The University Of Sheffield.

Frictional Behaviour of Coated Self-locking Aerospace Fasteners

Giuseppe Tronci

Supervisor: Dr M.B. Marshall

Submitted in partial fulfilment of the requirements for the degree of

Doctor of Philosophy

January 2017

ABSTRACT

Nuts and bolts used in aero-engines are manufactured from heat-resistant super-alloys. These materials have a high CoF, and frequently seizure occurs. In order to prevent this, a silver coating is applied to the nut threads, providing a low friction boundary at the interface. Additionally, a radial crimp is applied to the nut, in order to provide a self-locking feature preventing vibration self-loosening.

In this study, the CoF of the thread contact will be investigated both during initial joint assembly, and after thermal ageing. Additionally, a finite element model will be employed to investigate the contact mechanics as a consequence of the crimp.

The low CoF observed during initial assembly was found to be a consequence of shear flow of the silver coating, with an approximate doubling of this value once the coating aged. Areas of silver removal were found to be coincident with areas of high contact pressure in the joint, attributable to the crimp feature.

Additionally, new alternatives coating were tested in order to identify a replacement for the electroplated silver. Through a series of analyses, similarly done for the silver coating, from a list of 19 different thin films and paints, the list is reduced to three possible films, Chromium, Titanium and Nickel-Titanium.

Finally, through the FEA approach, a new self-locking design was developed, with an axial deformation instead of the radial crimp typically used. Thereafter, few nuts were manufactured, tested and compared to the elliptical, demonstrating it is a promising design with respect to the contact pressure distribution and silver removal.

TABLE OF CONTENTS

NOMENCLATURE

3D	Three Dimensions
CAD	Computer Aided Design
CAM	Computer Aided Manufacturing
CNC	Computer Numerical Control
CoF	Coefficient of Friction
EDM	Electrical Discharge Machining
FEA	Finite Element Analysis
rpm	Revolutions per Minute
RR	Rolls-Royce
TPI	Threads per Inch
UNF	Unified National Fine thread series
UNJF	Unified National Fine thread J series
VMC	Vertical Machining Centre

ACKNOWLEDGEMENTS

Firstly, I would like to express my thought that this PhD has been a marvellous experience, where I have had the pleasure of meeting fabulous new people.

I would like to express my gratitude to my supervisor, Dr Matthew Marshall, for the continuous support throughout my Ph.D., for his patience and motivation. His guidance has helped during all of the research and writing of this thesis, I could not have imagined having a better supervisor. I wish him every success in the future and a strong and rewarding career. I still remember the first time we met, when you helped me even though I could not speak any English, you gave me this opportunity, and all the necessary support. It has been a pleasure having coffee and good laughs together.

A sincere thanks to Glen Pattinson and Lloyd Pallett, my industrial supervisors. I hope they enjoyed the meetings, or at least the coffees.

I am also grateful to Carlo and Davide, who convinced me to move to Sheffield. Carlo also suggested to me that I take this experience, and has immensely helped me these past years. I thoroughly enjoyed these years with Davide, as we spent lots of free time together and enjoyed hundreds of barbecue steaks.

I would like also to wish a great future to the Sardinians; Michele, Mattia, Nicola, Marcello and Emanuele, hoping that they are able to utilise and grow their precious skills.

I consider it an honour to have worked with the colleagues and friends from Leonardo centre, doctors and doctors to be, such as Tom, Hiro, Mike, Andy, Martin, Pete, Wendy, Juan, Robin, Steve, Ben, Luke and many more, and of course all the staff of the Department of Mechanical Engineering.

A sincere thanks to our brilliant technicians, Dave, for his enormous contribution to the building of the test rigs, and Jamie, for his help in the last year.

Last but not least, my FAMILY. Firstly, Roberta, who supported and sustained me during the joy and the stress of this experience, I hope we can help each other for the rest of our lives. I am deeply grateful to my family: my parents Natalino and Pina, and my sister Carmen for supporting me spiritually throughout this experience and life in general. Even if distant, they are always present and I have truly missed them in the last four years, far from home.

CHAPTER 1

INTRODUCTION

1.1 MOTIVATION

Threaded fasteners play an important role in connecting parts that are subjected to static or dynamic loading. In addition they are reliable, and quickly assembled and disassembled. Aero-engine manufacturers use fasteners made from heat resistant super-alloys, as they must withstand temperatures above 1,000°C in the turbine section of an engine. These types of joints are widely used, with more than 15,000 bolts throughout engine (Figure 1.1).

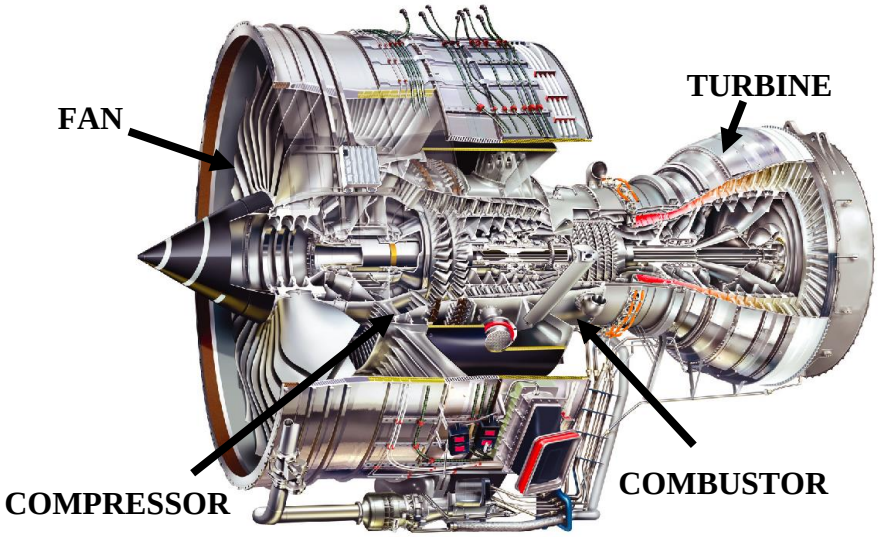

Figure 1.1: Trent 900 (Pattinson & Reade 2012)

In this study, Inconel 718 and Waspaloy fasteners are investigated, which are used in aero-engines over a range of temperatures from –50 to 760°C. They also operate in the presence of fuel contaminants, for example Sulphur and Chlorine, and are subjected to relatively high loads and vibration. When used in a like couple super-alloys have high coefficients of friction, for example 0.8 for Inconel on Inconel (Fox & Liang 2010), and seizure frequently occurs. To prevent this, in such applications, silver coatings are normally applied to the nut threads, which reduces the coefficient

of friction (CoF) and acts as a barrier between the surfaces in contact, preventing galling and seizure.

Generally, during engine build the joint must be disassembled and reassembled several times, whereas during repair and overhaul every fastener is changed. Prior to thermal cycling, silver coated fasteners can be re-used up to 5 times, fulfilling this requirement. Conversely un-coated nuts can be used only once.

To prevent vibration loosening, a radial crimp is applied to the end of the nut, prior to the silver coating process. This type of locking method, known as a prevailing locking device, generates a resistance torque while screwing. The crimp pattern can be elliptical or triangular depending on the joint (Figure 1.2), both of which acting to localise the stresses in two or three small areas, thus providing a locking feature but at the same time increasing the risk of removing the silver from the nut threads.

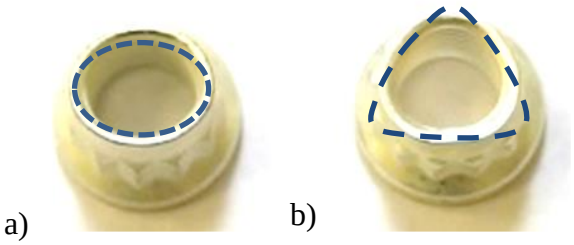

Figure 1.2: Crimp Patters: (a) Elliptical and (b) Triangular

Recently however, a problem with silver has been identified in aero-engines, where silver transfer can occur from coated nuts to other parts of the engine. Silver transfer to titanium parts in the engine (such as turbine discs), combined with the high temperature and loads present can cause stress corrosion cracking which may induce component failure. This problem is accentuated when the exhaust gases enter the engine, for example when the aeroplane is in a queue on the runway, as they act as a further catalyst to this process. Stress corrosion cracking was explained in a recent study by Saunders et al. (Saunders et al. 2016), which analysed the characteristic ‘blue spot’ seen in titanium alloys, as shown in Figure 1.3, which can lead to the failure of the component. Overall, this problem has been found to add significantly to inspection and maintenance costs.

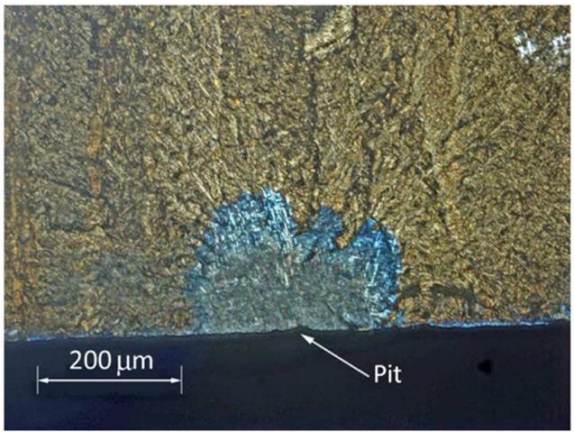

Figure 1.3: Stress Corrosion Cracking in Titanium Parts (Saunders et al. 2016)

Until recently there has been a lack of knowledge with respect to how silver works as an anti-seizure coating (Robinson 2009; Zhu 2012), with a recent study seeking to investigate its functional properties. If the behaviour of the silver is known, such as the CoF over the re-uses or the ageing capabilities, it could be replaced with another coating material, reducing the issues concerning the stress corrosion and the maintenance cost. Furthermore, a Health and Safety issue has also been recently discovered in the electroplating process used to apply the silver coating onto the nut (Robinson 2009). On a separate note, the elliptical crimp typically used was found to be magnifying the silver removal problem, as it increased contact stresses, promoting the removal. Thus, in recent years new locking designs are being investigated, in order to distribute the stresses along the nut, whilst still providing an anti-loosening capability for aerospace applications. Ideally, a new locking geometry must generate the required prevailing torque and must be as simple as a standard nut, such as the current elliptical design.

All of the above factors provide a motivation for this study, be it in the long term to replace silver, or in the short term to re-design the crimp feature to reduce silver removal.

1.2 PROJECT SCOPE

The principal aim of this study is to investigate the mechanical behaviour of the silver coating both experimentally and through Finite Element Analysis (FEA). An original experimental test platform is developed to investigate the CoF of crimped fasteners during tightening. The CoF is one of the most important parameters for joint designers, as an under or overestimation of the clamping load can lead to a loosening

or a failure of the joint. The performance of the silver coating is investigated over multiple tightening cycles, and its durability assessed. Removal of silver in the joint, and the associated contact pressures required for this to occur are then further analysed through a FEA approach, as a novelty in this area.

Following on from this, samples are aged at 760°C for 50 hours in order to be representative of aero-engine operating conditions. The CoF post-test is examined to identify the effects of temperature on the silver properties. Another key outcome will be to identify important material requirements for the coating, with the aim of determining an alternative coating to replace silver. Thus, a selection procedure is developed in order to test possible alternatives and compare them to the currently used silver film.

A further objective of this study is to develop an innovative self-locking design, to reduce the silver removal from the threads and thus alleviate problems related to the transfer of material to nearby parts. This new design must be suitable for aero-engine applications, as simple as the current design, and be capable of surviving multiple re-uses. Compared to the current elliptical design, a lower stress field is required, but which still provides the resistance torque and the anti-loosening capabilities.

1.3 LAYOUT OF THE THESIS

In Chapter 2 an overview of the previous studies related to this work are summarised, such as those relating to the fastener mechanism and vibration loosening. FEA studies are also discussed and the various locking methods analysed. Finally, the silver coating literature and the issues specific to aerospace applications are presented.

In Chapter 3 the mechanism by which silver functions as a low friction coating is analysed through a newly developed test platform. Firstly, the test rig and samples are described, along with the experimental tests, at room temperature and after a thermal cycle at 760ºC. The CoF in the threads is analysed, as well as the nano-hardness of the silver film pre and post ageing. Additional discussions consider the self-locking torque pattern and the speed dependency of the tightening process.

In Chapter 4 a FEA approach is used to analyse the contact mechanism of the elliptical self-locking nut, focussing particularly on the contact pressure and the stresses during the whole tightening process. Firstly, the model and the dynamic simulation will be carefully explained and the material properties defined. A pin on disc test for the silver coating is performed to find the relationship between the CoF and the pressure, as to

provide an input to the FEA model. Additionally, the tribological mechanism of the silver is analysed and used, along with a discussion of the stripping of the silver, to define a pressure threshold to cause the silver to strip.

In Chapter 5 multiple alternative coatings are tested, in order to find a suitable replacement for the silver coating typically applied on the threads of the nut. Different tests are performed and compared to silver at room temperature and after a thermal cycle. Additionally, a shortlist of optimum coatings are identified through use of nano-hardness and pin on disc tests.

In Chapter 6 a new self-locking design is introduced, using an axial deformation in the threads in the chimney of the nut to produce a resistant torque. Firstly, a FEA approach is used to analyse the stresses and the self-locking torque at different axial deformations. Afterwards, a CNC program is developed in order to machine the selected candidates. After machining, the nuts are tested in the platform and the results compared to the radially crimped nuts.

Finally, in Chapter 8 the findings and the conclusions of the previous chapters are summarised.

CHAPTER 2

LITERATURE REVIEW

2.1 INTRODUCTION

In this Chapter an overview of the previous studies related to this work are presented. Firstly, the tightening mechanism of the joint is examined, analysing the forces acting on the joint and the analytical relationship between the key parameters, such as torque, load and CoF. Vibration loosening studies performed over the past century are also summarised and the more recent technique of FEA explained as an ongoing developing method. Additionally, the different categories of locking devices are introduced followed by their related studies, aiming to analyse the anti-loosening capabilities. As the low friction silver coating is applied in the locking nuts analysed in the current work, the benefits and the issues related to the use of the coating in aerospace applications are presented, along with studies relating to the different self-lubricant coatings used for high temperature applications. Finally the gaps in previous research are highlighted and the motivation of this thesis explained.

2.2 BOLTS

2.2.1 *Overview*

When a bolt is rotated clockwise into a nut (assuming a right-hand screw thread), and torque is applied to tighten the joint, forces are generated into the three main components of the joint; the bolt or the male threaded part, the nut or the female threaded part and the clamped component, which is compressed in between the first two. Tightening of a bolted joint produces a compressive force in the clamped component, along with a tensile load in the bolt as shown in Figure 2.1.

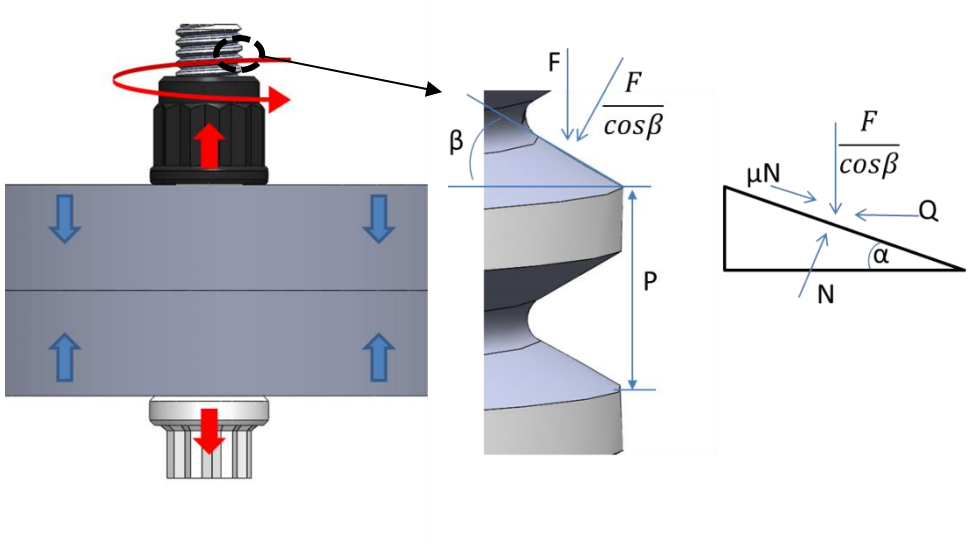

Figure 2.1: Forces in the Bolted Joint

As shown in Figure 2.1, reaction forces (*N*) due to the clamping load (*F*) and the thread half angle (β), are generated on the thread during tightening (*Q*), as the bolt becomes elongated. Due to the nature of the helix (with angle *α*), these reaction forces also generate a moment that tries to unscrew the joint, with thread friction providing a resisting force. From a geometrical perspective, a larger pitch (*P*), defined as the distance between adjacent threads, produces a higher moment. When a bolted joint is tightened, approximately 10% of the applied torque is used to clamp the components together. The rest is absorbed by friction under the bolt head and at the thread contacts. The under head friction is defined as the friction between the clamping plate and the bearing material of the bolt or the nut, depending on which member is being rotated. The thread friction is defined as the friction between the mating threads (Bickford 1998; Budynas & Nisbett 2010).

2.2.2 *Analytical Relationships*

Bolted joints have been the subject of multiple studies, with the aim in many cases of formulating equations to predict the relationship between applied torque and generated pre-loads (Juvinall & Marshek 2006; Shoberg 2000; Budynas & Nisbett 2010).

During tightening and un-tightening of a joint the total torque required is made up of different factors. The loading torque is the torque applied to induce a compressive load under the bolt head and creates a clamping load that tensions the bolt. The breakaway torque is the torque required to unscrew a locking device (if present) with

no clamping load on the fastener and is a parameter used to measure the performance of a self-locking device. Finally, the break-loose torque is the torque applied to start disassembling the loaded joint.

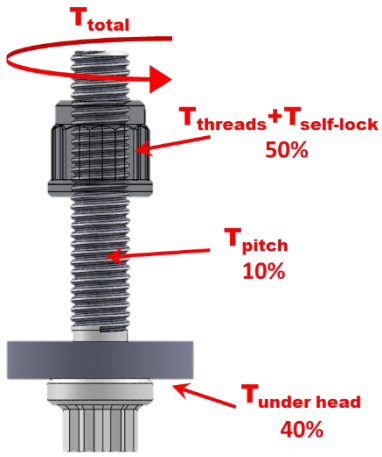

Figure 2.2: Torques Diagram (adapted from Shoberg 2000)

On a basic level, the torque required to tighten a joint can be approximated. For a given clamp force, *F*, nominal diameter, *D*, and the table-valued nut factor *K*, the torque is the result of the multiplication of these parameters.

$$T = K\ D\ F \tag{2.1}$$

The adimensional nut factor depends on the mating materials and can be found in look-up tables (Shoberg 2000; Rolls Royce 2011; Budynas & Nisbett 2010)

The loading torque can be broken down, and is the sum of four components (Figure 2.2): the clamp or pitch torque, defined as the amount of torque that is used to stretch the bolt, the thread friction torque, describing the torque to overcome the friction in the engaged threads, the under head friction, defined as the torque required to overcome the friction in the bearing surface, and finally the self-locking torque, the torque necessary to screw a locking device. It should be noted that the self-locking torque is the same as break-away torque, and is frequently included as a component of the loading torque.

$$T_{tot} = T_{pitch} + T_{threads} + T_{under\ head} + T_{self\text{-}lock} \tag{2.2}$$

Provided the thread pitch and the other geometrical parameters are known, along with the coefficients of friction both on the threads and under the head, the total torque required to tighten a joint becomes:

$$T_{tot}=F\left(\frac{P}{2\pi}+\frac{r_1\mu_1}{cos\beta}+r_2\mu_2\right)+T_{self\text{-}lock} \tag{2.3}$$

Where

$$r_1=\left[\frac{Min\ major\ bolt\ dia+Max\ dia\ or\ nut\ dia}{2}\right]\div 2 \tag{2.4}$$

$$r_2=\left[\frac{K_{min}+E_{max}}{2}\right]\div 2 \tag{2.5}$$

where F is the clamping load, P is the thread pitch, β is the half thread angle (30), r_1 is the mean thread engagement radius, and r_2 is the mean radius of the abutment face (Rolls Royce 2011). This equation, without the self-locking term, was published for the first time in J. Bickford's '*Introduction to the Design and Behavior of Bolted Joints'* in 1990, and attributed to N. Motosh (Motosh 1976).

In practice, the equation used in many standards in the aero-space industry is an approximation of this equation, and is as follows:

$$T_{tot}= F\ (a+b\mu)+T_{self\text{-}lock} \tag{2.6}$$

As shown, the self-locking torque is independent of load in both Equations 2.3 and 2.6. In Equation 2.6, a and b are geometrical factors calculated for fasteners, and μ is the coefficient of friction, assumed to be approximately the same for both the threads and under the bolt head. However, if the coefficients of thread and under-head friction are known, Equation 2.3 can be used (Rolls Royce 2011).

In order to calculate friction, torque and clamping load should be measured. Different methods are employed to calculate the load, such as load cells, ultrasound or measuring the elongation of the bolt. The torque is usually measured with resistant torque sensors, rotating torque sensors or torque wrenches (Fastenal: Industrial & Construction Supplies 2005).

2.2.3 *Experimental Studies on the Loosening of Bolted Joints*

The vibration loosening process by which bolts tend to unscrew has been studied for over a century, with Bickford (Bickford 1998), Eccles (Eccles 2010) and more recently Temitope (Temitope 2015) analysing all the studies done in this area. Researchers in this field have focused their work to identify the causes of loosening, considering factors such as axial and transverse dynamic loading, slip at the interface, bending moment and impact. In this section the most influential studies related to the aero-engine application will be presented.

Joint loosening was known from the industrial revolution, in particular in the rail industry, with most of the effort made to improve the design, instead of analysing the process. For example, in the documented patent of Ibbotson and Talbot (Ibbotson & Talbot 1877), a new self-locking method was introduced, where the nut was forced into the bolt threads. Thus, they claimed to have improved the joint design by preventing loosening by vibrations. Another example was seen in the patent of Lawrence and White (Lawrence & White 1861), who invented a locking device which secured the nut to the clamped components, preventing rotation and loosening induced by the vibrations of the trains.

Although the loosening of fasteners was known in the 19th century, the first study analysing the process was seen in 1945, when Goodier and Sweeney (Goodier & Sweeney 1945) investigated loosening due to clamping loading and axial vibration, through a fatigue test. They stated that the loosening was due to the dynamic clamping load, which radially contracts the bolt and dilates the nut, by a process termed the 'frictional ratchet'. They also identified the factors which influenced the loosening, such as bolt length, bolt diameter, pitch and thread tolerance of the joint.

A few years later Sauer et al. (Sauer et al. 1950) performed similar fatigue tests applying axial dynamic loads, and discovered that loosening rate is large at the beginning, and decreases with the number of cycles. They also found that clean surfaces improve the locking capabilities, reducing the rate of loosening. Interestingly they also found that loosening rate decreased with the preload, increased with increasing dynamic force, and decreased in used nuts compared to unused.

The theory of loosening due to dynamic transverse loading was first introduced by Junker (Junker 1969). He stated that the principal cause of the self-loosening failure is caused by vibration due to dynamic loads. He stated that when thread friction is

overcome, the loosening can occur, and when loosening starts, a smaller force can cause further loosening. This was explained considering an inclined plane, as shown in Figure 2.3a, where the nut is the block and bolt is the plane. The block remains in equilibrium until an external force is significant enough to overcome the friction. If transversal vibrations are applied and the inertial force is larger than the frictional force, the block slips down the plane.

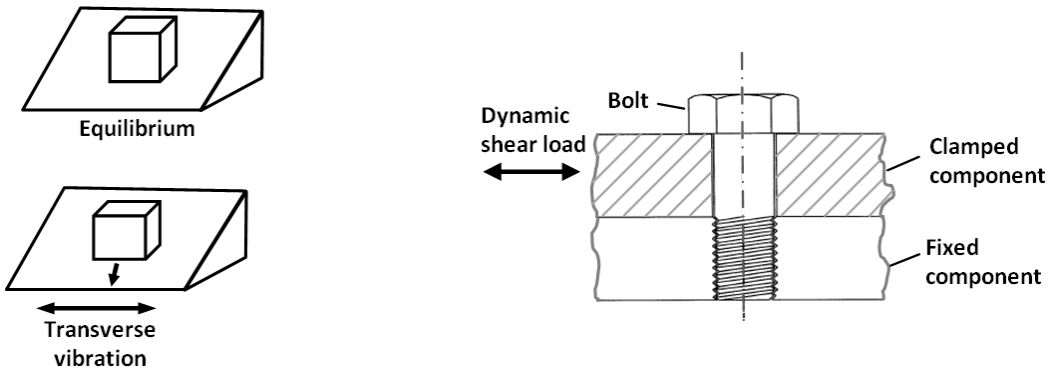

Figure 2.3: Junker Findings: (a) Block on incline plane and (b) Bolted joint subjected to dynamic shear load

The same principle can be applied to the preloaded joint, as shown in Figure 2.3b. Junker affirmed that when shear forces are higher than the friction force in the transverse direction, the joint will be free in any direction. Hence, because of the helix, a torsional force provides a loosening moment, which can initiate the loosening and eventually the joint can completely turn loose. He also stated that the transverse vibration is the most severe condition for loosening.

These studies were conducted using a newly developed machine, now popularly known as the 'Junker Machine', as presented in Figure 2.4.

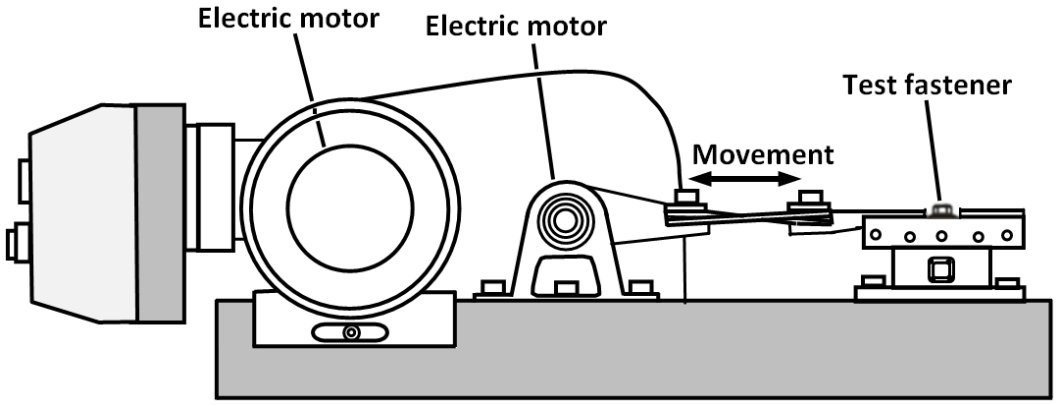

Figure 2.4: Junker Test Machine (Temitope 2015)

As shown in Figure 2.4, cyclic loading is applied by an electric motor to the preloaded test sample. This platform was used to investigate vibrational effects in the transverse direction, plotting the preload decay over a number of cycles. He also concluded that loosening is dependent on the amplitude of displacement, but is independent of frequency. This test platform is still widely used to measure the loosening resistance of locking fasteners, and is precisely detailed in a DIN standard (Deutsches Institut für Normung 2004).

A few years later, Finkelston (Finkelston 1972) used the Junker test machine to investigate the effect of initial preload on the loosening process. He stated that a high preload increases the loosening resistance in the joint for a given vibrational scenario. He also found that fine threads perform better than coarse threads and that locking devices reduced the loosening rate. Furthermore he confirmed the Junker finding that transverse vibrations are the most severe cause of loosening.

Latterly, Haviland (Haviland 1983) more specifically affirmed that in order to avoid self-loosening of the joint, movement in any direction must be avoided, such as rotational, transverse and axial movements.

The Junker theory was also explored considering the micro and macro movements during loosening, in particular in three sections of the bolted joints where frictional forces sustain the load, such as the interface between the clamped parts, the contact area in the threads, and the contact surface between the bolt head and the clamped components (Temitope 2015).

Pai and Hess (Pai & Hess 2002b; Pai & Hess 2002a) in their study analysed the localised slips causing loosening of joints in both the bolt head and thread interfaces, further validating the results using a three-dimensional (3D) FEA model (further explained in Section 2.3). They stated that loosening happens when the resultant of the tangential forces in the threads overcomes the frictional force, thus causing slip.

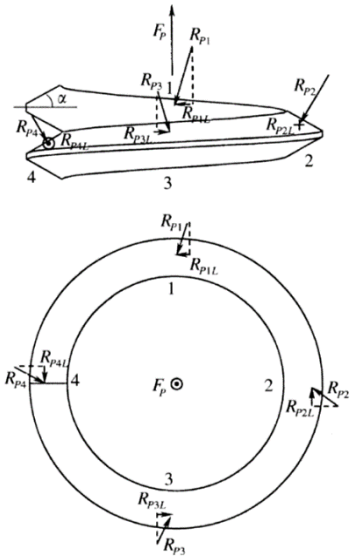

Figure 2.5: Loosening Process (Pai & Hess 2002a)

As shown in Figure 2.5, if the resultant reaction force *R*, opposed to the applied preload F_p is overcome in the tangential direction by a shear loading, then loosening starts. Furthermore, when the friction force is overcome, because of the helix of the threads, the preload generates a tangential force, which can turn loose the joint. The torsional torque applied during the tightening can also cause the loosening to start, as presented by Yamamoto and Kasei (Yamamoto & Kasei 1984).

In fact, Yamamoto and Kasei stated the loosening is caused by a restoring of the tightening torsion, which leads to a movement in the threads, also aggravated by the bending moment generated by the transverse vibrations. They also confirmed that localised slips accumulate, as earlier presented (Chesson & Munse 1965; Groper & Hemmye 1983), which can completely turn loose the joint. Finally they also supported the findings of Junker, showing that loosening is dependent on the amplitude but not the frequency of vibration.

The loosening of the joints was divided into non-rotational and rotational stages by some researchers. Jiang et al. (Jiang et al. 2003) defined the early stage as a non-rotational stage, with the reduction of the clamping force without relative rotation between the nut and the bolt. Afterwards, the clamping force further reduces as the joint rotates, as explained by experimental and FEA by the same authors (Jiang et al. 2004; Zhang et al. 2007). They stated that the cause of the early stage of loosening was due to localised cyclic plastic deformation, called 'cyclic strain ratcheting', which caused loss of preload as a redistribution of stresses occurs. As previously stated, they

also confirmed the importance of the transverse displacement amplitude during this stage.

Additionally, Zhang et al. (Zhang et al. 2006) analysed the rotational stage of the loosening of joints subjected to transverse vibrations, identifying the causes to be repeated micro-slips between the surfaces in contact, and the bending moment exerted on the joint. Similar results were previously obtained by Pai and Hess (Pai & Hess 2002a; Pai & Hess 2002b) and Groper and Hemmye (Groper & Hemmye 1983). Yamamoto and Kasei (Yamamoto & Kasei 1984), as previously explained, analysed the rotational stage of the loosening, stating that it is caused by the restoring of the torsional moment at the thread contact during vibration. They also introduced a numerical model to determine the required transverse force to cause the 'critical slip' at the bearing interface. Furthermore, Kasei et al. (Kasei et al. 1988) and Kasei (Kasei 2007) also found that loosening usually starts with undetectably small slips, with small or even in absence of macroscopic sliding at the bearing interface. The loosening reduces the clamping load, thus facilitating further loosening. These studies were further investigated by Jiang et al. (Jiang et al. 2004) and Zhang et al. (Zhang et al. 2006), finding that the Yamamoto and Kasei defined 'critical slip' for loosening to occur depends on the preload and the clamped length. They also stated that a washer and normal nuts have better anti-loosening performance than a flange nut. An additional analysis of a washer capability has been seen in the work of Marshall et al. (Marshall et al. 2011) in their test assessing the capabilities of different washers in distributing contact pressure. They showed that an improvement in the pressure distribution under transverse vibration loading can be achieved with the use of plain washers, spring washers and in particular Nordlock washers, compared to the case of a washer not being used.

Izumi at al. (Izumi et al. 2005), analysed the tightening and the loosening processes of the bolted joints not only with experimental studies but also through a 3D FEA, as further explored in Section 2.2.4. Similarly to Pai and Hess, they found that the loosening process starts at the thread interface, due to transverse vibrations. Comparing their results with Yamamoto & Kasei, they found a smaller value of 'critical slip' for the loosening to start.

2.2.4 ***Finite Element Studies***

In order to further understand the different mechanisms behind the tightening and loosening of bolted joints, FEA techniques have been widely used, with Mackerle (Mackerle 2003) summarising the studies performed in this area from 1990 to 2002. However, due to the ongoing innovation of the technique, this area is in continuing development. As explained in his work, the FEA results are affected by different factors such as the element type used, the constitutive equations, the time step size, the kinematic description, etc.

FEA studies have been employed to investigate multiple mechanisms, such as the stress concentration factor in the thread roots, the load and the pressure distribution along the threads during tightening, the self-loosening process caused by vibrations, the helical effects influencing joint behaviour, the fracture and crack propagation, along with the interaction between the clamped parts and the joint.

FEA models can be classified into three categories, 3D non-threaded joints, 2D threaded models and 3D threaded models. As explained by Mackerle, the fasteners should be modelled in 3D, in order to take into account the helix of the threads, the sliding surfaces and the joint interactions. However, 3D threaded models are time consuming, in terms of modelling and solving, with 2D and 3D non-threaded models normally preferred, as a compromise between solving time and accuracy of the results. However, 3D non-threaded models do not take into account the threads and the load transfer into them, and are mainly focused on the pressure in the bearing surface and in the clamped parts (Kim et al. 2007; Yang et al. 2011; Nassar et al. 2010; Oskouei et al. 2009). Furthermore, 2D axisymmetric studies do not take into account the helical effect of the threads, and are generally focused on the load distribution along them (Chen et al. 2010; Liao et al. 2009; Fukuoka 2005; Maruyama 1973; Fukuoka et al. 1985; Dragoni 1994; Englund & Johnson 1997; Lehnhoff & Bunyard 2000; Tanaka & Yamada 1986). Therefore, the most influential 3D threaded models are analysed in this section, which are used principally to take into account the helical effects on the joint.

Zadoks and Kokatam in their work (Zadoks & Kokatam 1999; Zadoks & Kokatam 2001) were the first to use a realistic 3D model to study joint behaviour. They analysed the axial stiffness of the bolt during tightening, as a critical parameter of the loosening failure of joints, validating the previous experiments. In order to reduce the number of elements in the model, the joint was split in two different parts, as shown in as shown in Figure 2.6, using finer meshes in the areas of interest. They

compared the results with 2D FEA and analytical results, which showed good agreement.

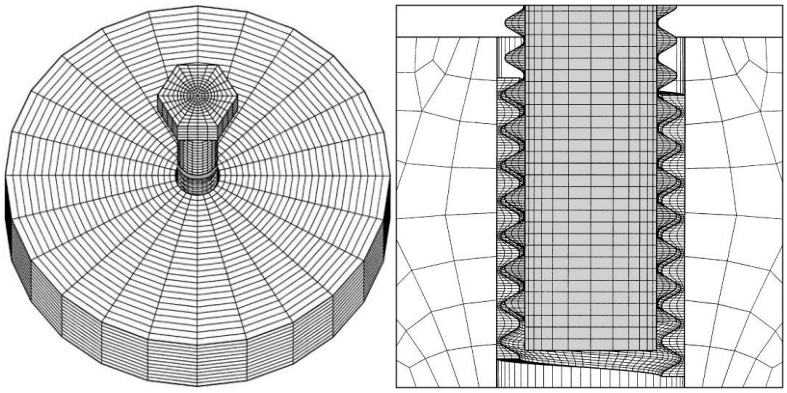

Figure 2.6: Zadoks and Kokatam FEA Model (Zadoks & Kokatam 2001)

Pai & Hess (Pai & Hess 2002b) in their 3D FEA work analysed in detail the failure of the fasteners by vibration induced loosening due to dynamic shear loads. They identified the different loosening steps observed in the experiments, and they concluded that the loosening caused by localised slips, found to be critical in the joint design, can occur at lower shear forces than loosening by complete slip.

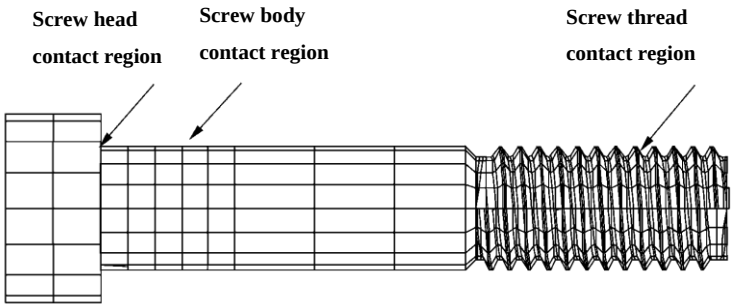

Figure 2.7: Pai & Hess FEA Model (Pai & Hess 2002b)

Izumi et al. (Izumi et al. 2005) studied tightening and loosening behaviour using FEA, and compared the results with experimental studies. It was found that the load distribution in the joints slightly differed. However as latterly highlighted by Yang (Yang et al. 2013), the mesh used, shown in Figure 2.8, was not accurately refined. Izumi et al. also highlighted the capability of FEA to contribute to the selection of the appropriate self-locking device, and further compared their results with 2D results and those obtained by Yamamoto and Kasei results (Yamamoto & Kasei 1984).

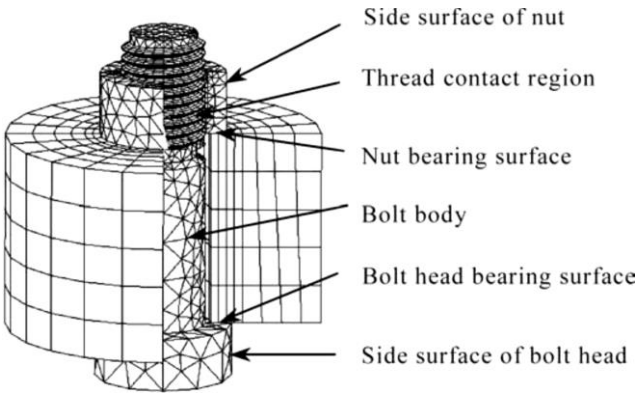

Figure 2.8: Izumi FEA Mesh (Izumi et al. 2005)

Fukuoka (Fukuoka et al. 2006), after their 2D studies (Fukuoka et al. 1985; Fukuoka 2005), analysed the effects of the thread helix on the root stresses along a fastener through a 3D model. In this work, a parametric mesh of the joint was seen for the first time, as shown in Figure 2.9. It was demonstrated that the maximum stress occurs at half a thread pitch from the nut loaded surface, and which then gradually decreases towards the top face of the nut. They also found that the load distribution experienced in the 3D simulation varied from the axisymmetric 2D analysis simulation, due to helical effects.

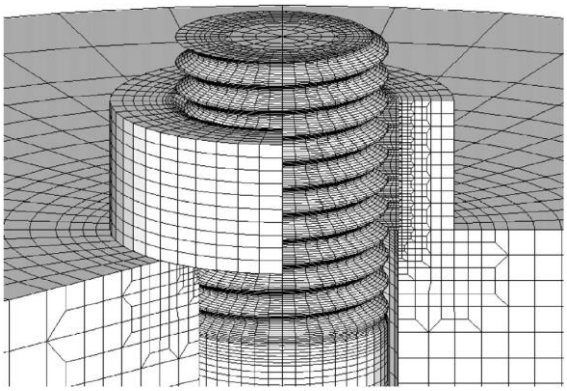

Figure 2.9: Fukuoka FEA Model (Fukuoka et al. 2006)

Yang et al. (Yang et al. 2013) in their study used a 3D parametric mesh to analyse the contact pressure at the interface for fine and coarse threaded fasteners, considering the helical effects. Accurate hexahedral elements were employed, as shown in Figure 2.10, to analyse the tightening mechanism and the effects of the clearance between the mating threads. They found that a better clamping load distribution can be achieved with a slight release after tightening and they also highlighted the advantages of using 3D simulations to take into account the helical effects in the tightening mechanism.

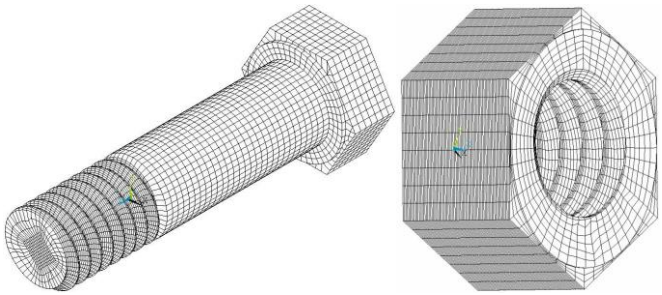

Figure 2.10: Yang FEA Model (Yang et al. 2013)

2.2.5 *The Role of Friction in Loosening*

As seen in Section 2.2.2, both through analytical and FEA studies present the torque required to tighten the joint is a function of the CoF. Whilst low friction is required to maximise the ratio of the clamping load to applied torque, high static friction helps to maintain and support the end load by preventing loosening. In the aero-engine industry, a particular challenge exists, as due to the temperatures experienced, heat resistant super-alloys are typically used. In a like on like couple these materials have high CoF, as therefore is not feasible to simply apply a higher torque to achieve a given clamping load and overcome the high friction. Additionally, high friction fasteners can also cause to further issues, such as damage to threads due to seizure and galling, which may lead to the failure of the joint.

Galling, often referred to as a cold-welding process, is surface damage due to adhesive wear and material transfer between sliding solids at high pressures (Fastenal: Industrial & Construction Supplies 2005). In threaded fasteners, damage typically occurs on the tapped threads of the nut, as the bolt threads are usually rolled, resulting in a rougher surface. Generally in aero-engines, due to limited access, seized fasteners may damage neighbouring critical components. Therefore aero-engine manufacturers found a compromise, applying a low friction coating to the nut preventing assembly damage, and a locking feature to avoid loosening.

As further explained in Section 2.3, among the different locking methods, elliptical deformed nuts are currently used in aero-engines in order to generate a resistant torque in the deformed threads. This is explained further in the following chapters of this study.

2.3 SELF-LOCKING METHODS

In order to prevent self-loosening of joints, design precautions are usually required (Bickford 1998; Kulak et al. 1987) such as

- increasing the friction forces between the bearing surfaces of the joints,
- reducing the hole clearance to reduce misalignments,
- increasing the preload,
- increasing the ratio between length and diameter to compensate for eventual misalignment,
- reorientation to have clamping loading instead of transverse loading.

Despite the above however, loosening can still occur and locking devices are often employed to prevent it. In an aero-engine, working space is limited and the environment is aggressive, therefore more complex locking devices are not suitable. Typically, crimped nuts are used, which are easy to assemble and disassemble, are as small as a normal nut, and if the preload is lost complete backing off is still prevented.

In this Section an overview of the categories of locking methods available and a critical view with respect to the aerospace applications are given.

2.3.1 *Fastener Locking Methods*

In order to counteract joint loosening, a variety of self-locking devices have been developed and investigated in the literature. Hess (Hess 1998) in a chapter of 'Handbook of Bolts and Bolted Joints' classified the locking methods in four groups (Figure 2.11):

I. Free spinning preload independent locking methods. Similar to standard nuts, but with an external locking feature, which acts only when tightening is complete, and is independent from the clamping load, e.g. jam nuts and lock wire. One of the benefits is the prevention of loosening even without clamping load. However they are not cost, time and weight effective for aero-applications.

II. Free spinning preload dependent locking methods. Similar to the previous category, they are free to rotate until clamping starts. At this point an additional locking feature acts to prevent loosening, such as lock washers

which deflect with the load, and spring nuts. However, because locking functionality depends on clamping load, if the joint is not sufficiently tightened complete loosening can easily occur.

III. Prevailing torque locking methods. Generally, an additional torque, the prevailing torque, is required to overcome the resistance imposed by an additional material or thread deformation feature, during tightening, e.g. elliptical nuts, as used in this work. However, the locking properties can decrease with re-uses of the joints. Additionally, complete loosening has been found to still occur occasionally with this method.

IV. Adhesive locking methods: In this category of locking fasteners, adhesive fluids are applied to the threads, locking them in position. However, lubricants and contaminants can affect thread adhesion, thus degrading the performance of the bond. Additionally, being a more permanent solution, lower strength adhesives can be used if required to permit multiple disassemblies, which can cause partial loosening.

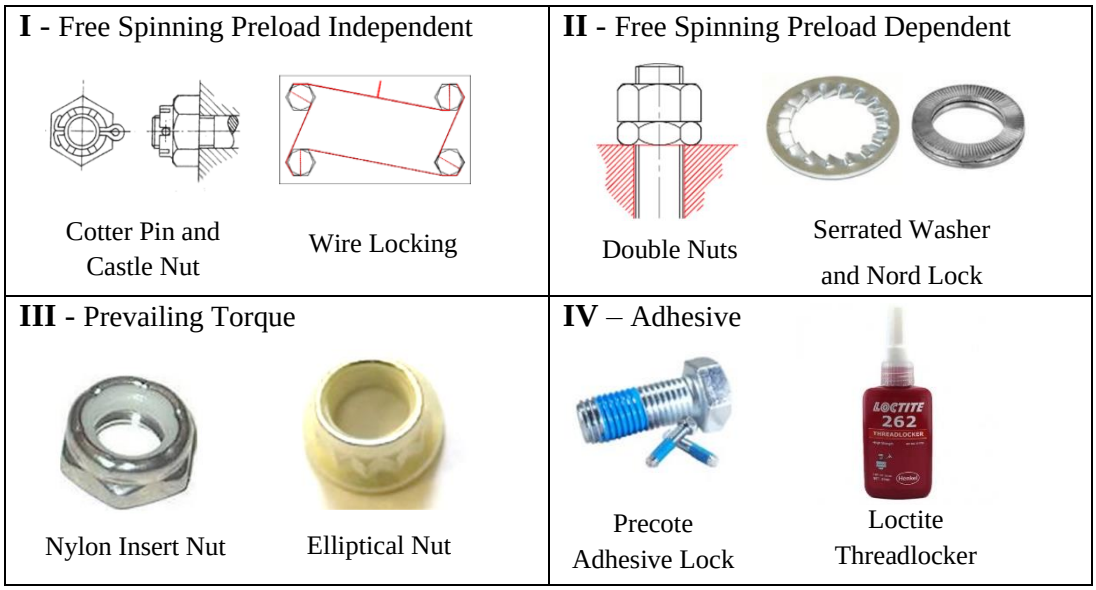

Figure 2.11: Self- Locking Joints (adapted from Temitope 2015)

2.3.2 *Testing of Locking Features*

Innumerable studies have been done in this subject, analysing the various types of locking methods, and highlighting their associated strengths and weaknesses. In this section different studies related to aero-engine applications are summarised.

The Junker Test Machine (Figure 2.4), as previously described in Section 2.2.3, or similar, are widely used to assess the anti-loosening performance of self-locking

devices, Junker's theory having been widely accepted. One of the most significant Junker's conclusions was that self-loosening of a joint can be prevented by using a self-locking feature alone, and this has been tested in various studies. Among the various studies related to the Junker theory and the loosening process, as previously introduced, Finkelston (Finkelston 1972) performed a comparison between free spinning and prevailing devices. He found that prevailing devices reduce the rate of loosening, and prevent complete loosening when transverse vibrations are applied. Meanwhile, Pearce (Pearce 1973) tested a broad range of locking fasteners using a Junker machine and introduced a shock movement through use of an air hammer. Comparing different types of washers, he concluded that helical spring washers improved anti-loosening capabilities, when compared to a plain washer.

Furthermore, the experimental studies of Barrett (Barrett 1990) stated that jam nuts and double nuts are too unpredictable for aerospace applications. In fact, the torque required to tighten each nut is not well understood, similarly the load distribution at the clamped interface is also variable. Another implication of the use of jam nuts and double nuts is the increase of the joint weight, which becomes particularly problematic when thousands of bolts are utilised in an aircraft engine (Juvinall & Marshek 2006; Budynas & Nisbett 2010).

Different platforms to investigate and assess the anti-loosening capabilities of locking devices were later introduced, such as two new platforms developed by Sase at al. (Sase et al. 1996; Sase et al. 1998): the 'Displacement-based loosening device' and the 'Acceleration-based loosening device'. In their work, they stated that these two platforms were easier to adjust in amplitude and frequency compared to the Junker machine. As shown by Figure 2.12, they concluded that serrated flange nuts, edged spring nuts, metal inserted nuts, and cover rings had poor anti-loosening capabilities compare to conventional nuts, while nylon inserted nuts performed slightly better. The best performing locking devices in their experiments were found to be double nuts and eccentric nuts, which significantly reduced the loosening rate, albeit under limited conditions.

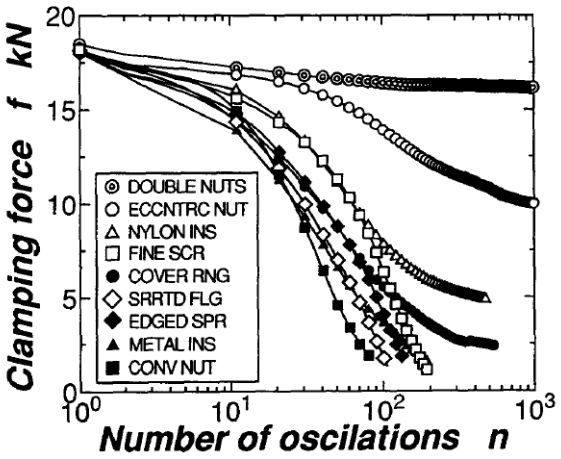

Figure 2.12: Sase et al. Results (Sase et al. 1996)

In 2009, different external locking methods were analysed using a Junker test machine by Cheatham et al.(Cheatham et al. 2009), who investigated locking devices on fine ¼" (6.35 mm) threaded fasteners, such as standard free-running Heli-Coil inserts with high vacuum grease, and standard free-running Heli-Coil inserts with Loctite thread-locker. Analysing the load versus the number of cycles they showed that standard free-running Heli-Coil inserts with Loctite thread-locker have the best anti-loosening performance compared to the other two.

Further analysing adhesive locking methods, as highlighted by Martinez et al. (Martínez et al. 2011) and Petrova and Lukina (Petrova & Lukina 2008), adhesives used as a thread-locker are very sensitive to temperature changes and are not reliable if subjected to multiple assemblies. Similarly, Kumar (Kumar 2014), investigated the anti-loosening capabilities of Nylock nuts, which use a nylon collar to increase the CoF in the threads. However, this type of locking feature is only applicable to applications with an operating temperature lower than the melting point of the nylon (150ºC) (Smith 1990).

Different prevailing nuts were investigated in a recent study by Eccles et al. (Eccles et al. 2010) using a modified version of the Junker machine. In order to analyse the loosening in the locking devices, they introduced clamping loading from 0 to 5 kN intermittently to the transverse vibration. In their experiments they found that prevailing joints can completely detach if the clamping loading exceeded the residual preload. This conclusion regarding clamping loading was in contrast to previous studies, which stated that prevailing fasteners cannot completely detach. They also developed an analytical model to identify how the loosening of the joint might be

prevented, which included the tensile load, the prevailing torque and the pitch of the screw. They found that free spinning nuts can completely turn loose with only transverse vibration and that the majority of self-locking devices can tolerate some degree of loosening under transverse loading.

Interestingly, in the work of Panja and Das (Panja & Das 2013), in which they analysed the locking properties of different self-locking devices including washers, they found that washers did not significantly prevent loosening as is widely believed. Additionally, they concluded that spring washers and inside or outside serrated washers performed only marginally better as anti-loosening devices.

As highlighted in this review, multiple test platforms are used to evaluate the locking capabilities, with the Junker test being the most widely used. Additionally, due to obvious safety concerns, aerospace manufacturers often employ other test methods in order to achieve a documented standard, such as the SAE standard test (SAE International 2014). Therefore, for applications in harsh environments, such as those found in the aerospace industry, fasteners with a mechanical locking feature are frequently used. However, because of the aforementioned issues, a physically deformed nut is generally preferred in the aero-engine industry, which provides a loosening-resistance effect and is easily assembled and disassembled. As previously stated, in this study, locking nuts which have a silver coating applied into the threads and in the bearing face to prevent seizure and reduce friction are explored, as will be introduced in the next section (Section 2.4).

2.4 SILVER COATINGS

2.4.1 *Introduction*

In aero-engine applications, as discussed, the bolts must withstand temperatures exceeding 1,000°C, manufactures use fasteners made from heat resistant super-alloys, such as Inconel and Waspaloy. However, when used in a like couple, seizure is likely to occur as there is a very high CoF. Indeed, in the work of Fox & Liang (Fox & Liang 2010), Inconel was found to have a CoF varying between 0.6 and 0.8. To limit this, a coating barrier is normally applied in the surfaces in contact, as examined in this work, where silver is applied in the threads and in the bearing surface of the nuts. Silver plating is prohibitively expensive for most fastener applications, with the aerospace industry being a notable exception.

2.4.2 *Silver as a Low Friction Coating*

The applied silver coating serves both as a corrosion inhibitor and a dry lubricant, reducing galling of the threads in high temperature environments. Additionally, it has a good high-temperature performance due to the plated layer's high melting point of 962°C (Pauleau 1996), and it can be successfully used as a solid lubricant up to a maximum temperature of 650°C. In aero-engine applications the silver coating is electro-plated onto the threads with a thickness of 6 μm, resulting in low coefficients of thread friction of the order of 0.10-0.15 (Robinson 2009). The limited variation in the CoF is important when predicting the torque required to achieve a given end load. It is thought that silver provides low friction between hard surfaces during relative motion due to its low shear strength, which allows it to plastically deform thus providing solid lubrication, however limited investigations have been performed (Pattinson & Reade 2012). Silver belongs to a family of soft coatings, and can easily shear to reduce friction. Yang et al (Yang et al. 2003), further investigated the tribological behaviour of the silver, finding three wear regimes: mild, moderate and severe wear, where the CoF induced by the coating was found to gradually increase as it sustained increased levels of damage, as shown in Figure 2.13.

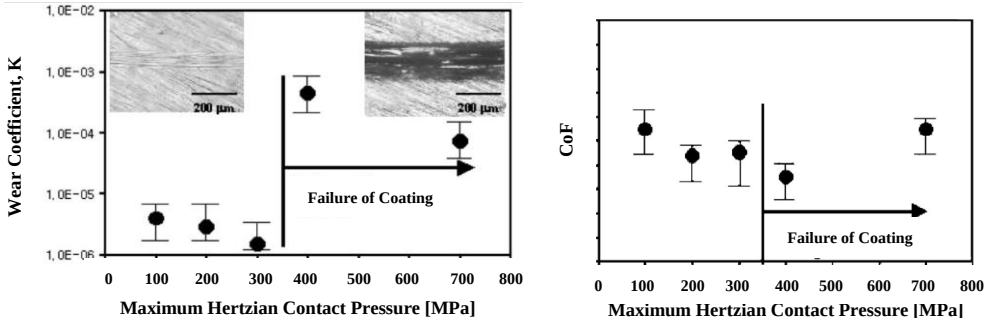

Figure 2.13: CoF of Silver Films against the Contact pressure (adapted fromYang et al. 2003)

Furthermore, El Sherbini et al (El-Sherbiny & Salem 1986) analysed different coating methods, and found ion-plating to be the most effective for tribological applications. At present, however, ion plating is found to be cost disadvantageous, and electroplating is the preferable compromise between cost and capability.

Marechal et al (Marechal, Pauleau, et al. 1994; Marechal, Quesnel, et al. 1994) have examined the tribological properties of the silver coating at different thicknesses (from 0.4 to 20 μm) at room temperature and at 500°C (Figure 2.14). They found a lower value of CoF when the coatings are less than 5 μm, as the substrate instead of the

coating supports the load. Above 5 µm, the friction increases along with the thickness, as the soft coating starts to support the load, increasing the contact area. Because of the softening of the silver coating above ~l50°C, they found a reduction of friction with temperature for very thin coatings (less than 3 µm), and an increase for thicker coatings, compared to the room temperature results, as with softening, the load is supported by a larger contact area.

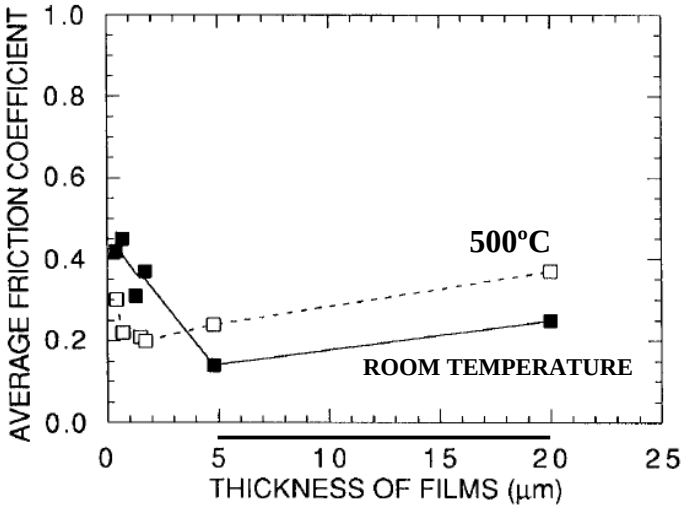

Figure 2.14: CoF at Room Temperature and at 500ºC for Different Silver Coating Thickness (Marechal, Pauleau, et al. 1994)

Additionally in tests at elevated temperature the study also found no significant difference between tests in air and nitrogen atmospheres, further highlighting the oxidation resistance of silver coatings.

At this moment no experimental works have been performed to assess the mechanical properties of the silver coating after thermal ageing, to understand the coating conditions of the aero-engine fasteners during engine maintenance. In fact, during joint disassembly, post cooling at room temperature, seizure is frequently seen and in combination with the limited working space, it can lead to catastrophic failure of nearby components.

2.4.3 *Issues Surrounding the Use of Silver*

As highlighted in the introduction, silver migration may occur with degradation of the coating and, if the silver comes into contact with titanium parts, stress corrosion cracking can occur. In order to try and limit this problem, silver coated joints are only used in applications where the service temperature does not exceed 300°C. However, at high loads and in combination with contaminants present in the aero-engine

environment, migration is accelerated. Silver coatings have also be found to vary in thickness, with undistributed thicknesses of 20 μm reported (Robinson 2009), which is likely to be ploughed off and entrained into the engine.

Additionally, silver plating is also being phased out with the introduction of European Union Reach legislation, which has highlighted the health, safety and environment issues associated with the cyanide baths used as part of the plating process (Robinson 2009).

These are all requirements that any future replacement coating for silver would have to meet. At present no satisfactory alternatives have been found, which is in part due to a lack of understanding with respect to silver behaviour and functionality. Its low plating cost (approximately £0.30 per nut), in conjunction with a low CoF, mean it is still used in aero-engines, although inspection intervals are now increased. Any alternative coating would also have to meet the stated six times re-use criteria (Robinson 2009).

Finally, most studies performed to date have been limited to ball on flat tests, and have not investigated the behaviour of silver coatings in bolted joints, despite this type of coating being widely used in the aerospace industry in conjunction with a crimp feature, therefore a significant knowledge gap exists.

2.4.4 *Low Friction Coatings for High Temperature*

An ongoing research area for coatings is investigating low friction and wear resistance at high temperature for aerospace and machining purposes, where temperatures can reach 1,000 ºC. In this section the most significant research in this area is summarised. Typically, based on the temperature requirement, these types of coating are used in combination with super-alloys. For example, in a recent study, Houghton (Houghton 2015) investigated different solid lubricants for Inconel alloys, with the aim of reducing the wear rate. He stated that in the selection of a suitable coating, not only the lubricating properties are taken into account, but also the ability to support load, the thermal properties, the cost and the ability to improve the tribological properties of the materials in contact. In his work, Nitrides and DLC (Diamond-Like-Carbon) coatings were investigated. Nitride coatings improve the surface hardness of a wide range of alloys, but also the wear resistance, due to the formation of a protective oxide layer. Nitride based coatings, such as Titanium Aluminium Nitride, Zirconium Nitride, Hafnium Nitride and Boron Nitride are widely used in the cutting tools

industry. DLC coatings are a category of hard coatings known for their high load capacity and resistance to abrasive and adhesive wear. Different types of DLC coatings are available on the market, with exact formulae kept secret by each manufacturer, generally however, degradation at high temperature occurs.

More widely, a review of research done up to 1982 was done by Sliney (Sliney 1982), summarising the different solid lubricant coatings for high temperature applications (journal bearings in particular), where the use of other lubricants is restricted. In fact, above 300 ºC most oils and greases are not stable and solid lubricants are generally applied.

MoS_2 (molybdenum disulphide) and WS_2 (Tungsten disulphide) are commonly used due to their low shear strength. These coatings showed good lubrication properties up to 350-400 ºC or slightly higher for short durations. Similarly, graphite, which must adsorb vapours to develop good lubricating properties, rapidly oxides at high temperature, and additives such as Cadmium Oxide (CdO) can be applied to improve the properties.

Other coatings are used for high temperature bearings, such as Graphite Fluorides, Polyimide coatings, and hard coatings such as alumina, silica and silicates, which showed good wear resistance but high friction. Thus, soft oxides are normally added, such as lead monoxide, to reduce the CoF, especially at high temperature where their shear strengths are reduced.

Bi et al. (Bi et al. 2013) in their overview of high temperature self-lubricating materials, highlighted the intention to develop synergetic lubrication materials, combining low and high temperature lubricants. Fluorides and molybdates appeared to be promising high temperature wear resistant solid lubricants, while Zirconia ceramics were potential candidates especially at high temperature, but the high CoF was not acceptable for engineering applications. Thus, additive such as graphite, MoS_2, BaF_2, CaF_2, Ag, Ag_2O, Cu_2O, $BaCrO_4$, $BASO_4$, $SrSO_4$, $CaSiO_3$ are applied as effective solid lubricants. Similarly, Alumina, with its good chemical stability and low price, showed high friction and poor wear resistance at high temperature, and for this reason, better performance are achieved adding Ag and fluorides as solid lubricants.

The NASA Lewis Research Center successfully developed the heat resistance coatings, such as PS100, PS200, PS300 and PS400 series of plasma sprayed coatings. PS100 was a nickel-glass-solid lubricant, PS200 a hard nickel-cobalt-bonded chrome carbide matrix with the addition of solid lubricant such as Ag and BaF_2/CaF_2. PS300

replaced the harder chrome carbide of PS200 with chrome oxide, and more recently the issues related with the previous coatings were solved in the PS400 series.

An additional successful heat resistance coating is Ni-hBN, in which the non-wettability and the poor sinterability of the hexagonal Boron Nitride (hBN) is improved by the use of the Nickel matrix. Despite the fact that its properties are strongly dependent on temperature, it is used as a self-lubricating wear resistant coating up to 800 ºC.

An emerging class of coatings is adaptive tribological coating, which are a new developing method of 'smart' materials, such as VN/Ag, which adjusts their chemical structure as a function of the environment and temperature they are subjected to, improving their lubricating abilities. In fact, while silver provides good lubrication at low temperature, the Ag_3VO_4 phase reduces the friction at high temperature due to its layered atomic structure.

Likewise NiAl alloys, which show poor ductility at room temperature and low strength and creep resistance at high temperature, can be improved with the addition of soft oxides in order to reduce the friction and the wear rate at high temperature, due to the softening oxide and a low shear strength. A Ni_3Al matrix containing Ag, Mo and BaF_2/CaF_2 in a multi-layer structure also improves the stress concentration between the coating and the substrate and reduces the porosity in the interface increasing the adhesion to the substrate. In fact, multilayer structures are normally used to reduce the stress concentration and improve the bonding strength. It is believed that no universal lubricant can operate at a wide range of temperatures, with a synergetic lubrication mixing two or more lubricants being a promising alternative.

A recent review by Voevodin (Voevodin et al. 2014) presented a series of hard coatings for high temperature applications, particularly for dry machining. As commonly known, hard coatings have high coefficients of friction, thus soft additives are applied, such as silver and gold. In fact, these soft metals are reliable solid lubricants due to their low shear strength over a range of temperatures, from below ambient to their melting points. Being sensitive to the thickness, they work best on a hard supporting substrate and in thin films (up to 1 micron). In fact, when a thick film is applied, part of the load is carried by the soft coating, generating a significant 'ploughing force' and increasing the frictional force. At high temperature soft coatings were found to exhibit a low wear resistance and are easily damaged due to their softening. Thus, nanocomposite coatings were developed, which include the solid

lubrication of the noble metals while maintaining wear resistance of a hard matrix, such as binary yttrium stabilized zirconia and the gold or silver nanocomposite coating materials.

In order to progress this class of coating and address some of the issues in their application, the thermal management of the mechanical contact is being promoted. The aim is to reduce heat spikes and redistribute the thermal load of the sliding components, in order to prevent the deterioration of the base materials, which can be achieved using multilayer coatings, such as TiN/CrAlN.

In conclusion, most of the studies reviewed above aimed to reduce friction at high temperature, while scarce research was done to analyse the frictional properties after a thermal cycle. In fact, a key focus of this thesis is the examination of the lubricating properties of the silver coating and the possible alternatives post-ageing. Cost and chemical affinity were not taken into account in this review, although are significant in the coating selection. For this reasons up until recently silver was found to provide a good compromise between friction, cost and chemical stability in the aero-engine environment.

2.4.5 *Summary: Application of Crimped Nuts & Silver Coatings in Aero-Engine Fasteners*

High contact loads due to the elliptical crimp and high temperatures result in high shear stresses and differential thermal expansion between the fastener and the coating. These conditions create the risk of coating breakdown and wear particle formation, leading to an increasing probability of seizure or damage to the threads. Adhesion of the coating to the substrate (nut) plays an essential role in avoiding failure, and has been one of the key drivers behind the choice of silver, as opposed to other low shear strength materials (Pattinson & Reade 2012). In this application silver has been found to have sufficient adhesion to the nut threads during tightening and un-tightening of the fastener assembly, protecting the mating threads with a physical boundary, thus in most cases avoiding galling (Robinson 2009). Previously, silver's ability to withstand temperatures in the range between –50 and 760 °C was also critical, though as discussed this has now been found to be limited. Engine fluid, engine oil, fuels, high humidity and fuel contaminants such as Sulphur and Chlorine are present in the engine and can penetrate into the nut through the unloaded thread flank. In fact, the current design specification of thread tolerance allows a coating thickness of 5-13μm, with

the penetrants having been identified as a key issue with respect to the silver migration (Zhu 2012). Additionally, in most cases fasteners are made from nickel-based alloys, Waspaloy and Inconel 718, and corrosion resistant steels A286 and FV535, and silver has been found to not activate any failure mechanisms with respect to these alloys. Indeed, up until recently it was thought to be inert with respect to all of the engine materials it contacted, such as titanium, carbon steel, aluminium, and magnesium (Robinson 2009).

In conclusion, at this moment there is a lack of knowledge concerning the elliptical crimped locking device in combination with the soft silver coating applied in the threads which were found to cause the failure of the joints in the aero-engine. For these reasons, the tightening process of the coated crimped nuts will be analysed in this work. Additionally the lubricating properties of the silver coating after a thermal cycle are not well understood, and will therefore provide a key objective for this thesis. Alternative coatings and locking design are also investigated, in order to reduce the issues seen with the current method, with the aim of minimising the contact stresses experienced.

CHAPTER 3

FRICTION OF SILVER COATED FASTENERS

3.1 INTRODUCTION

As discussed in Chapter 2, mechanical components in aero-engines operate over a temperature range from –50 to 760 °C. As a consequence, the fasteners used to join components together are manufactured from heat resistant super-alloys, which can generate high coefficients of friction, causing seizure. To prevent this, a silver coating is normally applied on the fasteners. Additionally, in order to avoid vibration loosening, a radial crimp is added to the end of the nut providing a self-locking feature. Unfortunately, this also has the effect of localizing the contact stresses in two small areas, increasing the risk of removing the silver coating from the nut threads and triggering seizure. Whilst seizure of the joints is undesirable, as discussed transfer of removed silver from the nuts to other parts of the engine is also a significant issue. In particular, silver can combine with corrosive species in the presence of moisture and attack Nickel and Titanium alloys leading to an increased inspection requirement.

Multiple researchers have been working on developing fasteners over the past century (as described in Chapter 2), with a similar approach being followed by Nassar et al (Nassar et al. 2007; Nassar et al. 2005; Nassar & Zaki 2009; Nassar & Yang 2007; Nassar & Yang 2007). As described in Section 2.3, they investigated various anti-loosening methods, in addition to different tightening speeds and different coatings. However, the performance of the silver coating, being used mainly in aerospace, is not fully understood, in particular when used in conjunction with a self-locking feature.

In this chapter the mechanical behaviour of the silver coating has been investigated experimentally on a bespoke test platform, developed to investigate the CoF of crimped fasteners during tightening up to a maximum load of 11.6 kN. The

performance of the silver coating is investigated over a period of 6 re-uses, and its durability assessed. Following on from this, samples were aged at 760 °C for 50 hours, and the CoF post-test analysed.

3.2 EXPERIMENTAL SET-UP

3.2.1 *Test Rig Development*

To investigate thread friction and the behaviour of silver coatings a new test rig was developed. The aim was to measure the clamping load, torque and the tightening angle, as a function of time. Through this approach it was possible to calculate the CoF on the threads, a key parameter in understanding the screw mechanism. In this section the development of the test rig is described.

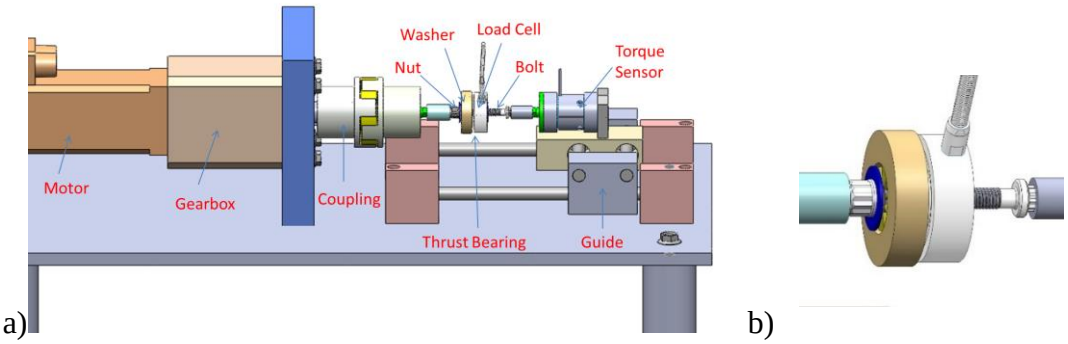

Figure 3.1: (a) Test Rig and (b) Joint Close-Up

The CAD image of the manufactured test platform is shown in Figure 3.1. As shown in the figure, the motor turns the nut into the bolt, compressing a load cell used to measure the clamp force. The bolt is fixed in a torque sensor, which in turn measures the reaction torque. With this test arrangement it is also possible to rotate the bolt with the nut fixed, by swapping their position. The overall capability of the test platform was designed based on the Rolls- Royce standard for the fasteners under investigation (Rolls Royce 2011). The load cell is donut shaped, and has the form of a thick washer with a ¼” (6.35 mm) diameter hole in the middle. It is a LTH350 compressive load cell manufactured by Futek, with a peak measurement value of 22 kN, and was calibrated from 0 to 20 kN, with an error of 0.5 %. The torque sensor is a reaction sensor (TFF350 by Futek), with a maximum measurement capability of 56 N·m, with an error of 0.4 % and was calibrated within the range 0 to 25 N·m. The torque sensor has not been calibrated for its maximum torque as the error depends on the calibrated

range; thus an error of 0.1 N·m is achieved instead of 0.2 N·m over the reduced range. This type of sensor works in both the clockwise and anti-clockwise directions. Both the load cell and the torque sensor are connected to a computer via USB.

The motor and gearbox shown in Figure 3.1 are used to drive the nut. The motor is a Baldor BSM63N-375AA unit, with a power of 375 W, and has an integrated position encoder. It is capable of delivering a 2 N·m rated torque with a peak output of 8 N·m, and has a rated speed of 4,000 rpm and a maximum speed of 10,000 rpm. Included in the experimental set-up is a 50:1 reduction gearbox, meaning the maximum output is 90 N·m (due to the mechanical loss) at 200 rpm.

The motor is mounted rigidly to the rig base plate, and a flexible coupling is utilised between the gearbox output shaft and the socket for the nut. A rotary encoder measures the rotation of the output shaft in combination with clamping load and torque measurements. On the opposite side, the torque sensor is mounted on linear guide rails so that the bolt is unconstrained and free to move in two dimensions.

A steel washer is also included in the set-up, to ensure load is applied on the correct face of the load cell, and also accommodates a thrust needle bearing used to reduce under head friction during a given test. Finally, two different adapters for the flexible coupling and torque sensor (each with 3/8” (9.52mm) square drives) were manufactured, allowing a range of fasteners to be tested. All components are mounted on a 12 mm thick steel table, which is fixed in the floor to prevent unwanted movement.

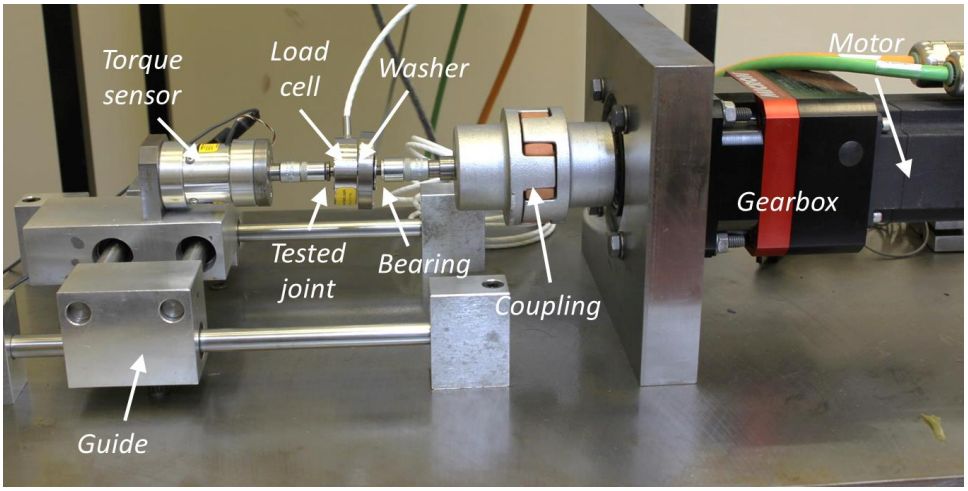

Figure 3.2: Test Rig

The motor speed along with the acquisition of positional, load and torque data is controlled via a LabVIEW program (version 2012). Figure 3.3 shows the user interface, while in APPENDIX A an overview of the developed program is provided.

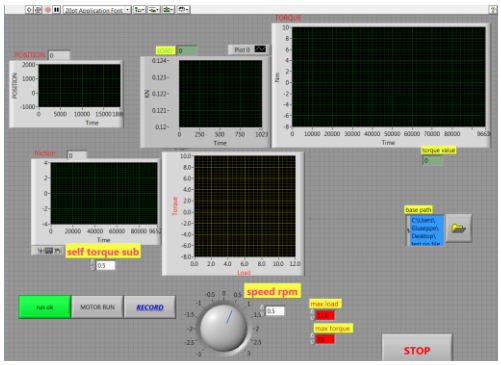

Figure 3.3: LabVIEW Interface

Motor speed is set pre-test, with an end load or torque target also specified. When the end load or torque limit is reached, the motor stops running and after a short dwell the process is reversed and the joint is un-tightened. As shown in Figure 3.3, the front panel of the program graphs and displays the measurements in real-time during a test. Torque, time, load and shaft position are continuously recorded in a text file, allowing the CoF in the threads to be calculated throughout the tightening process. The maximum acquisition speed is 1,000 values per second, but a sample rate of 100 values per second was found to be satisfactory, since the maximum speed used in the test was 3 rpm, thus providing 2,000 values per rotation.

3.2.2 ***Materials and Equipment***

AS48824 bolts and AS49211F nuts were tested in this study. The AS48824 bolts are ¼" (6.35) diameter, 38 mm long with a 20 mm threaded section containing 28 threads per inch UNJF (Unified National Fine thread J series), and have a 5/16" (7.94 mm) 12 point head. UNJF threads differ from the more common UNF variant by the root radius of the male thread, being larger in order to improve the tensile performance of the fasteners and to reduce the stress concentration factor as defined in the Standard MIL-S-8879C (Military Specification 1991). Additionally, the requirement for high strength is achieved with 3A and 3B classes of fit. The bolts are manufactured from Waspaloy, an age-hardenable, nickel-based super-alloy, with high strength properties up to 1,000 °C. Furthermore Waspaloy has good corrosion and oxidation resistance,

and has a Yield Strength of 910 MPa and an Ultimate Tensile Strength of 1335 MPa at room temperature. This combination of properties makes it ideal for extreme environments, such as those found in aero-engines.

AS42911F coated and crimped nuts were used in conjunction with the bolt. The nuts had 28 UNF threads per inch (TPI), were approximately 10 mm long (therefore containing 11 threads), and had a 3/8" (9.525 mm) 12 point outer form. Similarly to the bolt, the material used for the substrate was Waspaloy. The applied crimp was elliptical, and was produced by the clamping arrangement shown in Figure 3.4, where the nut chimney was compressed until a displacement of 0.35 mm was achieved.

Figure 3.4: Crimping Vice

The silver coating was previously applied by electroplating by Rolls-Royce, resulting in a coating 5-13 μm in thickness on the threads. The clearance required for the coating was taken into account, during the manufacturing process.

Mobil Jet Oil II (ExxonMobil 2015), a high performance synthetic gas turbine lubricant, was applied to the bolts prior to testing. All tests were carried out as per the Rolls- Royce Design Standard JDS 829_03 (Rolls Royce 2011) where the end load used to clamp a 0.2500" (6.35 mm) joint is 11.6 kN. Prior to lubricant application acetone was used to decontaminate the specimens. An image of the test samples is shown in Figure 3.5.

a) 

b) 

Figure 3.5: (a) Mobil Jet Oil II and (b) Joint Sample

3.2.3 *Experimental Procedure*

In this section the experimental procedures for the needle bearing calibration and for both the room temperature (‘cold use’) and thermally aged tests are explained.

3.2.3.1 Bearing Calibration Test

Whilst the under head friction can be assumed to be minimal due to the use of the needle thrust bearing, as a consequence of its low CoF compared to that of the threads, it is more accurate if the torque dissipated in the bearing is subtracted. Therefore an additional experiment was performed to determine its value. The needle thrust bearings (AXK0821TN by SKF) have inner and outer diameters of 8 and 21 mm respectively, and are 2 mm thick. The cage consists of two hardened washers, with a single bearing capable of supporting a maximum clamping load of 20 kN.

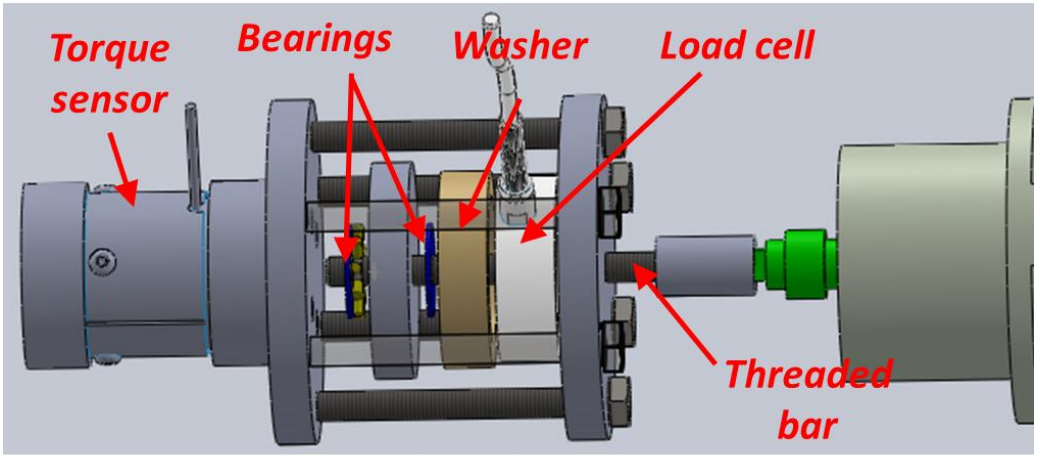

Figure 3.6: Bearing Calibration Test

Figure 3.6 illustrates the calibration test setup used to calculate the bearing torque. As shown in the figure, the bearing is placed between the nut and the washer, and by tightening six M6 screws a variety of loading forces representative of the main test rig were reproduced. In this set-up, a bar with a fixed disc is rotated by the motor, with a second identical bearing used on the other side of the disc. The measured torque is that required to avoid the rotation of the two plates, and is the sum of the friction torque of both bearings. The load was measured through the donut load cell, with the torque sensor used to measure the bearing torque. A similar LabVIEW program to that presented for the main test platform was used to record the test data.

3.2.3.2 Cold Use

As highlighted, during engine assembly joints are typically assembled and reassembled multiple times, with 6 re-uses being a common target. Thus, 6 cycles were performed on an as new joint, with an end load of 11.6 kN targeted. Mobil Jet Oil II was applied to the bolt and a thrust bearing used to isolate the thread torque as previously described. The joints were assembled at rotational speeds of 3 rpm during wind on and wind off, and at 0.5 rpm during the final tightening and untightening, in order to achieve a satisfactory accuracy with respect to the targeted clamping load. Torque and clamping load were recorded, enabling the CoF to be calculated for each cycle. The test procedure is summarised in Figure 3.7.

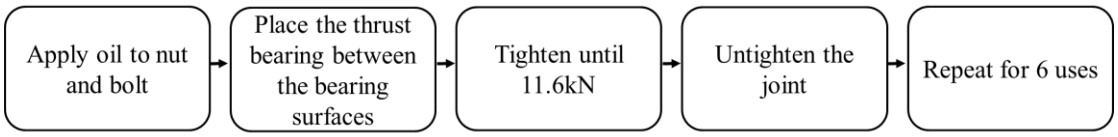

Figure 3.7: Flowchart of the Cold Test Procedure

3.2.3.3 Ageing Test

During engine operation, the joints must operate at high temperatures, up to 760 °C, which can cause the coating to deteriorate. Thus, assembled joints were thermally aged at 760 °C for 50 hours, and their ability to prevent seizure investigated at room temperature post-cooling. Whilst in the practical application, a significant level of vibration accompanies engine operation, this has not been considered in this case. The aim of this study is to consider a worst case seizure event, and in the case of vibrations these are likely to reduce the level of seizure experienced, and have thus not been included in the study. In order to prepare these samples for ageing, the torque required to reach the end load was first evaluated using the load cell, and the joint then re-assembled to the same torque with a Waspaloy spacer replacing the load cell (Figure 3.8). The Waspaloy spacer had similar dimensions to the load cell, and was used since the load cell could not withstand the ageing process. Mobil Jet Oil II was once again used as a lubricant.

The specimens were then placed in the oven, which gradually reached 760 °C as per Rolls-Royce Standard (Rolls Royce 2011). After 50 hours at constant temperature, the specimens were left in the oven switched off to slowly cool down till room temperature, and then disassembled on the test rig. The torque profile was once again

measured. As the load cell was not in place, the CoF in the threads was calculated using the torque as the joint began to unscrew, i.e. where the joint load was known. In order to estimate the CoF in the threads, the equations previously defined in Section 2.2.2 were used, assuming the end load of 11.6 kN remained during the thermal cycle. As in the cold test, the surface torque must be subtracted from the total torque. Thus, the spacer plate was rotated with respect to the joint, to estimate the surface torque, which was then subtracted. Once disassembled, the joints were re-tested using the load cell, as described previously, in order to fully characterise the CoF in the threads using Equation 2.3, with the overall test procedure summarised in Figure 3.9.

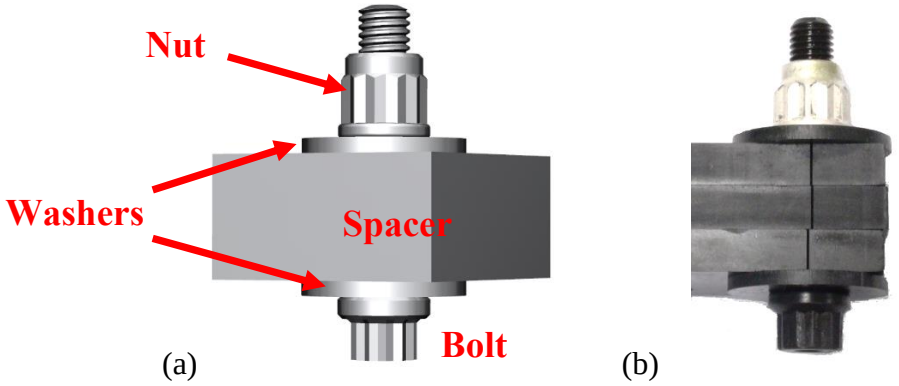

Figure 3.8: Thermal Ageing Test Assembly a) Schematic and b) Real Joint Tested

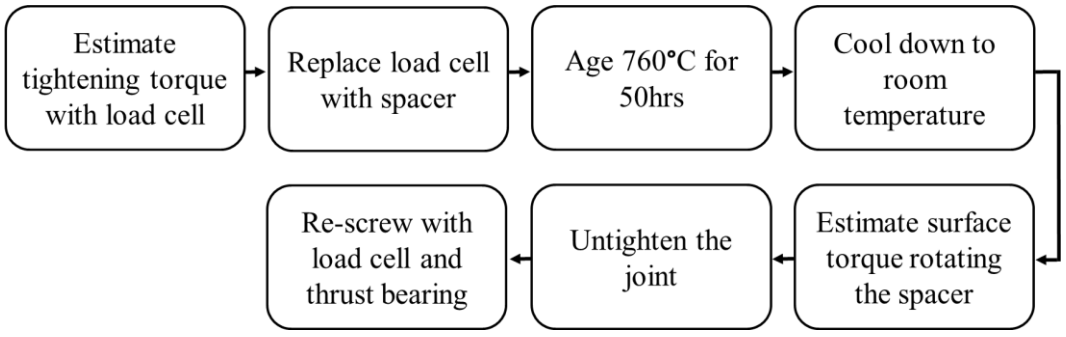

Figure 3.9: Flowchart of the Thermal Test Procedure

3.3 RESULTS

3.3.1 *Bearing Calibration Test Result*

The torque required to overcome the bearing friction was calculated. Five tests for a series of applied loads were performed using Mobil Jet Oil II as the bearing lubricant, with the torque and the load during clamping measured each time. Figure 3.10 shows the results of the test. As shown, a linear relationship was observed between bearing torque and load, where the line of best fit was characterised by Equation 3.1.

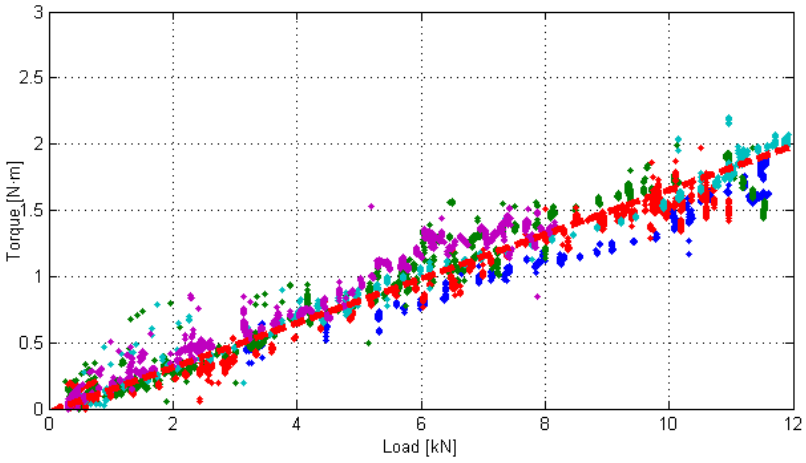

Figure 3.10: Bearing Test Results

$$Torque=0.168*F-0.0223 \quad (3.1)$$

The torque shown in the figure is half of the torque measured, as two bearings were used at the same time. The equation has been subsequently used to subtract the bearing torque from the total torque measured during tightening experiments using the main test rig, as further explained in Section 3.3.2.

3.3.2 *Calculation of Coefficient of Friction*

From a given data file, torque and load are extracted as a function of the angular position as shown in Figure 3.11.

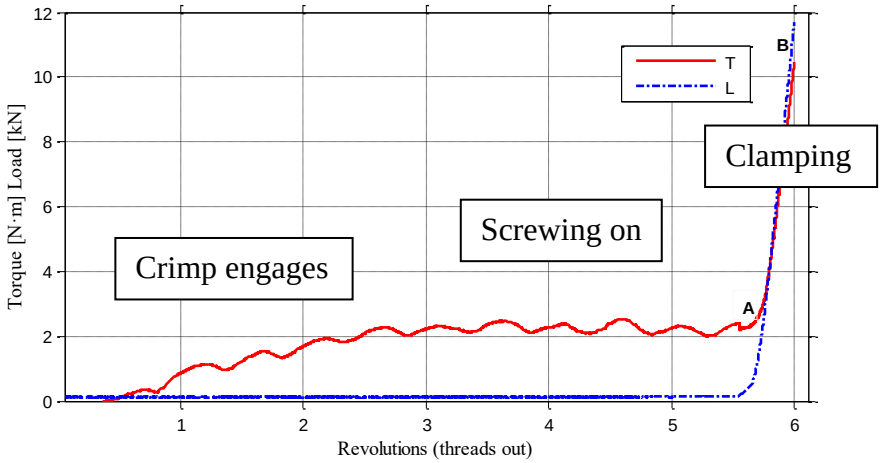

Figure 3.11: Torque and Load during Screwing

The example data set in Figure 3.11 shows the torque and clamping load recorded during the tightening as a function of the position of the bolt with respect to the nut. As shown, the horizontal axis is plotted in terms of the number of complete threads out of the nut. This value is determined by counting the number of threads that are observed out when the end load is reached, and provides a frame of reference for the test.

As previously stated, in this work elliptical self-locking nuts are used, which produce a resistive torque whilst engaging, as per the prevailing torque locking methods described Section 2.3. In practise, the self-locking feature is achieved by deforming the chimney and will be further investigated in Sections 3.4.1 and 4.7.1

As shown in Figure 3.11, at the start of the test the bolt threads engage with the crimped nut threads, producing the locking torque. The locking torque is almost constant until axial force is developed, with a sinusoidal pattern evident. As the fastener begins to clamp the load cell (point A), torque and load rapidly increase before reaching the 11.6 kN set point (point B). Figure 3.12 shows the load plotted as a function of torque, where a higher torque is measured during the first tightening with values becoming approximately constant with re-use. It was also found that torque values were lower during the un-tightening phase.

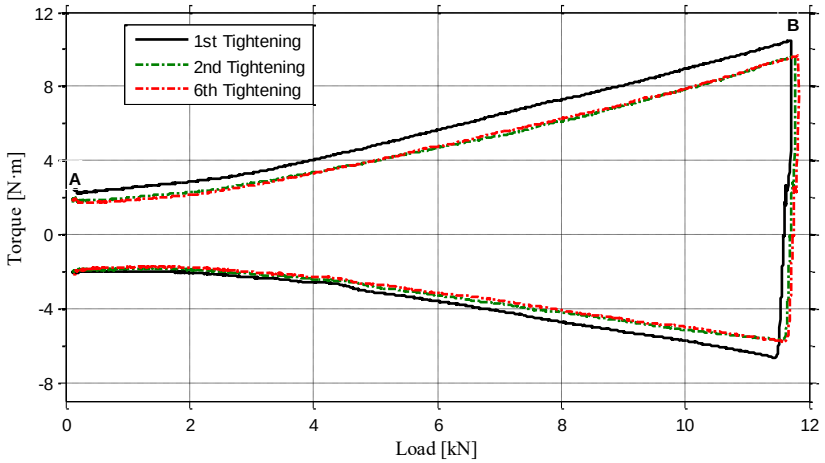

Figure 3.12: Torque vs Load for 6 re-uses

When the clamping load is zero, the measured torque is due to self-locking only, and results from the resistance due to the crimp in the nut chimney. At the end of the load cycle, when the pre-set end load is reached, the motor stops and the torque reduces. The motor stops after 50 milliseconds and the end load is usually surpassed by approximately 0.1-0.2 kN.

As previously defined in Section 2.2.2, the total torque required to tighten the joint is the sum of four factors, the pitch torque, the bearing torque, the threads torque and the self-locking torque. In order to calculate CoF in the threads, the threads torque should be isolated and the other factors subtracted. The pitch torque, required to stretch the bolt, is calculated as:

$$T_{pitch} = \frac{P}{2\pi} F \tag{3.2}$$

Thus, subtracting the bearing torque, defined in Section 3.3.1, and the self-locking torque, the CoF in the threads has then been calculated as:

$$\mu = \frac{cos\beta}{r_1} \frac{T_{thread}}{F} \tag{3.3}$$

Assuming the self-locking torque is constant, with the average value taken over the final revolution of the nut prior to compressing the load cell and generating clamping load, the CoF can be calculated and plotted against position, load and torque (an example is shown in Figure 3.13).

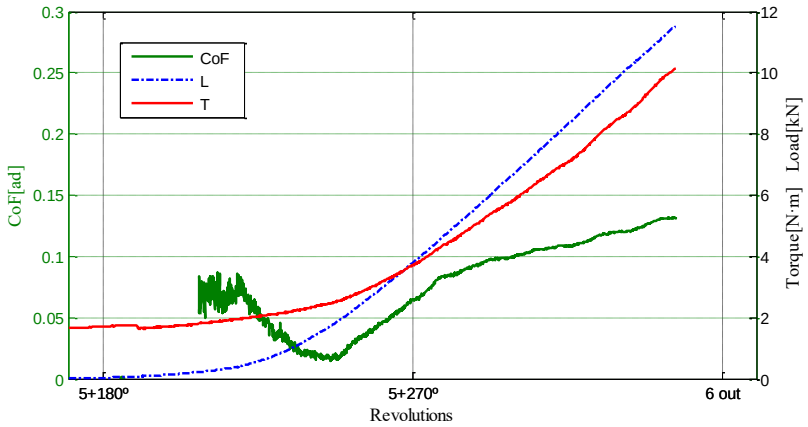

Figure 3.13: CoF in the threads

As shown in Figure 3.13, the CoF changes as the joint is loaded, which may indeed be the case, but the calculation procedure may also contributing to such observed trends. In fact, the self-locking torque has been assumed constant, and this is clearly not the case based on the observed sinusoidal pattern in the torque data as the crimp is engaged. Thus, it was assumed that the self-locking torque continues with its sinusoidal pattern, even when the clamping load is developed, as shown in Figure 3.14.

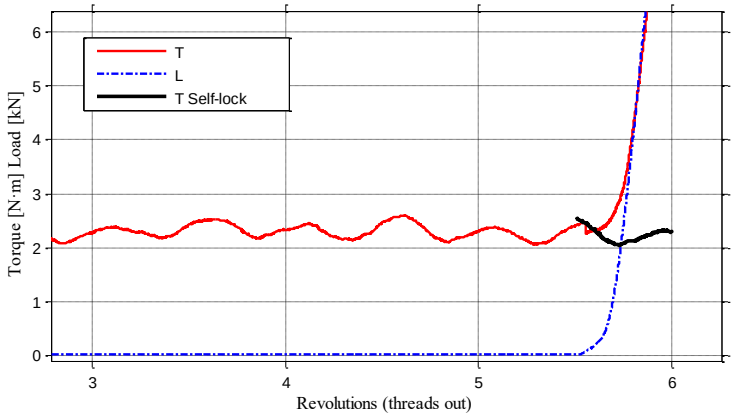

Figure 3.14: Self-Locking Torque Assumption

Figure 3.15 shows the resulting CoF in the threads calculated by subtracting the assumed self-locking torque and using Equation 3.3.

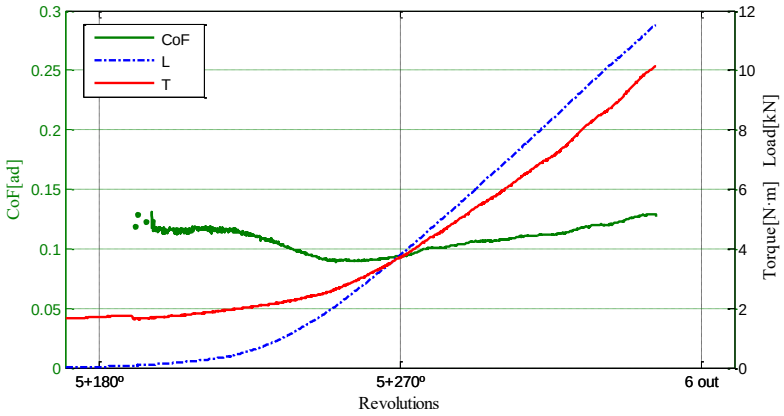

Figure 3.15: CoF in the Threads

As shown in Figure 3.15, the CoF in the threads shows less scatter compared to Figure 3.13, in particular at the beginning of the clamping. However, the friction value at the end load remains constant, in the range of 0.125-0.13. This refined calculation method was thus used in the rest of this work.

3.3.3 *Cold Use*

During the cold test the torque, the load and the angular position were acquired continuously during the 6 cycles.

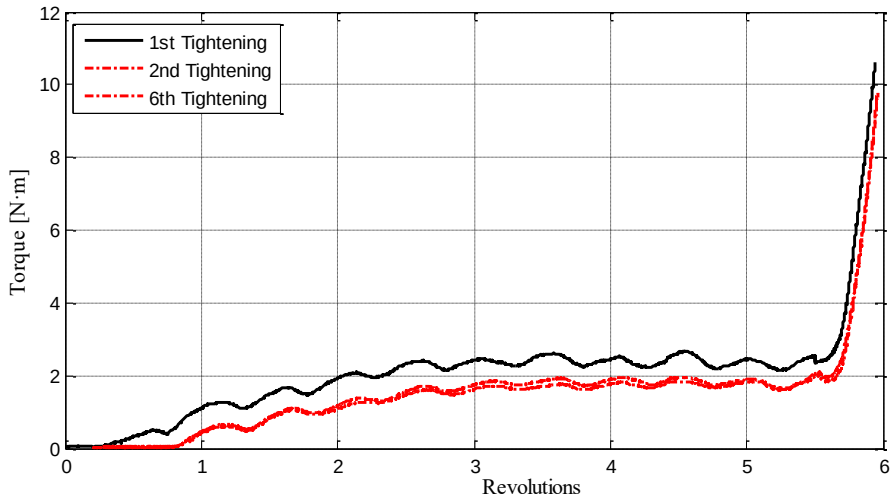

Figure 3.16: Self-Locking Torque over Re-uses

As shown in Figure 3.16, the torque can be plotted against the angular rotation, showing a sinusoidal pattern of the self-locking torque over the whole test, with the first cycle being slightly higher than the following cycles, and will be further investigated in the following sections.

Upon post-processing, using the approach and the equations previously described, the CoF in the threads was isolated and plotted for all six re-uses, along with the clamping load (Figure 3.17).

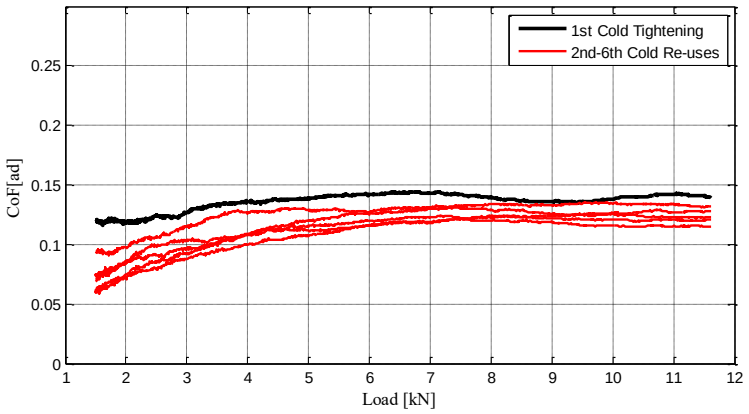

Figure 3.17: CoF for Cold Re-Uses

As shown in Figure 3.17, the thread friction over the cycle was found to range between 0.1-0.14, and shows a gradual increase with clamping load. Furthermore, the friction during the first tightening was found to be slightly higher with respect to the following cycles. These two behaviours of the silver coated crimped nut will be further investigated in the following sections of this work.

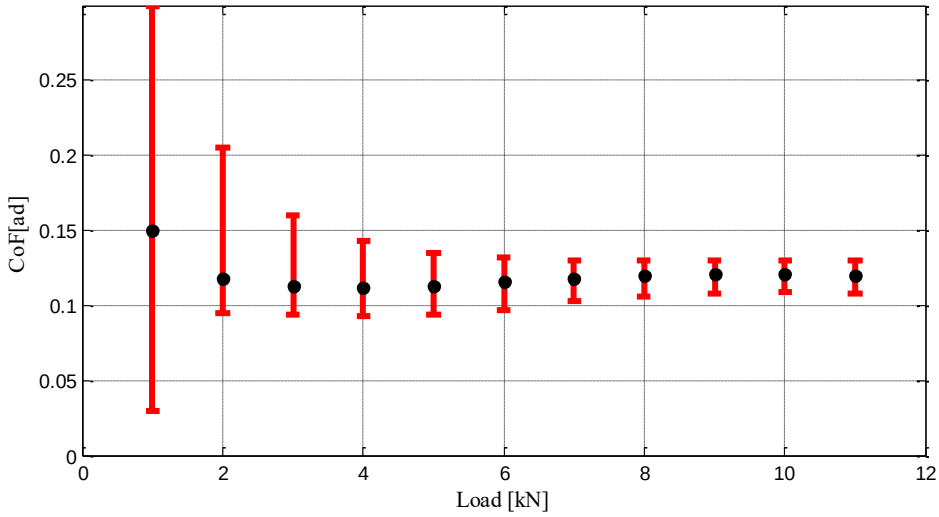

Figure 3.18: CoF for Cold Re-Uses, 5 Tests

Figure 3.18 shows the average CoF in the threads for 5 test specimens (6 cycles each), whilst also taking into account the minimum and maximum friction recorded at 1 kN

clamping load increments. As shown in the figure, the CoF results show some scatter at low load, which is attributable to the accuracy of the sensors at low values. Also, the self-locking torque was estimated as previously described and, at a low clamping load, makes up a significant part of the total torque (Equation 2.3). As highlighted in Figure 3.18, the scatter decreased with increasing clamping load, with a range of 0.11- 0.13 measured at peak load.

3.3.4 *Ageing Test*

Five silver coated joints were tested at 760 ºC for 50 hours and unscrewed after cooling at room temperature to evaluate the break torque, thus simulating the untightening process during engine maintenance. The results are summarised in Table 3.1.

Pre Thermal Ageing			**Post Thermal Ageing**			
CoF	**Tightening Torque**	**Untightening Torque**	**CoF Un-tightening (estimated)**	**Untightening Torque**	**Spacer Torque**	**CoF Re-tightening**
0.118	16 N·m	12.7 N·m	0.4	33.8 ± 5 N·m	11 N·m	0.24

Table 3.1: Ageing Test Results

In the first columns, Table 3.1 shows the torque measured for the joint prior to the thermal ageing process. As discussed this value was used to determine the torque necessary to achieve the required end load with the spacer plate as opposed to the load cell in place. Figure 3.19 shows the torque profile of the joint both pre- and post-ageing. As shown in the figure, the torque required to turn the joint is significantly higher post-thermal ageing. This result, along with the torque attributable to rotation of the spacer, was used to estimate the thread friction (Table 3.1). As shown in the Table, the thread friction has increased significantly as a consequence of the thermal cycle, and has more than doubled in value.

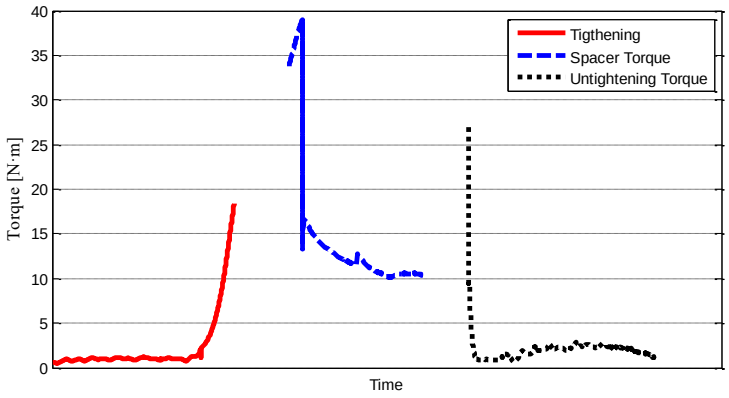

Figure 3.19: Torque during Thermal Ageing Test

As discussed, Figure 3.19 shows respectively the torque required to tighten the joint on the spacer, the torque required to rotate the spacer after ageing, and the torque required to unscrew the joint. The red curve shows the tightening torque, evaluated using the load cell, and used to re-assemble the joint with the spacer replacing the load sensor. The blue curve shows the torque required to rotate the spacer after the ageing process. When the spacer rotates relative to the joint, both bearing surfaces slide. However, in reality during the periodic engine maintenance, during the unscrewing process only one of the two surfaces slides, either the bolt or the nut side, and therefore in order to estimate the CoF in the threads only, the total torque was halved. A peak torque was calculated at the beginning of the test, attributable to breaking the seizure that occurred with ageing, further highlighted by the washer-joint interfaces shown in Figure 3.20a.

Finally, the black curve of Figure 3.19 shows the untightening torque post-ageing, indicating a higher torque than pre-ageing. During the test, silver removal and transfer to the mating threads and the spacer was also observed, as shown in Figure 3.20b, with silver clearly evident on the bolt threads. As highlighted by this discussion, the CoF in the threads measured directly from the un-screwing process is an estimation, not taking into account the seizure of the seating face, and accurately tested by re-tightening.

Figure 3.20: a) Typical Washer-Joint Interface, b) Silver Transfer Post-Ageing

As stated, multiple joints were tested using the previously described procedure, in order to detect any scatter in the results. In Figure 3.21 five tests were plotted.

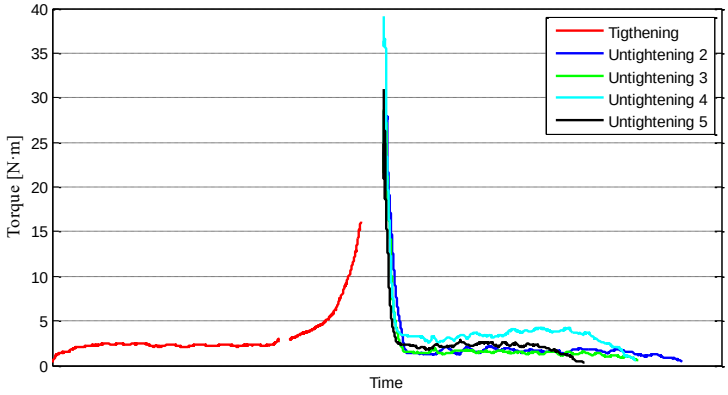

Figure 3.21: Ageing Test Results

As shown in Figure 3.21, the torque required to directly unscrew the joints after the thermal cycle was higher than the cold tightening torque in any test, with torque values between 28.5 N·m and 39 N·m (Table 3.2). This variance in the results was thought to be caused by varying degrees of joint seizure, as illustrated in Figure 3.20.

Cold Tightening	**Untightening post-ageing**				
16 N·m	**1st**	**2nd**	**3rd**	**4th**	**5th**
	35.4 N·m	28.5 N·m	28.5 N·m	39.1 N·m	31.0 N·m

Table 3.2: Ageing Test Results: Repeats

In order to further characterise the aged joints, once disassembled the joints were re-tested using the load cell. Figure 3.22 shows the torque and load curve for the aged joint compared to that for the cold test, further highlighting the increase in torque required to rotate the joint after the thermal cycle. Additionally, Figure 3.23 shows the CoF in the threads as a function of joint load, where a similar increase in value

with respect to load is once again evident, however, with a significantly higher overall value in the aged case as compared to the room temperature case, though less than determined from the aforementioned initial calculation (0.24 vs. 0.4 for re-assembly vs. un-screwing respectively (Table 3.1)).

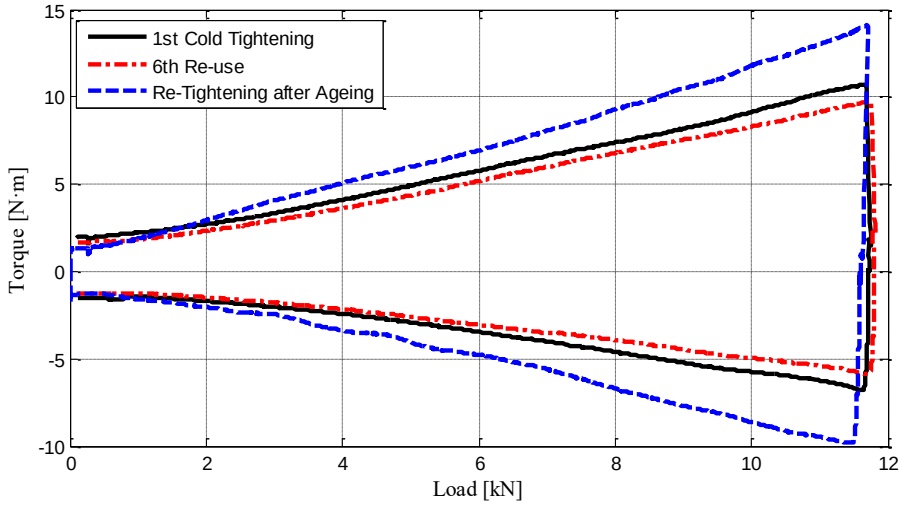

Figure 3.22: Pre- and Post-Heat Treatment Load vs Torque Curve

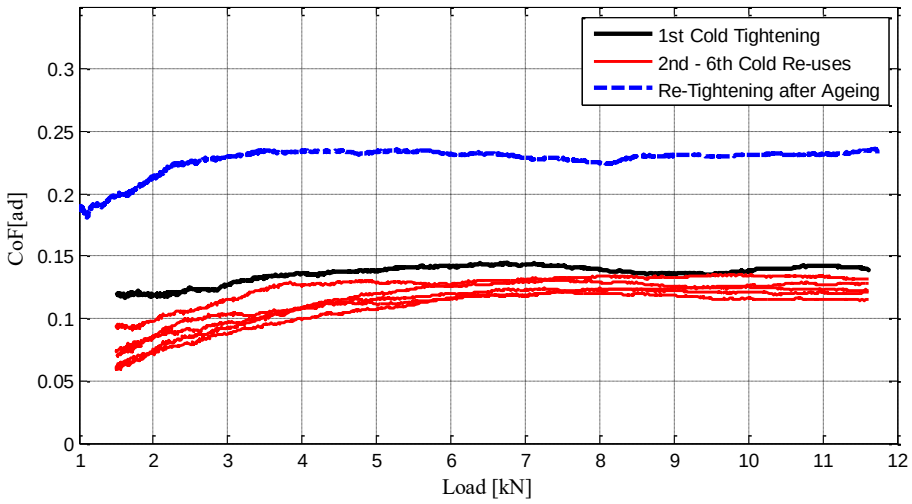

Figure 3.23: Pre- and Post-Heat Treatment CoF Curve

3.4 DISCUSSION

The self-locking torque was found to vary over the six repeats, and also follows a sinusoidal pattern as previously presented in Figure 3.16.

The self-locking torque during the first tightening process is higher than all other repeats, but where the same sinusoidal pattern is observed throughout. The reasons for this behaviour were thought to be the silver removal from the nut threads and the deformation of the elliptical nut chimney as further discussed in this section.
In this section the tightening speed will be also investigated, in order to assess the speed influence in the CoF during the screwing. Additionally the hardness of the coating will be analysed in both condition, pre and post ageing in order to assess the temperature effect to the silver coating, as a possible cause of the friction behaviour.

3.4.1 *Locking Torque Variation & Silver Removal*

The stripping process was analysed through an engagement test. Five different joints were assembled at different engagement lengths, with the number of bolt threads protruding from the chimney varying from zero to four, with no clamping load applied. Thereafter, the joints were cut using an EDM technique, and the silver removal assessed.

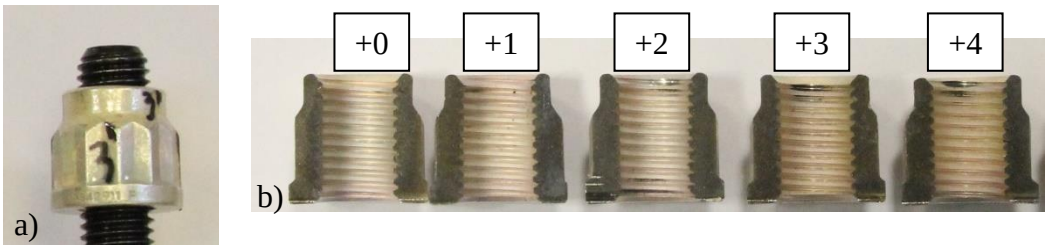

Figure 3.24: Engagement Test

As shown in Figure 3.24, the silver starts to strip from the first wind-on, particularly in the crimped section of the nut, and deteriorates further during continued winding. Obviously, this process is accelerated when the load is applied and with multiple tightening cycles. This change may effect friction in two ways. Firstly, removal of silver promotes a like on like couple increasing friction. However, silver removal increases clearance reducing contact and the locking torque. While sufficient silver is present globally and mobile with the nut, the latter effect is likely to dominate.
Additionally, the external diameters of the elliptical section of the nut were measured during the 6 cycle test, as shown in Table 3.3.

	Min dia [mm]	MAX DIA [mm]
Before 1st screwing	8.48	8.74
Clamped 1st	8.60	8.70
Before 2nd	8.55	8.72
Clamped 2nd	8.60	8.70
Before 3rd	8.55	8.73
Clamped 3rd	8.59	8.71
Before 4th	8.54	8.73

Table 3.3: External Diameter during the Test

As shown in Table 3.3, diametral change in the nut is observed from the first cycle. The minimum diameter in particular, in the first cycle deforms, and then does so elastically during the following cycles. Thus, the crimp section changes, along with the silver being partially removed, as seen in Figure 3.24, are thought to have caused the self-locking torque to reduce during the cycles. An additional analysis of the contact between the mating threads is therefore necessary to fully understand this effect and will be presented in Chapter 4, where the contact mechanics will be further analysed using the FEA.

3.4.2 *Self-Locking Torque Pattern*

As discussed, it has been observed that for the elliptically crimped nuts, the locking torque recorded has a sinusoidal pattern as the fastener is assembled (Figure 3.11 and Figure 3.16). As the bolt thread is continuous in form, it is unclear why this occurs, therefore a series of measurements were performed on the thread using the apparatus shown in Figure 3.25. As shown in the figure, a threaded upper plate (0.25” UNF) rests on the bolt, connected to a digital indicator with an accuracy of 1 μm. The plate is free to move, and can be used to measure changes in the bolt diameter as it is rotated.

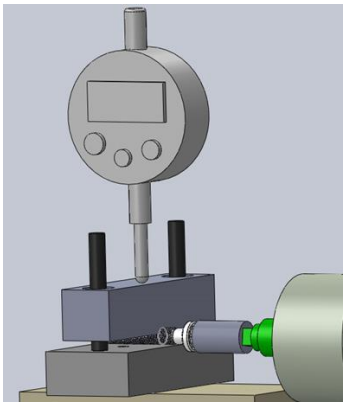

Figure 3.25: Diameter Test Device

Five bolts were tested, with each showing almost the same result, approximately 40-50 µm between the minimum and the maximum diameter recorded, with peaks of 60 µm. This difference is permitted within the tolerance of the bolt, and likely due to the process through which the threads are rolled. However, as schematically demonstrated by Figure 3.26, as the oval bolt interacts with the crimped section of the nut, high forces will be generated twice per revolution, resulting in the observed self-locking torque variation and the sinusoidal pattern.

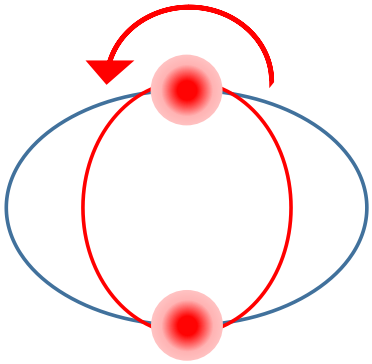

Figure 3.26: Oval Bolt and Crimp Interaction

3.4.3 ***Speed Dependency***

The speed used during the experimental test previously described was set at 3 rpm during wind on and wind off, and at 0.5 rpm during the final tightening and untightening. This speed was chosen in order to more accurately reach the required clamping load, and avoid any damage to the test rig, particularly to the load cell. In reality however, during engine assemblies wind-on speeds could reach 100 rpm (Rolls Royce 2015). Thus, further analysis is required in order to investigate the effect of the

tightening speed and the applicability of the test performed. As stated by 'Standard RRES90027', wind-on and tightening speeds for self-locking nuts are lower than those used for standard nuts, where speeds as low as 20 rpm may be required and must be specified in the assembly instruction. Thus, joints were tested at different speeds, up to 32 rpm. The same joint was tightened at 0.5 rpm, in order to accurately reach the required clamping load, and untightened at different speed, doubling it every two un-tightenings. After each speed increase, a tightening cycle at 0.5 rpm was performed, in order to observe any friction change, due to potential damage of the silver coating. Thus, the speeds tested were 0.5, 1, 2, 4, 8, 16, 32 rpm, and the recorded torque and load have been plotted in Figure 3.27.

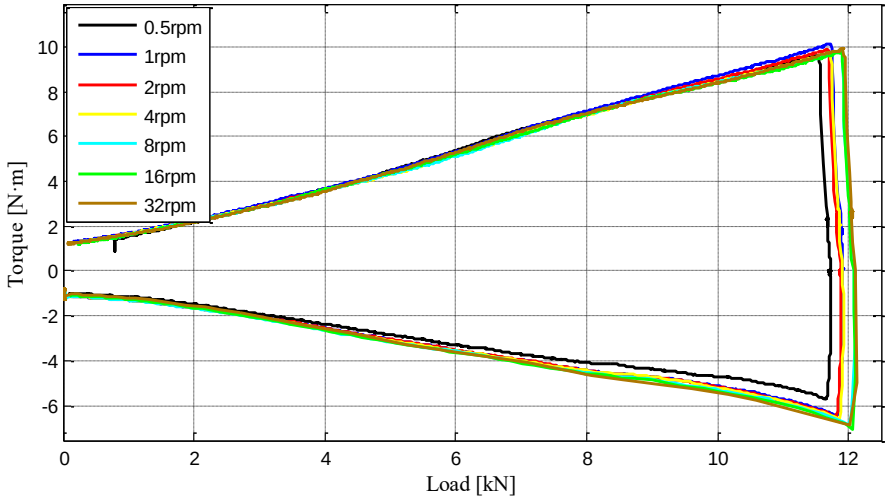

Figure 3.27: Speed Dependency Test: Torque against Load

As shown in Figure 3.27, during the tightenings, at 0.5 rpm, no difference was observed, proving once again the high repeatability and interestingly the limited impact of silver removal. However, during the un-tightenings at different speeds, a torque increase was noticed. In order to further analyse the data, the CoF was plotted against the clamping force (Figure 3.28).

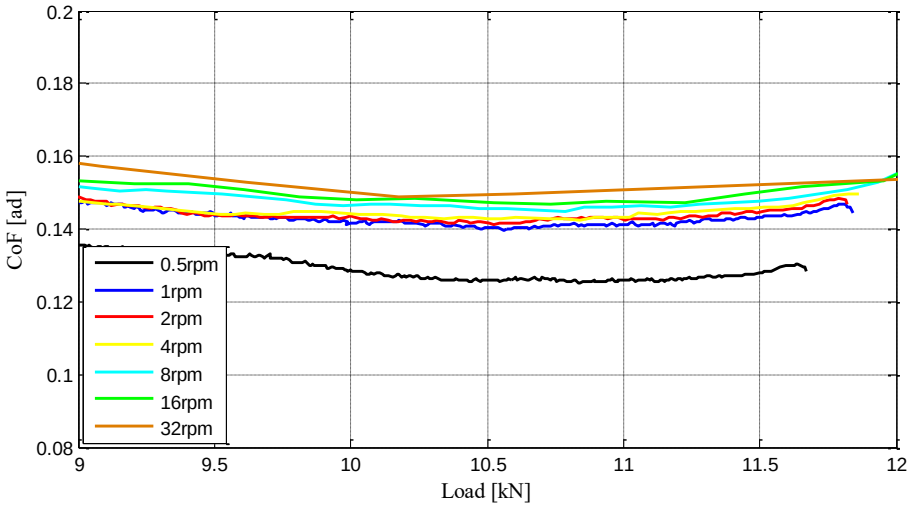

Figure 3.28: Speed Dependency Test: CoF against Load

As shown in Figure 3.28, a significant increase in the CoF was found, particularly in the first two speed increases (1 and 2 rpm). In order to numerically evaluate the increase in CoF as a function of the untightening speed, the friction during untightening was normalised using the datum CoF calculated at end load during the preceding 0.5 rpm tightening, as plotted in Figure 3.29.

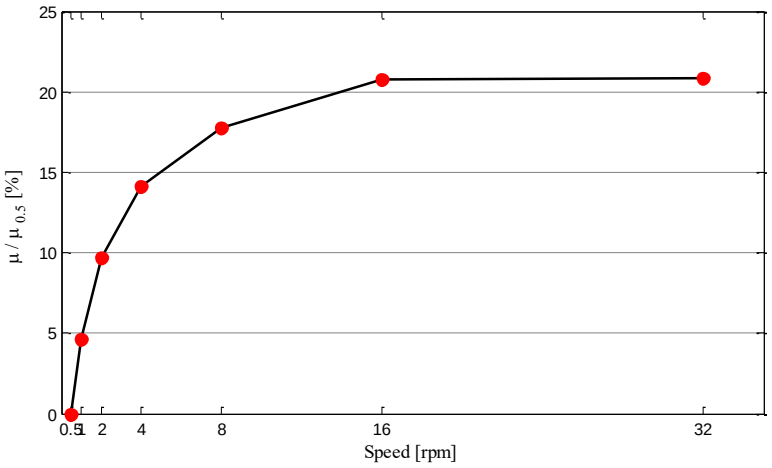

Figure 3.29: Increase of CoF against Untightening Speed

As shown in Figure 3.29, the CoF rapidly increases until 8 rpm, after which a more gentle increase is observed. The same test was done with and without the thrust bearing between the bearing surfaces, showing similar increases in the CoF in the threads and the bearing friction. The increase of CoF was expected, as seen in the literature. In fact, Arnell et al (Arnell & Soliman 1978) found an increase in CoF along

with the sliding speed using different soft coatings such as silver, indium and lead, at different thicknesses. Furthermore, Zou (Zou et al. 2007), analysed the CoF in the threads in the presence of solid lubricants, showing a speed dependency until 5 rpm in fine thread fasteners, in a range of speed between 1 and 100 rpm. Yang (Yang et al. 2003), in sliding tests from 20 to 1,000 mm/s, found an increase in CoF with sliding speed, as the formation of the transfer layer acting as a solid lubricant is affected by the speed, as well as the contact pressure, as will be seen in Chapter 4.

3.4.4 *Nano-Hardness Test*

As previously shown in Section 3.3.4, during the ageing process the frictional behaviour of silver changes, with an increase recorded. To further analyse the effect of ageing on the properties of the coating, a Hysitron Triboscope TS70, capable of a maximum load of 10 mN and maximum roughness of 3.5 µm, was used to measure the hardness both pre- and post-ageing. The measurements were taken on the flat bearing surface of the nut, as the geometry of the threads was found to be impractical. The pre-aged samples were polished with a 0.25 micron diamond suspension for 2 minutes before the first test, with a resulting roughness of 500-800 N·m (Figure 3.30a), and a coating thickness of 5.5-7 µm. With a Berkovic indenter (Fischer-Cripps 2011), a 10 cycle partial loading and unloading test was undertaken, with a maximum load of 10 N. Three locations on the sample were analysed, using a 3 by 3 matrix in a 50 µm square scan area. The same measurements and test were undertaken on the aged samples. While the thickness of the coating was found to be almost the same, the roughness was higher at 3-4 µm (Figure 3.30b).

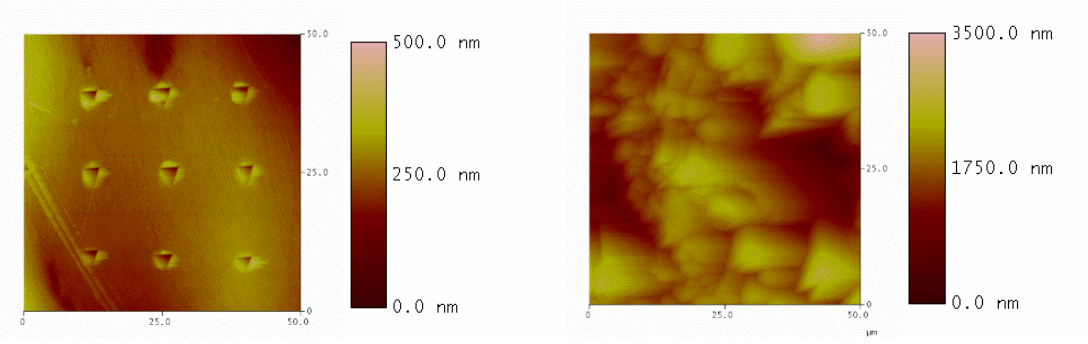

Figure 3.30: Comparison between pre-aged (a) and post-aged (b) silver coating

The hardness of the coated nut pre and post-ageing, automatically measured by the instrument from the partial unloading curve, was plotted and compared (Figure 3.31).

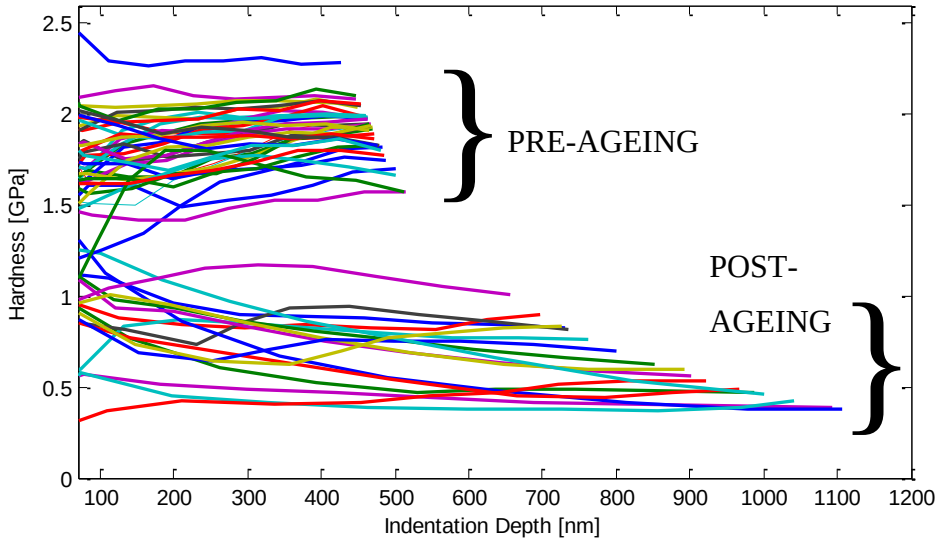

Figure 3.31: Silver hardness pre- and post-ageing

As shown in Figure 3.31 the hardness of the pre-aged sample is between 1.4 and 2.3 GPa, while the hardness of the post aged sample is lower, from 0.5 to 1.2 GPa. This result clearly indicates that the ageing process anneals the silver, leaving it susceptible to removal at lower contact pressures. In order to further explore this effect, split nuts were compared from the cold re-use test (Figure 3.32a) and in the aged condition post-unscrewing (Figure 3.32b). As shown in the Figures, a significant amount of silver was removed post-ageing, as evidenced by the dark appearance in many places of the threads. As a consequence of the severe damage to the silver coating, an increase in the CoF is expected, as the contact becomes chemically similar to a like on like couple. Similar behaviour has also been explored by Roberts et al. (Roberts et al. 1997), where softening and annealing of silver were considered in pin on disc tests. Additionally in tests at elevated temperature, the study also found no significant difference between tests in air and nitrogen atmospheres. This further highlights the oxidation resistance of silver coatings, and supports the authors' hypothesis that the observed effect was annealing related.

Figure 3.32: Sectioned silver nut (a) after cold use test and (b) after post-ageing test.

3.5 SUMMARY

The analysis of the silver coating behaviour in aerospace fasteners can be summarised as follows:

- The CoF in the threads in a silver coated joint was analysed during tightening, highlighting a dependency on the clamping load. However, the coefficient of fiction was found to be consistent, which is fundamental in order to estimate the torque required to reach the end load. Additionally, an overall low CoF of 0.125 was observed at room temperature.
- The silver coated joints were investigated after a thermal cycle at 760 ºC, as typical of engine operating conditions. The thermal ageing was found to effect the silver coating properties, leading to a significant increase in the CoF from 0.125 to 0.24 and a significant silver removal and transfer to the nearby parts.
- The nano-hardness test showed annealing of the silver coating with thermal ageing, resulting in easier removal of the silver coating. Therefore, the resulting contact between the bolt and nut threads becomes similar to a like on like couple, producing a rise in CoF.
- The tests developed within this chapter have enabled full investigation of silver coating properties within the context of this application. Thus, the test presented, such as the cold test, the thermal test and the nano-hardness test, can be used to investigate different coatings. In fact, in Chapter 5 different coatings will be analysed using the presented methods, in order to identify a replacement for the silver coating.

- The CoF was analysed at different speeds, showing a significant rise with speed increase, in line with previous studies. Thus, a strict assembly procedure should be carried out during engine assembly, using a specific speed, as identified when evaluating the tightening torque required to reach the peak load.

CHAPTER 4

FINITE ELEMENT MODELLING

4.1 INTRODUCTION

In Chapter 3, the silver coated nuts were tested using a newly developed platform, analysing the frictional properties at room temperature and after a thermal cycle. The tightening process for a bolted joint is generally analysed by measuring torque and clamping force directly, and calculating contact pressure and thread friction afterwards. These calculations rely on many assumptions and approximations, and for a given load yield a single value of CoF, assumed to apply uniformly at all contact sites.

In fact, previous work (Yang et al. 2003), has shown that silver has pressure dependent frictional properties, and it is widely known (Juvinall & Marshek 2006), that the pressure in a joint is not constant, varying throughout the tightening process, and also within the joint along the threads in contact. Additionally, this effect is further accentuated when a crimp is used, as clearly seen in Section 3.4, where the silver removal shows a non-uniform pressure distribution. Thus in this chapter, the crimped joint geometry along with the complete tightening process is dynamically modelled using FEA techniques. The joint is modelled in 3D using the FEA solver Simulia Abaqus 6.13, with pre and post-processing through Altair Hyperworks (Altair 2013b) (including Hypermesh and Hyperview), application of the crimp feature to the nut, the initial wind-on of the crimped nut, along with the subsequent tightening cycle are investigated, using the materials and frictional properties of the joint parts in order to fully represent the process.

The aim of this work is to investigate the contact of the mating threads, in the presence of a self-locking feature and a thin silver coating. Through this approach the contact pressure at the threads during both the wind on and during clamping, along with the overall CoF developed at these contacts can be investigated. Additionally, the FEA model will be a useful tool to investigate new self-locking joint designs in order to reduce the local contact pressures and decreasing the coating damage.

4.2 MODELLING APPROACH

Bolted joints have been widely investigated over the past century as previously described in Chapter 2, using both experimental and FEA approaches. Mackerle (Mackerle 2003) in his bibliography summarised the previous studies regarding the analysis of bolted joints through 2D and 3D FEA approaches. In this case a 3D study was undertaken in order to consider the effect of the helix and the asymmetric crimp in the nut chimney on the thread contacts. This analysis will yield local contact pressures in the screwing process, something that it is not possible to accurately determine from the experimental tests previously performed.

As previously explained in Section 2.2.4, studies involving 2D axisymmetric models and a non-threaded 3D model have previously been undertaken in order to analyse the mechanical behaviour of fasteners. Static models were preferred in these cases in order to analyse stresses and elongation along the joint, as dynamic analyses have significantly longer solution times. Fukuoka et al. (Fukuoka et al. 2006) analysed the effects of the thread helix on the root stresses along a fastener, demonstrating that the maximum stress occurs at half a thread pitch from the surface loaded by the nut, gradually decreasing towards the top face of the nut. Additionally, Yang et al. (Yang et al. 2013) showed the load distribution along the threads, as well as the stresses and the deformation along multiple joints for fine and coarse fasteners. In particular, this study highlighted the advantages of using a 3D geometry when considering the effect of helix dimensions.

The approaches undertaken in the highlighted studies, do not enable the complex interaction between the bolt and the self-locking nut to be fully investigated during the tightening process. Therefore in this study a full 3D dynamic FEA model was created, inclusive of the self-locking feature. The tightening of the joint is then simulated over eight revolutions, with interface friction included as a contact pressure dependent property. As in the previous studies, Simulia Abaqus was chosen as the FEA solver. This package is commercially available, and offers high precision when solving contact problems. However, as in all modelling approaches limitations exist. In this case, the thickness of the silver coating is five microns and has not been included in the model, as interactions between this layer and the substrate were too complex to include, particularly when considering the potential for material transfer. However, the frictional behaviour of this layer was still included in the model through

consideration of the CoF. Silver coatings are of low hardness and shear yield strength. In particular their friction response was identified to transition from asperity friction at low loads, through to bulk shearing as load is increased (Holmberg & Matthews 2009). Therefore, the CoF of the coating as a function of contact pressure has been studied using a pin on disc test, and the resulting relationship used as an input in the FEA model. Similarly, whilst the parts were accurately drawn with respect to their specified geometry (The Society of British Aerospace Companies Ltd 2004), the surfaces are assumed to be perfectly round and smooth. Therefore the issue of bolt roundness previously investigated in Section 3.4.2, and the surface roughness have not been considered in the analysis. Additionally, thermal effects as a result of high tightening speed, and their potential impact on the frictional properties of silver have not been considered here, as experiments have previously been performed at low speed. Finally, fillets and chamfers in both the nut and bolt modelled were simplified to reduce the solving time.

4.3 PIN ON DISC TEST

Due to the absence of previous studies regarding the CoF for thin silver coatings on Waspaloy as a function of contact pressure, a pin on disc test machine (Figure 4.1) was used to characterise this relationship.

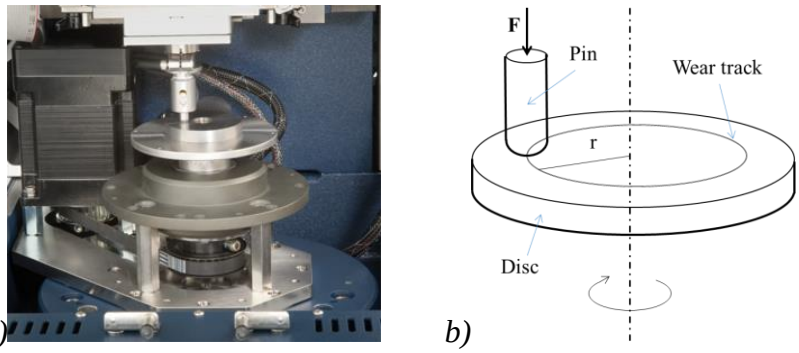

a) *b)*

Figure 4.1: a) The Pin on Disc Machine and b) Simplification of the Test Feature

4.3.1 *Test Procedure*

Known also as a ball on flat test, a disc rotates while a ball is normally loaded against it. Five mild steel discs, 70 mm in diameter and 6.5 mm thick, were silver coated by the same method and to the same thickness as the nuts, resulting in a coating thickness of approximately 6 μm. Balls, a ¼" (6.35 mm) in diameter, made from Inconel 625 (an alloy with analogous mechanical properties to Waspaloy) were used as the pin.

The Poisson's ratio of the coating was estimated to be annealed silver, 0.37, and the Young Modulus of the disc was found through a nano-indentation test that gave an average value of 99.5 GPa. The Inconel used had a Young's Modulus of 205.8 GPa and Poisson's ratio of 0.312 (provided by the manufacturer), as summarized in Table 4.1.

Part	**Material**	**Young's Mod. [MPa]**	**Poisson's Modulus**
Disc	Steel (silver coated)	99,500	0.37
Pin	Inconel 625	205,800	0.312

Table 4.1 Material Properties

The machine was set-up to measure the tangential force, changing the applied normal force step by step. The speed was pre-programmed, and the machine recorded force, speed and CoF as a function of time, and stored it as a text file. Using different load cells, the CoF was examined on a pressure range from 40 to 1,500 MPa. Three load cells of measurement limits of 0.5 N, 50 N and 200 N respectively were used. For each load case, the disc rotates for two revolutions at the same contact radius. In this way, the CoF is recorded both for a first loading as well as on a used track, simulating the second re-use of the joint. Afterward the ball was moved 0.5 mm radially outward to unused material, and the normal load increased. The linear speed was maintained as a constant during the whole test at 10 mm/min, similar to the relative speed observed in the screwing process. The entire test was executed in lubricated conditions, applying Mobil Jet Oil II, to represent the oil typically used in the aerospace application and in the tightening experiment.

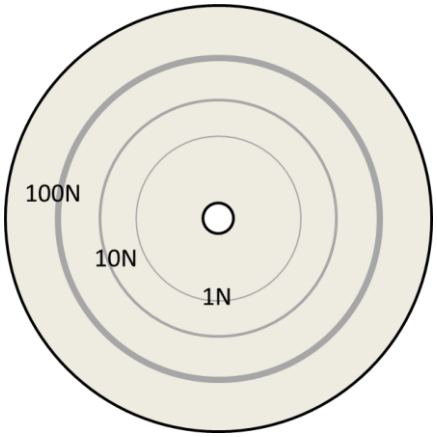

Figure 4.2: Different Tracks in the Disc Sample.

A Hertzian contact analysis was performed to estimate the contact pressure, p_{max} , for the contact between the ball and flat (infinite radius), with elastic contact conditions assumed (Williams & Dwyer-Joyce 2000):

$$a = \sqrt[3]{\frac{3}{4} F R_{ball} \left(\frac{1 - \nu_1^2}{E_1} + \frac{1 - \nu_2^2}{E_2} \right)} \tag{4.1}$$

$$p_{max} = \frac{3}{2} \frac{F}{A} = \frac{3}{2} \frac{F}{\pi a^2} \tag{4.2}$$

where *a* is the radius of the contact area, *E* and ν are respectively the Young modulus and the Poisson's ratio of the ball *(E_1* and *ν_1)* and the disc *(E_2* and *ν_2)*, and *F* is the normal force applied. The CoF was measured at different pressures, from 20 MPa to 1,500 MPa, in order to fully characterise this relationship. The load required was calculated using the previously defined equations for every pressure step of 10 MPa, from 20 to 250 MPa, or 25 MPa, from 250 to 1,500 MPa. Additionally, the contact width is measured through a digital microscope, in order to identify any potential difference from the Hertzian estimation to the actual pressure.

4.3.2 ***Results***

The measured CoF, calculated as the tangential force divided by the normal force, has been plotted against the Hertzian pressure.

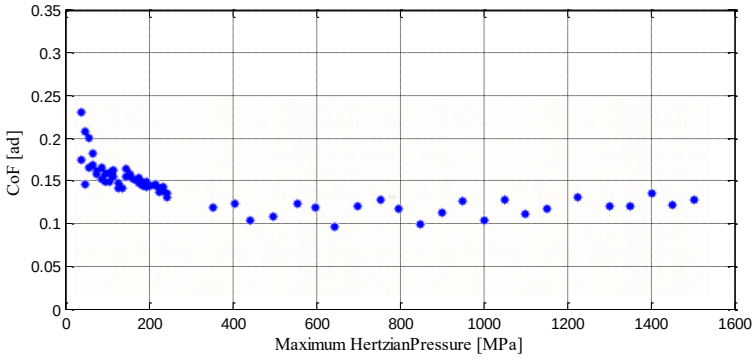

Figure 4.3: CoF against Hertzian Pressure

In order to further investigate the result, the contact width was measured using an optical microscope, showing a divergence from the elastic theory presented.

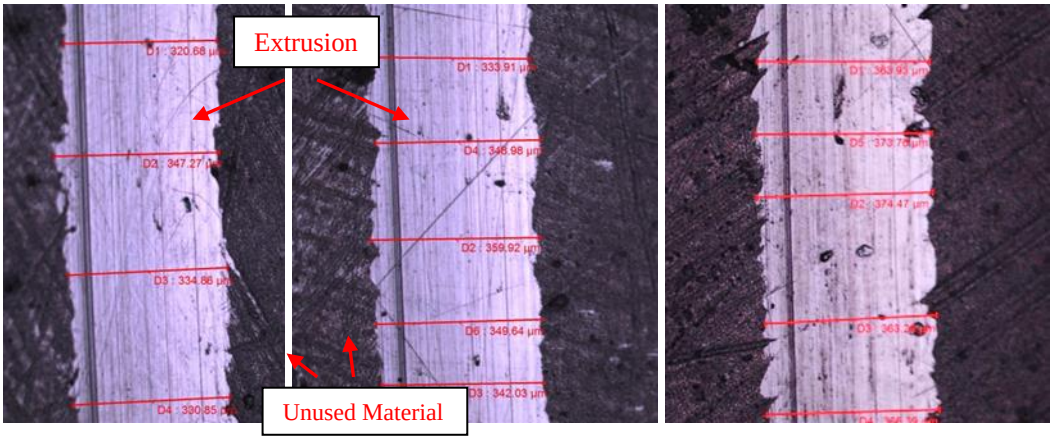

Figure 4.4: Area of Contact at 101N (a), 91N (b), 82N (c).

The measured radius of contact, obtained as half of the contact width, shown in Figure 4.4, was compared with the Hertzian theory, plotting the applied load against the radius of contact.

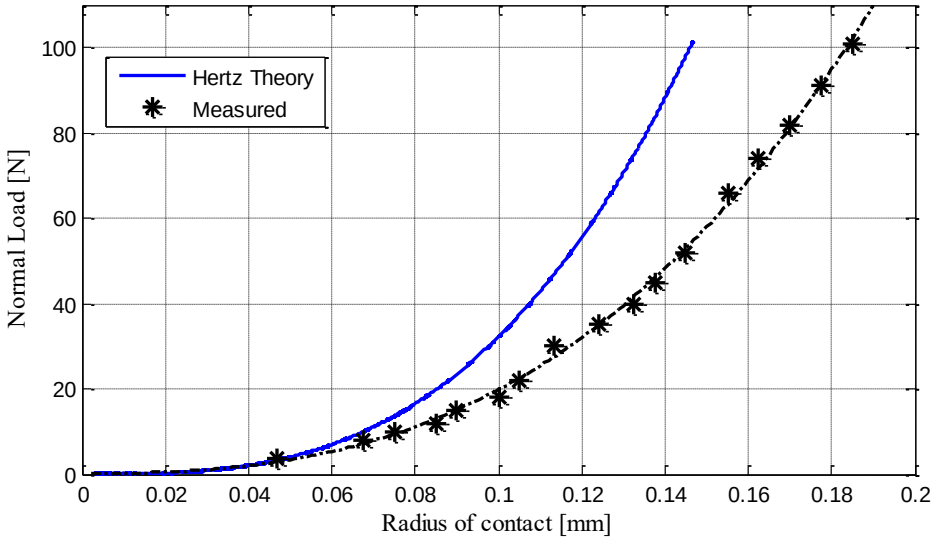

Figure 4.5: Comparison between the Measured Radius of Contact and the Hertz Theory

As indicated in Figure 4.5, the measured radius is considerably bigger than the estimated one, implying the contact pressure to be smaller. Thus, at high pressure, with a soft coating of 6 μm, the assumption of elastic behaviour was found to be inaccurate. This behaviour has been already analysed in the literature, such as Kogut et al (Kogut & Etsion 2002), who analysed the elastic-plastic contact of a sphere on a flat surface and E.D. Reedy (Reedy 2006), who investigated the contact on a thin coating, demonstrating that the contact changes with the square root of the normal load, instead of the power law relationship (two thirds) in the Hertzian theory. Hence,

as the area and the load applied are known, in line with the Hertzian theory, the contact pressure was estimated as the load divided by the area. Finally, the CoF has been plotted against the estimated pressure (Figure 4.6).

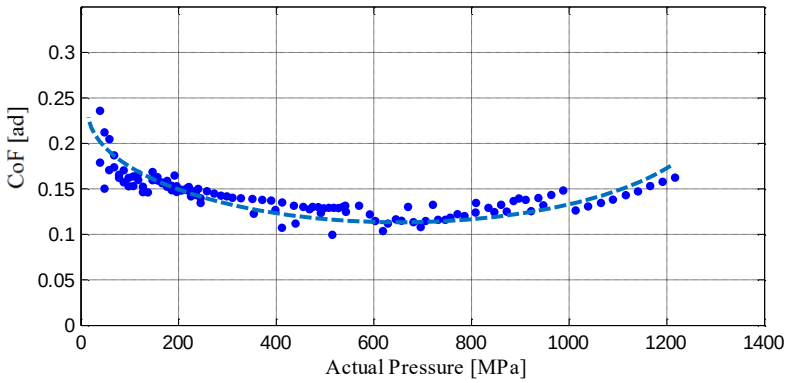

Figure 4.6: CoF against the Actual Contact Pressure.

The graph in Figure 4.6 shows the dependence of the CoF on the contact pressure, showing an initial decrease in friction with pressure, followed by a gradual increase. The result from the pin on disc test was also similar to that observed by Yang et al. (Yang et al. 2003), which analysed the tribological behaviour of the silver coating in a pin on disc test in a pressure range of 100-1,000 MPa, highlighting the wear and friction dependency on pressure.

The variation in CoF with respect to the pressure can be explained by considering the silver behaviour in the contact. In fact, the above experiment has shown the tribological behaviour of the coating, highlighting three different situations. At the beginning, an initial adhesion was found as the silver is intact, followed by shearing when the silver is bright, and progressive damage when silver is removed, as shown in Figure 4.7. Furthermore, it was noted that silver gives the lowest frictional resistance when shearing.

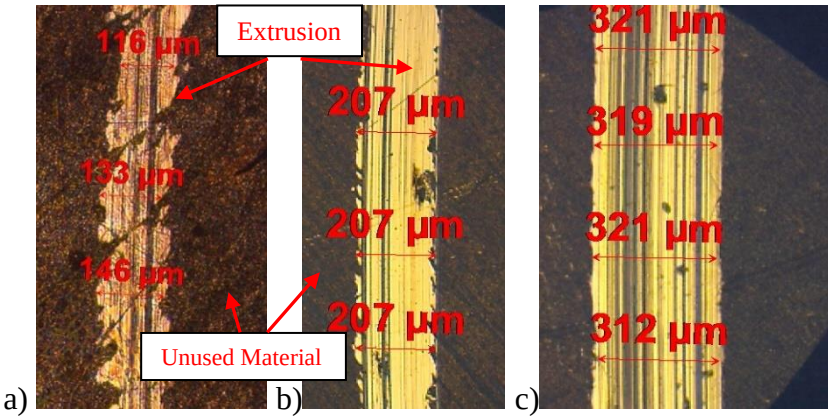

Figure 4.7: Silver Mechanism a) 450 MPa, b) 635 MPa c) 875 MPa

Additionally, the CoF obtained in the first revolution and in the second revolution have been compared, and plotted along with the contact pressure (Figure 4.8).

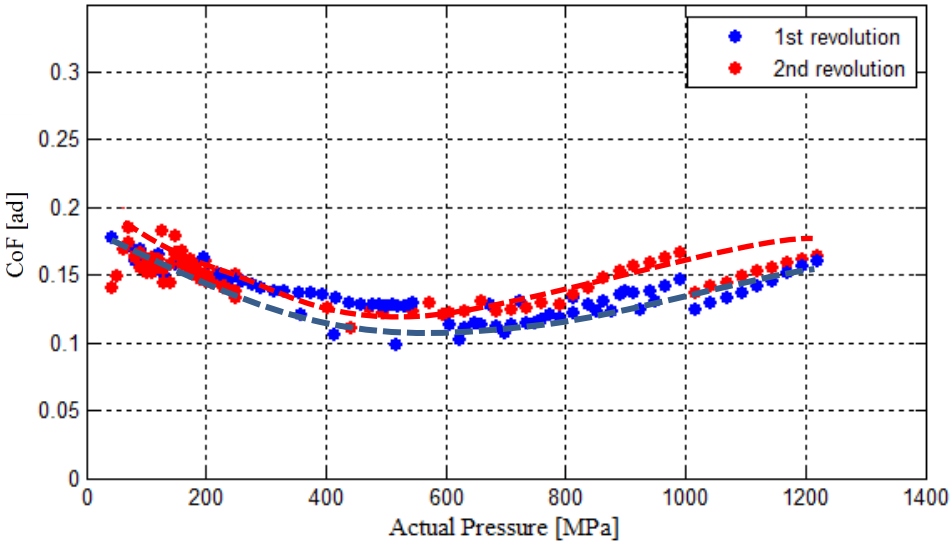

Figure 4.8: CoF versus Contact Pressure, as Result of the Pin on Disc Test.

As shown in Figure 4.8, the second re-use at low pressure showed an analogous CoF with respect of the first. However, at pressures above 700 MPa, the CoF in the second revolution is higher than the first revolution, due to damage of the coating. Additionally, the spike experienced at 800-1,000 MPa was due to the Inconel ball being overused and slightly damaged, while at 1,000 MPa a new ball was used. As highlighted in previous studies (Holmberg & Matthews 2009), this behaviour is typical of soft thin coatings, which are susceptible to high levels of deformation, leading to the substrate properties affecting the CoF.

4.4 FEA MODEL DEVELOPMENT

4.4.1 *Geometric Model*

The parts were drawn with the 3D software Solidworks 2012 using the appropriate joint dimensions, with simplifications applied to the geometry by deleting fillet radii and chamfers, as these were deemed to be inconsequential with respect to the model, as detailed previously.

The assembly is made of three components: the bolt (AS48824), the nut (AS49211F) and the load cell. The ¼" (6.35 mm) diameter bolt and nut are 10 and 35 mm long respectively, with a UNJF thread shape. To facilitate the solver, the 12-point bolt head was simplified as detailed in the previous section, while in the case of the nut all dimensions were considered. The steel load cell used to measure the clamping force in the joint (Section 3.2.1) has also been modelled, and has the form of a thick washer with a ¼" (6.35 mm) diameter hole in the middle and an outer diameter of 37 mm (LTH350 compressive sensor manufactured by FUTEK). Furthermore, the washer used in the experiments, also made from steel, was not modelled in the FEA, but its thickness taken into account into the load cell. Figure 4.9 shows a diagram of the completed model.

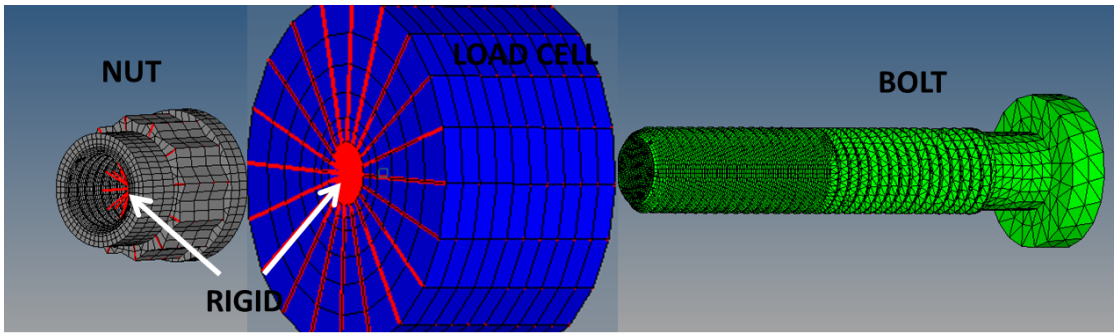

Figure 4.9: The Main Parts of the FEA Model.

4.4.2 *Elements, Boundary Conditions and Mesh Generation*

Altair Hypermesh 11 (Altair 2013a) was used as a FEA pre-processor, to make and handle the mesh, and also to apply load, boundary conditions and material properties. 3DS Abaqus 6.12 was used as the solver, importing the Hypermesh output file and generating a resulting file that can be read by Altair Hyperview, used for post-processing.

A refinement procedure was also performed to locally re-mesh the areas of interest. One of the key parameter of the analysis is the contact pressure in the threads surface, thus the contact between a slice of the nut and a slice of the bolt was analysed at different element sizes as shown in Figure 4.11, where the nut section is pushed against the bolt section, applying a radial displacement.

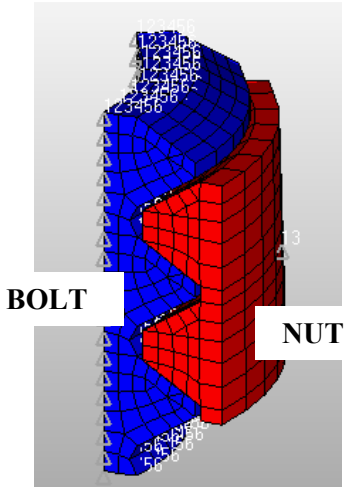

Figure 4.10: Mesh Refinement Model

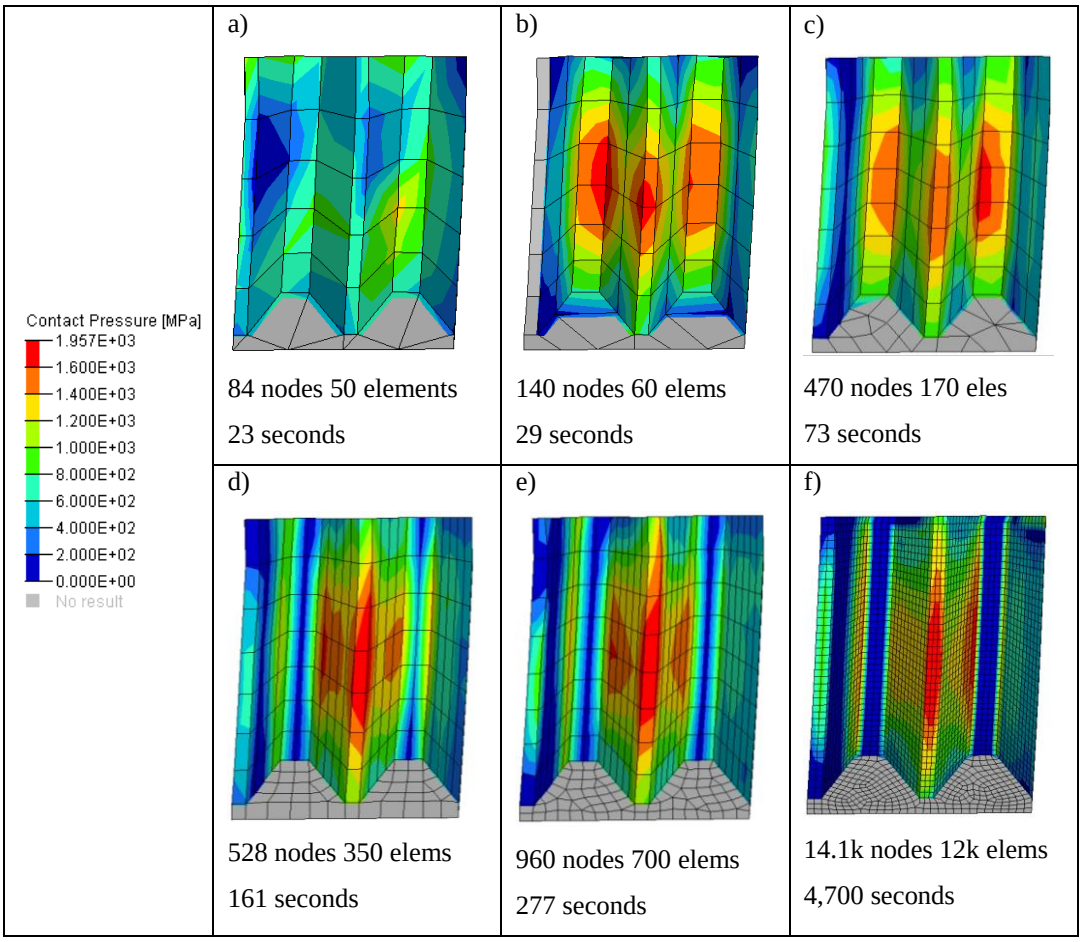

Figure 4.11: Mesh Refinement Procedure

As shown in Figure 4.11, the contact pressures for a portion of the joint threads were compared using different mesh sizes. The mesh used in this work, shown in Figure 4.11d was found to be an acceptable compromise between the pressure distribution and the solving time, being one week necessary using this method (30 weeks in the case of the example f). The volumes surrounding the areas in contact, were meshed using first order brick elements (hexa). These elements offer increased accuracy, while the rest of the model is maintained with larger elements such as tetra and pyramid elements, to improve the solution efficiency. Bolt, nut and load cell have 56k, 30k, 1.5k nodes and 158k, 75.5k, 1.2k elements respectively giving a total of 87,500 elements and 235,000 nodes for the completed model.

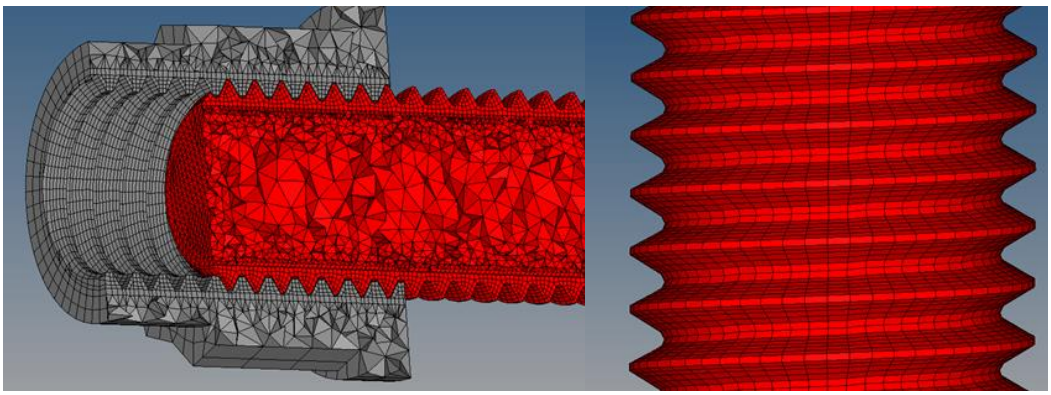

Figure 4.12: The Final Mesh.

Rigid elements, known as ‘spiders’, were used to apply boundary conditions. These elements allow displacements and rotations to be applied to the nodes the spider is connected to. For example, these elements were used to connect the external nodes of the nut to a centre node where the rotary displacement is applied. Six contact surfaces are included in the model in total, and were defined as CONTACT PAIR’s, using the Surface-to-Surface interaction function, reflecting proper contact between the bodies (ABAQUS 2013). In the contact between the threads on the nut and bolt, the nut surface was defined as SLAVE and the mating bolt surface as MASTER, in the master/slave rules, as the nut has a slightly finer mesh (ABAQUS 2013). The interaction used for this contact pair is hard pressure-overclosure, with a non-linear penalty also applied, allowing a small penetration between the surfaces in order to help the solving convergence. Furthermore, the bolt and the nut were positioned really close to each other, with a gap of 0.9 μm, and an adjustment of 1 μm was used to help the contact at the beginning of the simulation. The CoF at a given pressure between

contacting pairs is defined using the friction data from the pin on disc test (Figure 4.8), and was uploaded as a look-up table in the solver. Finally, the bearing surfaces of the bolt and nut, which are in contact with the load cell, were defined as frictionless, zeroing the torque to overcome the friction in the bearing surfaces. This assumption is acceptable when compared to the experimental study, as a bearing is used for these contacts, and bearing friction removed from test results during post-processing.

4.4.3 *Material Properties & Assumptions*

The bolt and the nut are made from Waspaloy, an age hardening austenitic nickel-based super-alloy, while the load cell material is Stainless Steel 17-4. As the load cell behaves elastically, the material specifications are only density (7,780 kg/m3), Poisson's ratio (0.27) and Young Modulus (197 GPa). As both bolt and nut undergo plastic deformation, Waspaloy was defined using the density (8,200 kg/m^3), the Poisson's ratio (0.29), the Young Modulus (231 GPa) along with the true stress true strain plastic curve, as presented in Figure 4.13 (ASM International 2002), and defined as isotropic hardening.

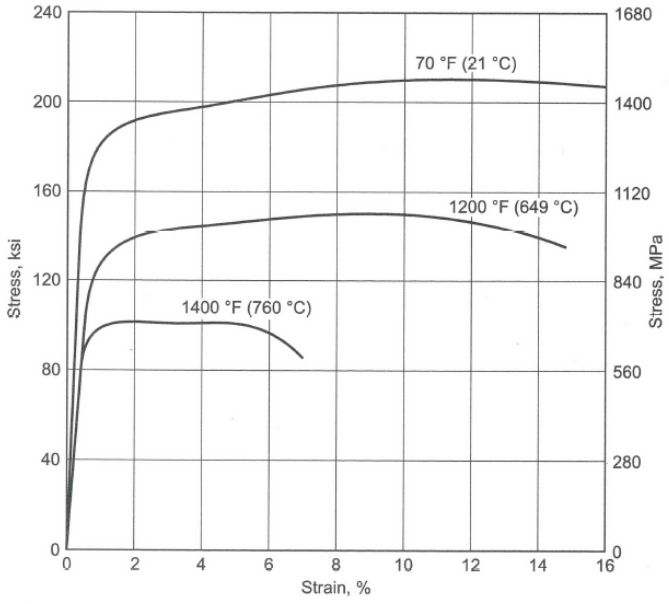

Figure 4.13 : Inconel 718(ASM International 2002).

Abaqus 6.13 Standard/Explicit was used as a solver, defining the analysis as dynamic, quasi-static, with effects due to temperature and speed not considered. The thermal effects have not been considered, as the screwing speed is relatively slow, meaning a significant temperature increase will not occur at the rubbing surfaces (ABAQUS 2013). Therefore, the increase in FEA solver time associated with the

inclusion of these parameters is not deemed worthwhile. The material properties used are summarised in Table 4.2.

Part	Material	Density [kg/m^3]	Young's Mod. [MPa]	Poisson's Modulus	Plastic behaviour
Load Cell	Waspaloy	7,780	197,000	0.27	Yes
Bolt /Nut	Stainless 17-4	8,200	213,000	0.29	No

Table 4.2 Material Properties

4.4.4 *Load Case & Solutions*

The analysis has three main steps: crimping, screwing and the final tightening of the joint. The first step involves applying the crimp, to re-produce the 0.35 mm squashing of the nut chimney, using displacement control instead of load. Practically, this is performed using a vice equipped with a micrometer (Section 3.2.2), while in the simulation a displacement of 0.175 mm was applied to 10 nodes in two opposite sides of the nut chimney. The bolt and the load cell do not take part in the first step, and they were suppressed.

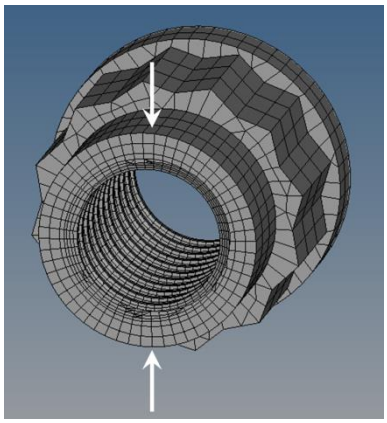

Figure 4.14 : The Boundary Conditions in the Crimping Step.

The second step is the screwing of the bolt through the crimped nut, in order to re-produce the wind on for eight revolutions prior to the application of the clamping force. In this step, the nut rotates on its axis for 50.3 radians, applying a rotational displacement to the spider attached, while the bolt head is fully constrained. Similarly, the load cell is free only in the axial direction. The resistance torque extrapolated from the centre node is the self-locking torque. As this step is generally solved in about 4,000 increments, in order to reduce the size of the output file and the writing time,

the output file is written at 5% intervals throughout this step, around every third revolution. Additionally, a restart file is required every 50 increments to avoid data loss.

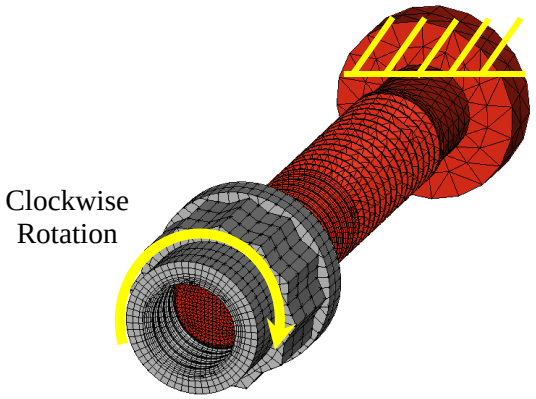

Figure 4.15: The Boundary Conditions during the Screwing and Tightening Steps.

The last step is the final tightening, where the bolt is tightened to the standard end load of 11.6 kN. The load cell and bolt are constrained as in the previous step, while the nut rotates only 2 radians. The output file is written every 1% of this step, every 0.02 radians (around 1.14º), as additional data points are needed at the post-processing stage. The clamping load was extrapolated summing the nodal force in the bearing surfaces for either the nut, the bolt or the load cell surfaces.

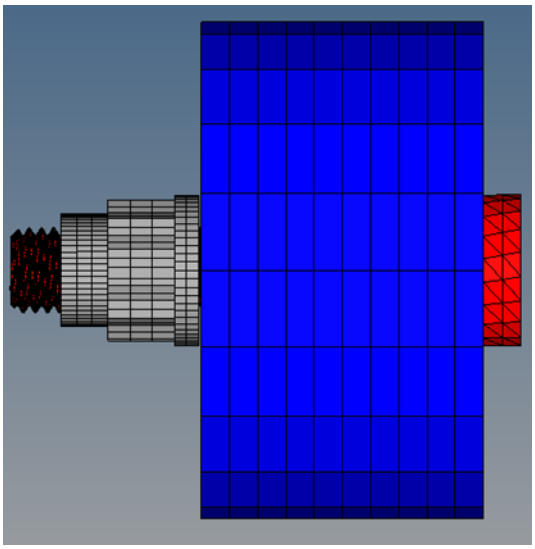

Figure 4.16: Final Output Clamping the Load Cell.

4.5 VALIDATION

The FEA has been validated using the experiment results (Figure 4.17), as the boundary conditions and geometries are the same. The torque required to tighten the

nut, the sum of the torque required to overcome the friction in the threads and the torque required to stretch the bolt, has been plotted along with the clamping load. The torque required to overcome the friction on the bearing surfaces has not been considered, because the interaction between the bearing surfaces was defined as frictionless in the FEA, and during the experiments the bearing torque was measured using the needle roller thrust bearing and subtracted (Section 3.2.3.1). In the model, the resistance torque was obtained from either the centre node of the rigid elements on the bolt or the centre node of the nut, while the clamping load was obtained by summing the nodal forces in the bearing surfaces.

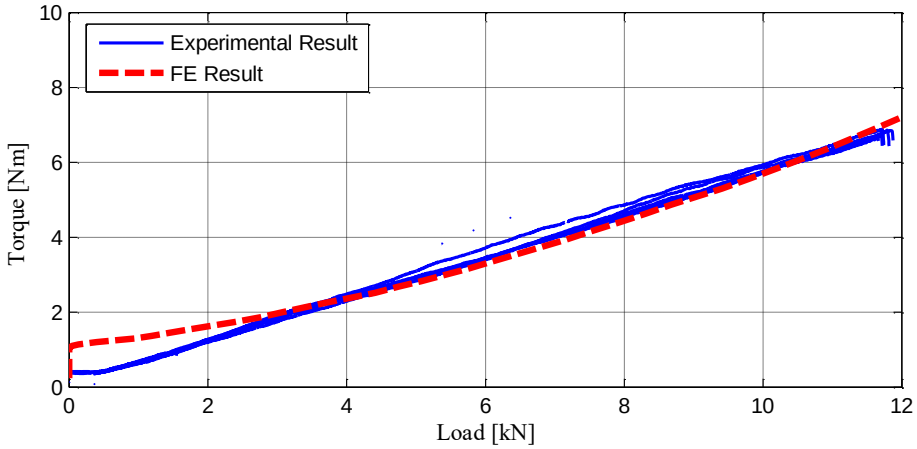

Figure 4.17: FEA and Experimental Results Compared: Load versus Torque.

Figure 4.17 compares the FEA result with a typical experimental result, showing similar curves. As shown, a significant variation occurs at the beginning of the plot, up to 3 kN, and is caused by a lack of accurate friction data from the pin on disc at the lowest contact pressures. In fact, a large number of nodes in the wind on process have a small contact pressure, where the pin on disc test is not able to achieve accurate results in this regime, due to the measurement accuracy of the load cell used. This point will be further explored in the following sections.

Furthermore, the surface roughness has been assumed negligible and is likely to have an increased effect on friction and therefore torque at this low load. However, overall the model appears satisfactory to investigate the contact conditions.

4.6 RESULTS

During the entire simulation stresses, pressure and deformation were recorded and analysed through Hyperview, the Altair postprocessor (Altair 2013b). In the first step

the nut chimney was squashed and ovalised. The displacement and the stresses have been graphically plotted (Figure 4.18a and Figure 4.18b). Von Mises stresses are shown when investigating the different components and load conditions, as they are an appropriate descriptor for an elastic-plastic stress state and are analogous to distortion energy.

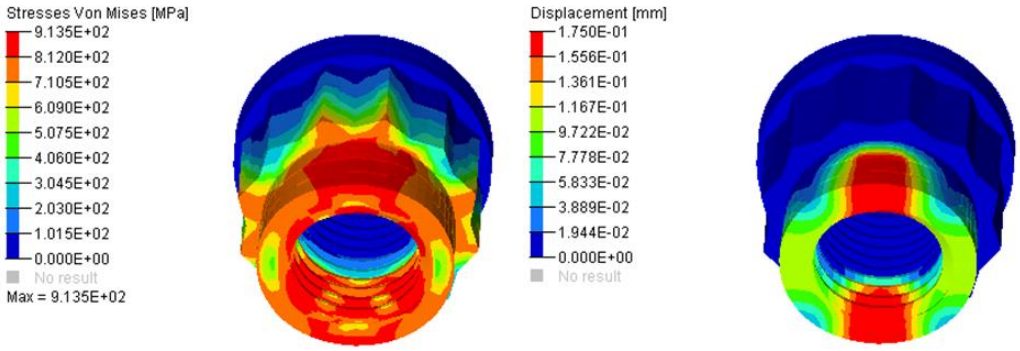

Figure 4.18: Von Mises Stresses (a) and Displacement (b) in the Nut after the First Step

Figure 4.18a and Figure 4.18b show the Von Mises stresses and the displacement at the end of the crimping step, showing the symmetric deformation of the nut, with a maximum displacement of 0.175 mm and a stress of 913 MPa in the nut chimney. During the second step the nut rotates into the constrained bolt. At the end of this step, the bearing surface of the nut is in the proximity of the load cell. At this point the clamping load is zero, as the joint has not yet clamped the load cell, and the resulting torque depends on the thread friction and is a consequence of the self-locking feature.

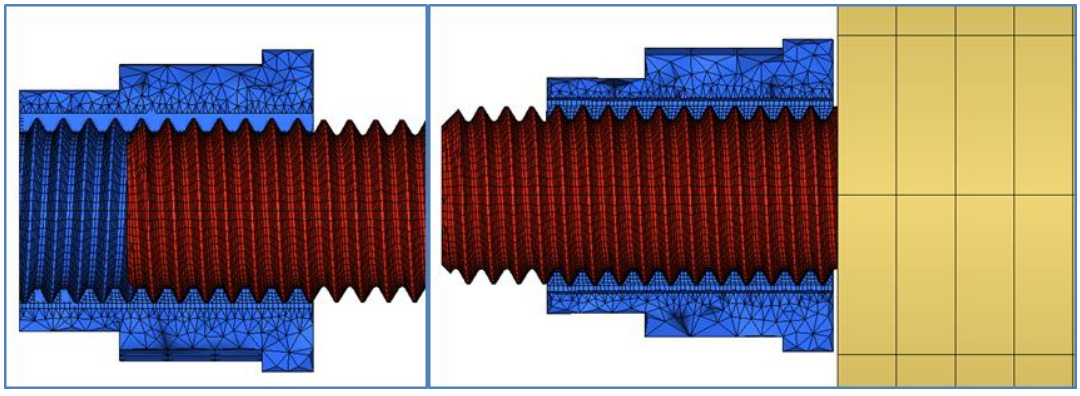

Figure 4.19: Nut Position at the Start and at the End of the Step with respect of the Engagement.

Figure 4.19 shows the position of the nut at the beginning and the end of this step. Obviously during the wind-on step, the bolt threads engage the crimp, which is plastically deformed.

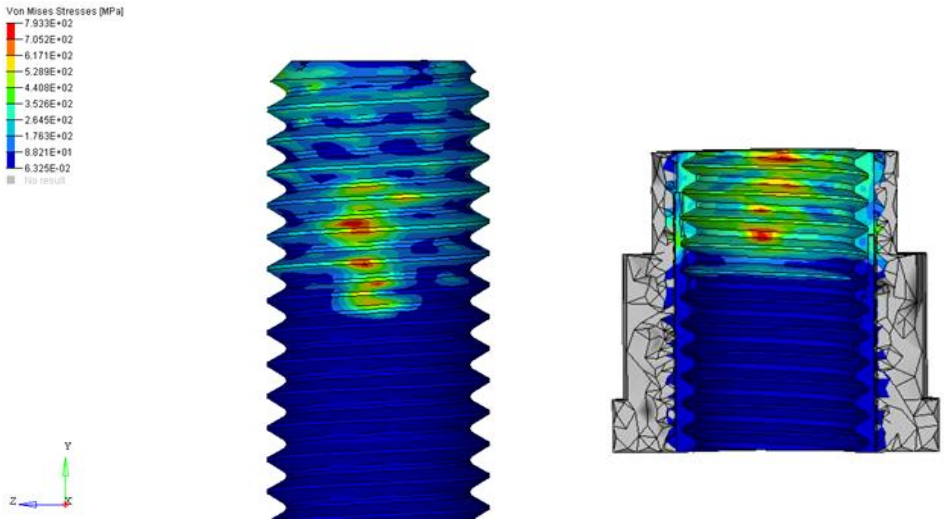

Figure 4.20: Von Mises Stresses in the Bolt (a) and in the Nut (b).

Figure 4.20 shows the maximum Von Mises stresses during the screwing step in the bolt (Figure 4.20a) and in the nut (Figure 4.20b), with a slightly higher stresses in the nut compared to the bolt, with maximum stresses of 850 and 800 MPa respectively for the two components. Furthermore, the stresses in the nut are concentrated in the crimp section, while the first threads are totally unstressed. The contact between the thread surfaces was analysed using the variable CPRESS, defined as the contact pressure at every node of the interface surfaces.

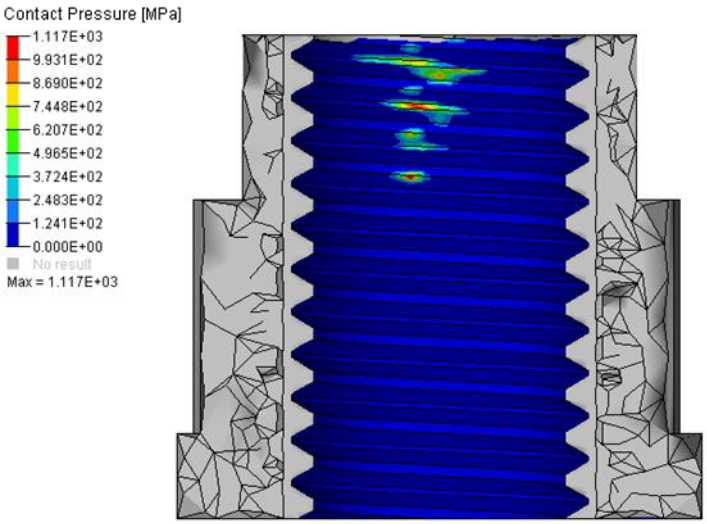

Figure 4.21: Contact Pressure along the Nut

As shown in Figure 4.21, contact only occurs during the wind on-step in the nut chimney, i.e. the crimped section. It is also interesting to note, that even at this early stage of the tightening process, that high contact pressures above 1 GPa were recorded.

During the tightening step the nut rotates into the bolt, clamping the load cell in between the two bodies. The clamping load, measured at the interface between the bearing surfaces has been plotted along with the resistance torque.

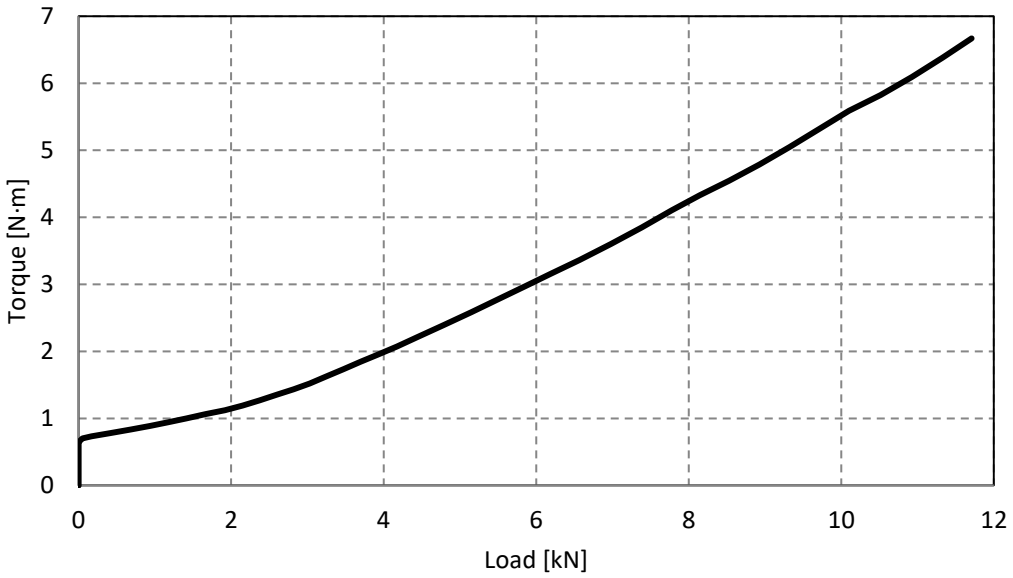

Figure 4.22: The Resistance Torque along with the Clamping Load.

The curve in Figure 4.22, as previously shown in the validation section (Section 4.5), indicates the gradual increase of the resistance torque, as measured at the bolt head, during the final tightening. Furthermore, Von Mises stresses in the parts are also plotted when the end load is achieved.

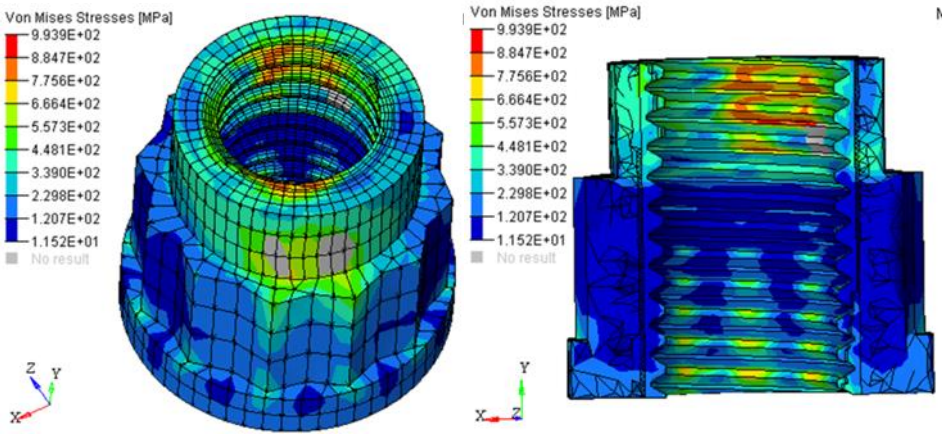

Figure 4.23: Von Mises Stresses in the Nut during the Tightening Step

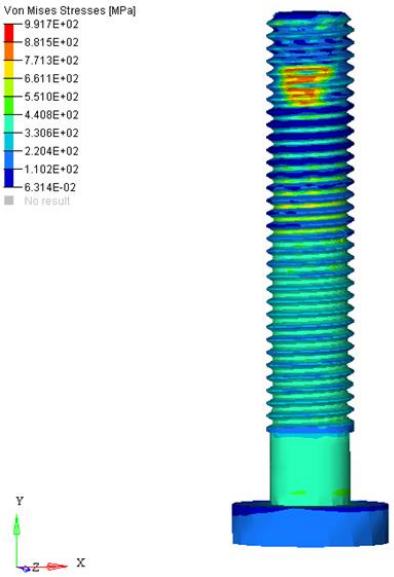

Figure 4.24: Von Mises Stresses in the Bolt during the Tightening Step

As shown in Figure 4.23 and Figure 4.24, maximum values in the stress distribution of the nut and bolt at end load, are similar to each other in the crimped section, and have approximate values of 990 MPa in both components. Additionally, a non-uniform pressure distribution were identified, due to the geometrical modelling. In fact, both the bolt and the nut were modelled as polygons, interacting with each other. However, the crimp effect in the contact pressure is observable.

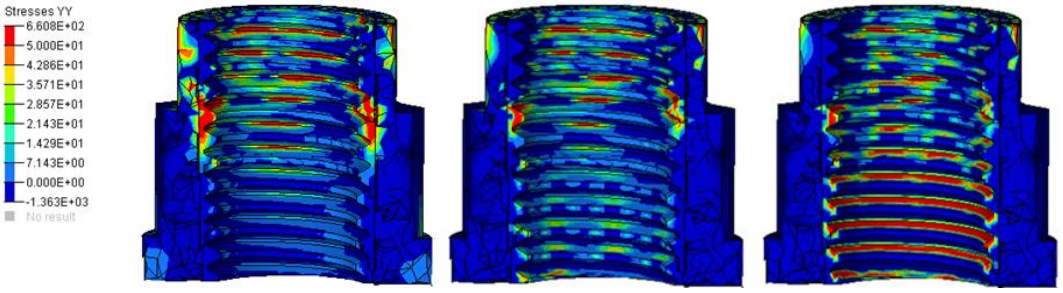

Figure 4.25: Stresses in the Axial Direction at Different Clamping Load: 1 kN, 3 kN, 11.6 kN

The stresses in the axial direction were analysed to map the distribution of the stresses due to the clamping load in the nut, and plotted using the same scale. As shown in Figure 4.25, the load is entirely taken by the crimped section until 3 kN, when the first threads start to be loaded. At the end load of 11.6 kN, the pressure is mainly in the first five revolutions, while in the crimp section the stresses are reduced. However,

the stresses in the crimp are still present, proving that part of the load is taken up by the crimp.

4.7 DISCUSSION

The model can be also used to investigate some of the features observed in testing the silver coated nuts in Chapter 3. In Section 3.4 the drop in self-locking torque with re-use was described, and it has been suggested that it is caused by either the deformation of the crimp and/or loss of the coating. In this section, these effects will be considered using the FEA model, by monitoring the diameter of the crimp section during the tightening process, and modifying the thread shape to simulate a loss in coating thickness. Similarly, in Section 3.4.1, several nuts were sectioned and the silver removal was investigated for different wind-on stages. These results will be compared to the FEA model with aim of identifying the contact pressure at which stripping occurs. Additionally, as shown in Section 3.3, the CoF was found to change during the tightening process. This result provided the initial motivation for the FEA study, and the accuracy of the calculated CoF will be considered.

4.7.1 *Locking Torque Reduction with Re-uses*

During the experimental stage of the investigation, it was observed that the self-locking torque reduced with re-use, with a significant difference recorded between the first and the second usage of the nut as seen in Figure 3.16.

The reasons for this behaviour were suggested to be either plastic deformation of the crimped section or removal of the coating. The effect of both of these factors will now be examined using the FEA model result. The external diameter was found to change in the experiment during the screwing process. Thus, in the FEA model, the external diameters, minimum and maximum, were monitored during the entire analysis of the tightening process. Additionally this analysis has included the removal of the nut to see if the deformation is recovered. In this case, instead of unscrewing the whole nut, for convenience the bolt was removed from the analysis, to enable the nut to elastically recover. This approach has allowed maximum and the minimum diameter of the crimp section to be plotted over the entire analysis (Figure 4.26).

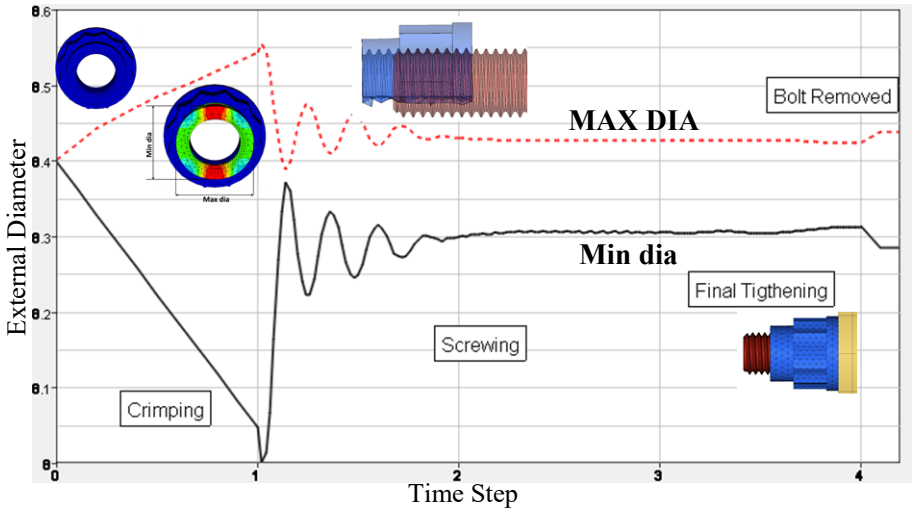

Figure 4.26: Diameter Changes during the Analysis

As shown in Figure 4.26 the chimney section is circular at the beginning of the analysis, reaching the maximum ovalisation at the end of the first step, when the crimp has been applied. During the first part of the screwing, the crimp is strongly deformed as it interacts with the bolt threads. After the first bolt thread engages the crimp, the diameter stays approximately constant, until the tightening step, when the nut is elastically deformed due to the clamping interactions. Removing the bolt, the crimp section relaxes, showing that the deformation is a sum of both plastic and elastic deformations.

To simulate the second re-use of the joint, the nut has been unscrewed one revolution, ensuring a zero clamping force, and re-tightened to the end load of 11.6 kN, with the second use pin on disc friction values applied. Pressure, stresses and torque were analysed, showing a similar result to the first tightening, with the crimp diameter also showing a similar trend, with an elastic deformation during the second use and in line with the experimental results. This indicates that the plastic component of the crimp deformation is not significant, and that plastic deformation is unlikely to account for the observed experimental reduction in locking torque. In addition, the slightly higher CoF in the second re-use does not increase the overall torque, as the percentage of nodes that experience high pressure is not significant.

Secondly, the nut threads were modified to simulate the thickness of the coating being removed (5-6 μm), leading to an increased thread clearance. This was achieved, through the pre-processor Hypermesh, where the nodes in the internal threads were moved 5 microns along their normal axis, reducing both the minimum and maximum internal diameter, whilst keeping the 60º angle between the flanks. With these

changes, the entire analysis was repeated and stresses, torque and pressure were evaluated as in the previous model.

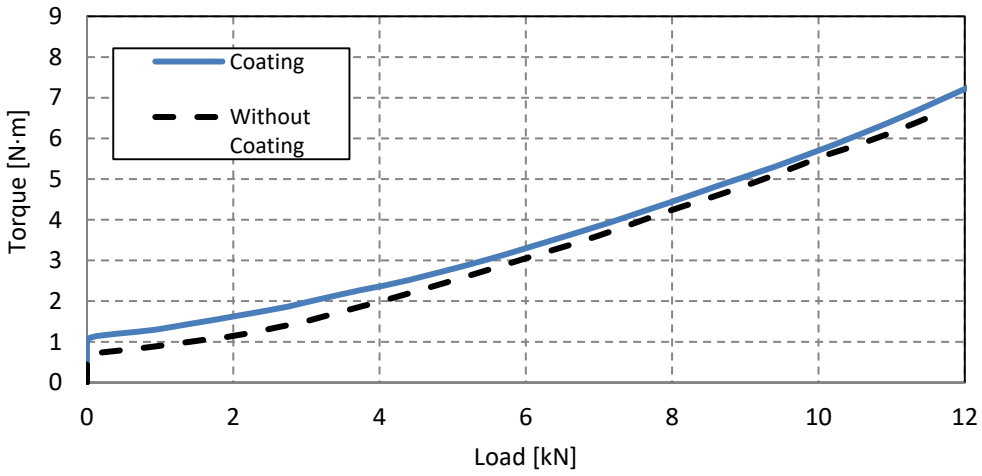

Figure 4.27: Tightening Curve in the Coated and Un-coated Nut.

Figure 4.27 show the torque-load profile with the silver coating thickness removed against the 5 microns coating in place. The curve with the coating removed was found lower, similar to the behaviour seen in the second cycle in the experimental results in Section 3.3.3.

Pressure, stresses and elongation were analysed, although a significant difference from the presented results has not been found. Based on the analysis undertaken, it is therefore suggested that loss of coating at the contact patch is likely to account for the drop in locking torque observed with re-use. This is particularly likely, as stripping of the coating (as discussed in the next section) was observed in most cases.

4.7.2 *Contact Pressure Investigation*

From the .odb file, the output file from the solver Abaqus, the variable CPRESS was used to evaluate the distribution of the pressure along the nut. The variable indicates the contact pressure at each node of the two contact surfaces. In this case the pressure data has been plotted as a distribution.

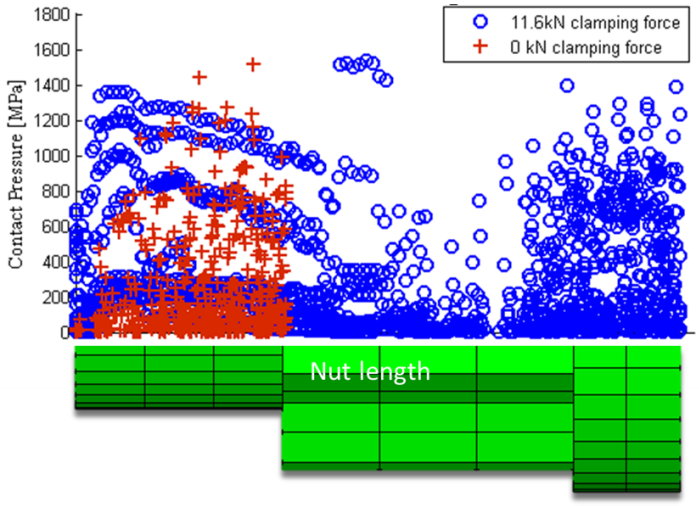

Figure 4.28: CPRESS Distribution along the Nut at 0 and 11.6 kN.

Figure 4.28 shows the distribution of the contact along the nut, highlighting the high contact pressure in the crimp, both before and after the end-load is reached. As seen in Section 4.6, not only the first threads take the load, but also the crimped section. Furthermore the number of nodes in contact has been plotted during the clamping.

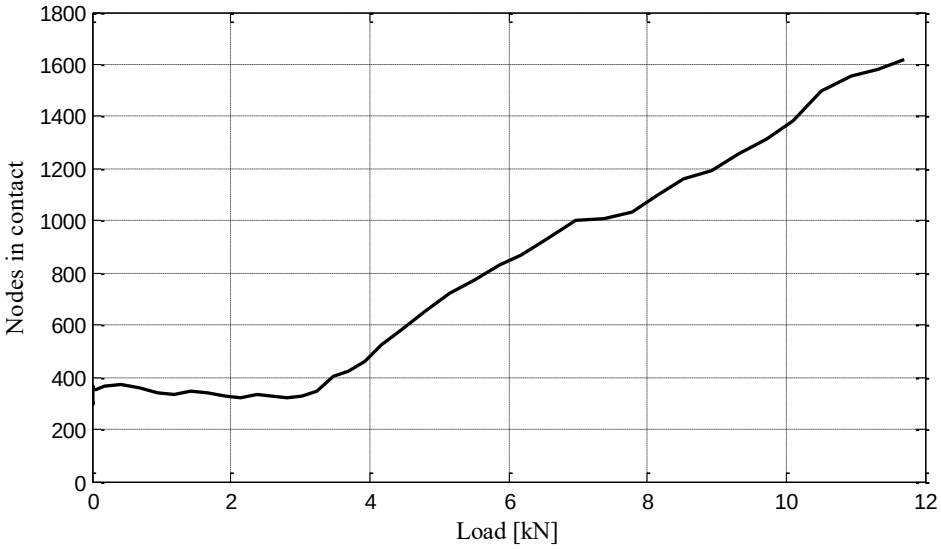

Figure 4.29: Number of Nodes in Contact during the Clamping

Figure 4.29 represents the number of the nodes in contact, mainly constant until 3 kN and linearly increasing with the clamping load. As the pressure in every node is not the same, the overall average is ineffective; thus the percentage of nodes with contact pressure below a series of threshold values have been plotted along with the clamping force.

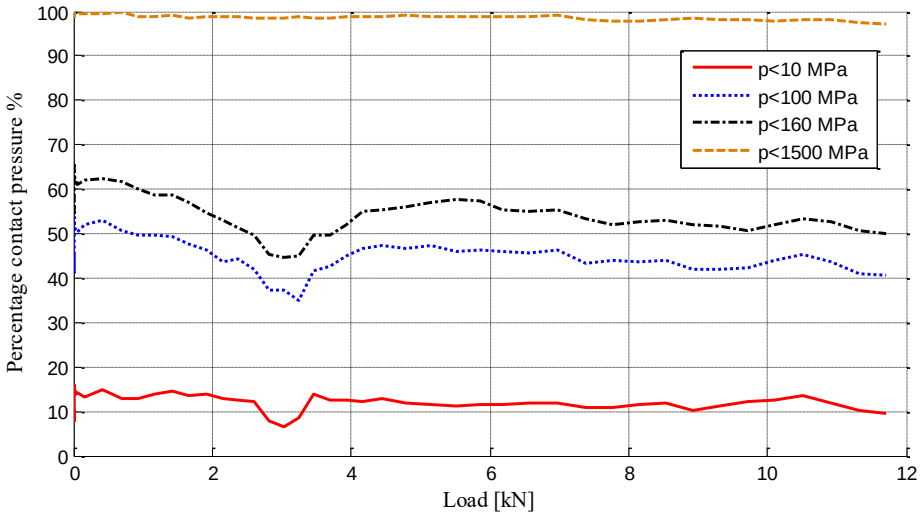

Figure 4.30: Percentage of Nodes in Contact for Different Pressures

Figure 4.30 shows this distribution, and highlights the percentage of nodes with a contact pressure lower than 10, 100, 160, and 1,500 MPa, indicating that 96% of the nodes have a pressure lower than 1,500 MPa, and that 50% have a value lower than 160 MPa. It can also be observed that at 3 kN a dip occurs in all of the distributions. This is caused by the gradual engagement of the first thread. Up until this point the load is sustained by only the crimped section (as shown in Figure 4.20 and Figure 4.25), increasing the average pressure. As discussed for the pin on disc test, as a low normal load is required and surface roughness effects become significant, measurements taken for values of contact pressure lower than 50 MPa are subject to error. The load cell used was also unable to measure loads below an equivalent contact pressure of 10 MPa for the samples tested. Thus, the 30% of the nodes with pressures lower than 50 MPa are poorly defined, while for the 10% of nodes with a contact pressure lower than 10 MPa, the CoF was roughly assumed equal to the value at 50 MPa. As highlighted, these nodes are a significant proportion of the distribution, and may be a source of error in the model.

4.7.3 *High Pressure Regions & Stripping Of Silver Coating*

During the experimental tests, the silver coating was found to be removed from the substrate, especially in the crimped sections. Using different joints, nuts were split at different axial engagements, in order to highlight the progressive stripping process, as previously seen in Section 3.4.1. In the FEA model the contact pressure was analysed at the same engagements, developing a comparison between the silver conditions and

the pressure distribution. The half nuts in Figure 4.31 were split when the first bolt thread is one, two and three revolutions out of the nut chimney respectively.

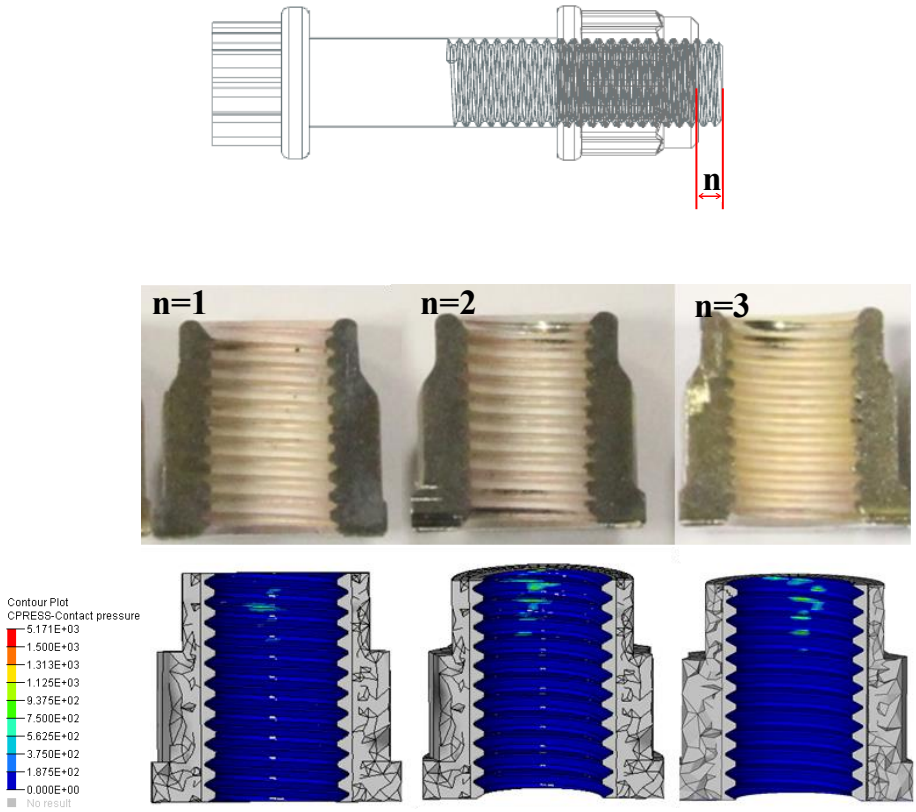

Figure 4.31: Silver Removed along the Screwing Process: Experiment and FEA Results.

As demonstrated in the Figure 4.31 the FEA result matches the experimental results well, with the silver removed in regions of high contact pressure in the crimped section. This result also suggests that a contact pressure of approximately 750 MPa will lead to stripping of the coating, when combined with relative motion. As seen in the pin on disc test, Section 4.3, at this pressure value, the silver coating starts to damage, but still provides low friction. Similar results were found in the literature by Yang et al. (Yang et al. 2003), analysing the silver coating wear and CoF at different pressures, where it was found that initial coating failure did not accompany a high friction, as the layer of silver removed acts as a solid lubricant.

4.7.4 *Coefficient of Friction*

As examined in Section 3.3, the CoF was observed to change in the experiment during the tightening process. However, it is still unclear as to how accurate the equation used to calculate this value is. As previously discussed, Equation 3.3 is used in the

experiment to calculate the CoF in the joint. As indicated, the CoF in the threads μ_1 is a function of the measured thread torque and joint load at a given point in the tightening sequence. The thread torque is calculated as the total torque minus the torque required to stretch the bolt and the self-locking torque. This value is then divided by the clamping load and a geometrical factor. However, this equation assumes the CoF is the same throughout the joint, and does not account for the pressure dependent behaviour of the silver coating. It can also not be considered to be an average CoF in this case, as the relationship between CoF and contact pressure is non-linear. This statement is highlighted by the FEA model (Figure 4.32), where the average CoF is calculated on a nodal basis and is plotted against load (a true average), along with the value calculated by Equation 3.3 using the thread torque and joint load. As shown, as a consequence of the relationship between friction and contact pressure, the calculated value significantly deviates from the true average, and can only be considered an indication of broad joint friction, with a particularly mis-leading result at low load. However, as previously highlighted, the CoF measured in the pin on disc test has shown scatter at low pressure (Section 4.3.2), which means that inaccuracies are also present in the FEA model. Finally, the different methods analysed to calculate the CoF converge to a single value at the end load, which is practical used in order to estimate the load at a given torque.

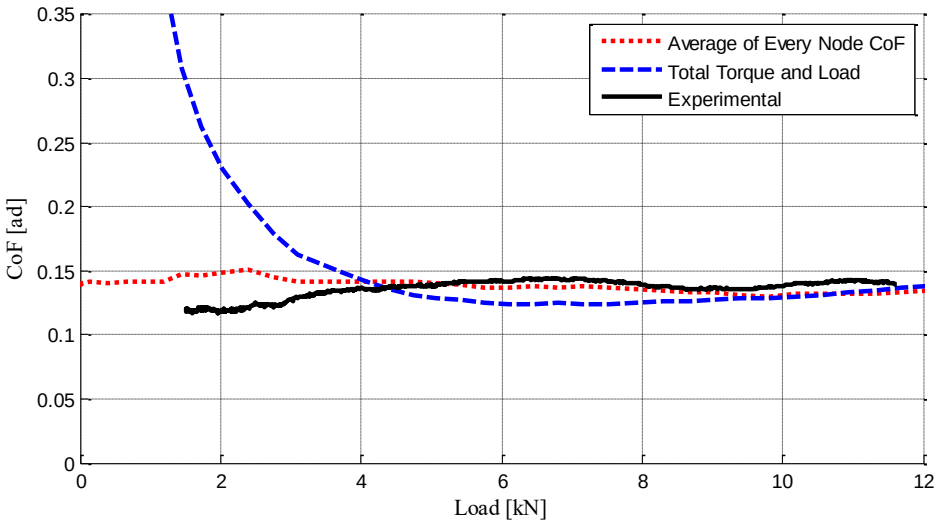

Figure 4.32: CoF during the Clamping.

4.8 SUMMARY

In this chapter the tightening process of the silver coated joint was analysed using the dynamic FEA model, and summarised as follow:

- The tightening process was analysed by the FEA method considering the self-locking feature and the variable CoF of the thin coating, showing a good match with the experimental result. Thus, future design and development of new coatings and self-locking features to replace the silver coated elliptical nut can be analysed using the FEA model and the pin on disc test.
- The stress distribution was analysed throughout the different steps of the crimping, the screwing on and the final tightening, identifying the concentration of the stresses along the crimped area of the nut, higher than the yield strength of the material.
- The relaxation of the locking torque was investigated in detail, and the factor behind the observed relaxation in self-locking torque with re-use investigated. Following this study, the removal of silver was identified as the most likely factor. In fact, a reduction of the torque profile was found if the thin coating was not modelled. The removal and the compression under loading of silver effects the clearance of the joint.
- The stripping of silver seen during the experiment, especially in the crimped zone, was compared to the contact pressure distribution in the FEA model, where pressure peaks were found to be coincident with silver removal. A threshold contact pressure of 750 MPa was identified.
- The equations previously used during the experiments were investigated using the FEA model, highlighting the weakness in the calculation, indicating that a true average CoF is not calculated. However, the different methods analysed converge at the end load to a single value, which is of primary importance as it is used to estimate the torque at end load during engine assembly.

CHAPTER 5

ALTERNATIVE COATINGS

5.1 INTRODUCTION

In the previous chapters, the silver coated nuts were tested and analysed. However, as previously explained in Section 2.4.3 some issues were associated with the use of this coating, such as stress corrosion cracking in nearby parts due to silver transfer. Additionally, the method used to apply the coatings, electroplating, is being phased out due to the introduction of new legislation, which has highlighted the health and safety issues associated with the cyanide baths used as part of the process (Robinson 2009).

In this work different alternative coatings were tested, following selection by Pattinson & Pallett in their internal report (Pattinson & Pallett 2015). In the selection, the requirements for the new coatings were various, for instance, the capability to withstand to the aero engine environment, such as the temperature range from -50 to 760º C. Furthermore, the silver replacement requires chemical stability in the presence of fuel contaminants, such as Sulphur and Chlorine, hydraulic fluid, fuels and lubricants. In addition to the capability to be applied to the internal threads and to the seating face of the nut, the replacement requires the resistivity to salt fog and high humidity, and must not cause stress corrosion cracking of nearby components. Furthermore, the new coating must be compliant with the Aerospace Standard JDS252.01 (incompatible materials), the Standard JDS002.01 (materials and processes to be avoided), and approved by REACh (Registration, Evaluation, Authorisation & restriction of Chemicals) (Pattinson & Pallett 2015).

As discussed above, the process typically used to apply the silver coating, electroplating, has been dismissed due to a lack of suitable materials that would fulfil the Health and Safety requirements. Thus, two other coating methods were found capable of depositing the coating onto the internal threads of the nut: lubricant doped paints and PVD (Plasma Vacuum Deposition).The lubricant sprayed paints offer the lowest cost option compared to PVD in terms of required equipment. These silicon resin modified dry film lubricants are generally used in high temperature applications,

and are suitable for steel, aluminium, magnesium and titanium alloys. Used on fasteners, they give an exceptionally good rubbing wear resistance (Indestructible, Specialist Coatings Manifacture 2016). However, there is a recognised risk of reduction in load carrying capability and stress resistance, which could affect the property consistency of the paints.

PVD technology is also being considered for deposition of coatings, as it offers a higher degree of accuracy and repeatability compared to paints. However, there is a perceived higher cost associated with this technology (Pattinson & Pallett 2015).

In the selection, in addition to mono-layer coatings, similar to the current silver, dual and multi-layer alternatives were also investigated. As discussed by Holmberg and Matthews (Holmberg & Matthews 2009) dual and multi-layer coatings (Figure 5.1) are frequently used for tribological applications for their benefits. In fact, these types of coatings may enhance the adhesion of the coating to the substrate, improve the wear and corrosion protection, and reduce stress concentrations and crack propagation.

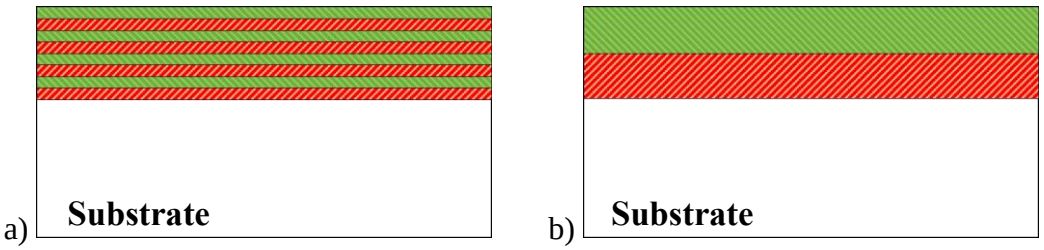

Figure 5.1: Structure of Multi-layer Coating (a), and Dual-layer Coatings (b)

Pattinson and Lloyd, in their internal report entirely analysed the periodic table of elements in order to find materials which can sustain aero-engine temperatures. Afterwards, they investigated affiliation with Chlorides which may induce stress corrosion cracking in nearby components, and the related Health and Safety issues. After a literature review of the remaining materials, different coating companies were asked to provide solutions for this application, fulfilling the described requirements. Thus, they provide different possible silver replacements, such as mono and multi-layer thin films and paints. However, as these materials are not on the market at present, full information was not available.

The alternatives selected and tested in this work are summarised in Table 5.1.

	THIN FILMS	Structure
1	Pure Nickel (Ni)	Mono-layer
2	Pure Chromium (Cr)	Mono-layer
3	Pure Titanium (Ti)	Mono-layer
4	Pure Platinum (Pt)	Mono-layer
5	Chromium-Nitride (Cr-N)	Dual-layer
6	Titanium-Nitride (Ti-N)	Dual-layer
7	Nickel-Platinum (Ni-Ti)	Dual-layer
8	Chromium-Nitride (Cr-N m)	Multi-layer
9	Titanium-Nitride (Ti-N m)	Multi-layer
10	Nickel-Titanium (Ni-Ti)	Multi-layer

	PAINTS	Structure
1	RB9-126	Silicone Resin
2	RB9-127	Silicone Resin
3	RB9-131	Phenolic Resin
4	RB9-138A	Inorganic Silicate
5	RB9-138B	Inorganic Silicate
6	SI-233	Yttrium Oxide
7	SI-234	Boron Nitride
8	SI-238	Mica
9	SI-239	Talc

Table 5.1: Coatings and Paints

As the alternatives outlined in Table 5.1 are possible replacements of the silver coating, similar investigations are needed to approve and compare them to the electroplated silver.

The aim of this work is to identify the suitable alternatives to the silver coating typically used. The consistency, the frictional properties and the related mechanisms will be investigated using the procedure developed for the silver coating in the previous chapters.

5.2 SELECTION PROCEDURE

In order to reduce the number of alternatives presented in Table 5.1, a selection procedure was created. Different steps, such as testing and characterisation are

required in order to fully examine the thin films and coatings. Similarly to the test performed with the silver nuts in Chapter 3, the alternatives were tested at room temperature and after a thermal cycle. Additionally, as the silver coating was characterised through a nano-hardness test, the alternatives were also analysed in the same way. As the analyses are time consuming, the tests are performed in ascending order, from the room temperature test, the heat treatment test, followed by the nano-hardness, as shown in Figure 5.2. The aim of this procedure is to eliminate at every step the alternatives which fail to fulfil the requirements of the test so as to only undertake further characterisation of credible coatings.

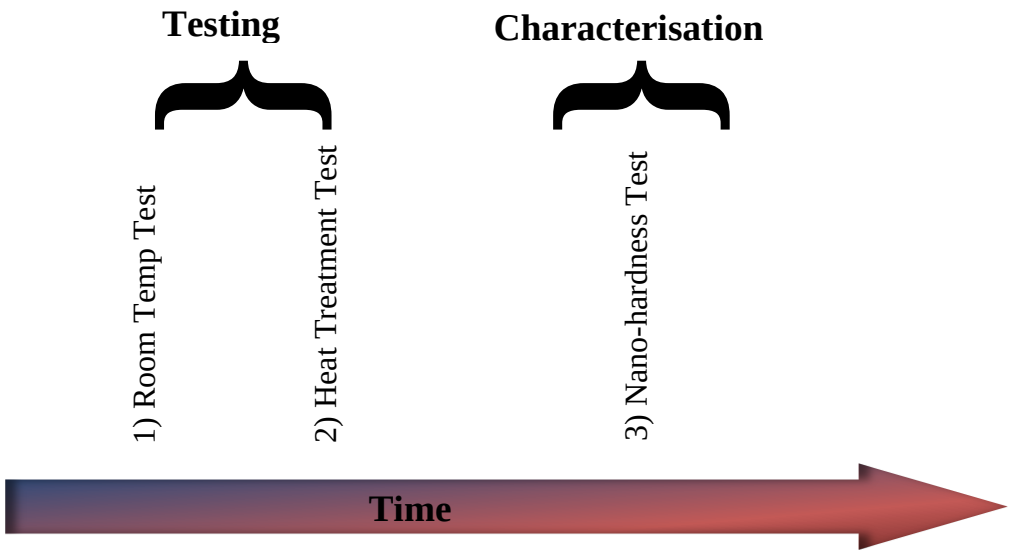

Figure 5.2: Selection Procedure

In the test at room temperature, the consistency of the result along with the value of CoF are investigated. In the test after the thermal cycle, the ability to withstand the high temperature without failure is analysed. In the nano-hardness test the roughness and the hardness of the coatings are examined before and after a thermal cycle in order to find and explain any observed differences in behaviour pre and post thermal cycle.

5.3 TESTING

5.3.1 *Room Temperature Test*

5.3.1.1 Test Procedure

Two nuts of each sample have been tested following the standard procedure performed with the silver coated nuts previously outlined in Section 3.2.3.2. The joints were tightened six times, with an end load of 11.6 kN reached in each case, as in Rolls-

Royce Design Standard JDS 829_03 (Rolls Royce 2011). As previously detailed, the aerospace lubricant Mobil Jet Oil II was applied to the bolt prior to assembling, and a thrust bearing was used to isolate the thread torque as described in Section 3.2.3.1. All the nuts have been crimped in the chimney section to provide a self-locking feature, deforming the diameter by 0.35 mm using a vice (Section 3.2.2). At rotating speeds of 0.5 rpm and 3 rpm, winding-on and clamping respectively, the torque along with the load were recorded, enabling the CoF to be calculated for the different joints during post-processing. Repeatability of both measured torque and CoF in the threads are the key parameters investigated.

5.3.1.2 Results

The torque at the end load and the CoF are analysed for all the 19 alternatives from Table 5.1.

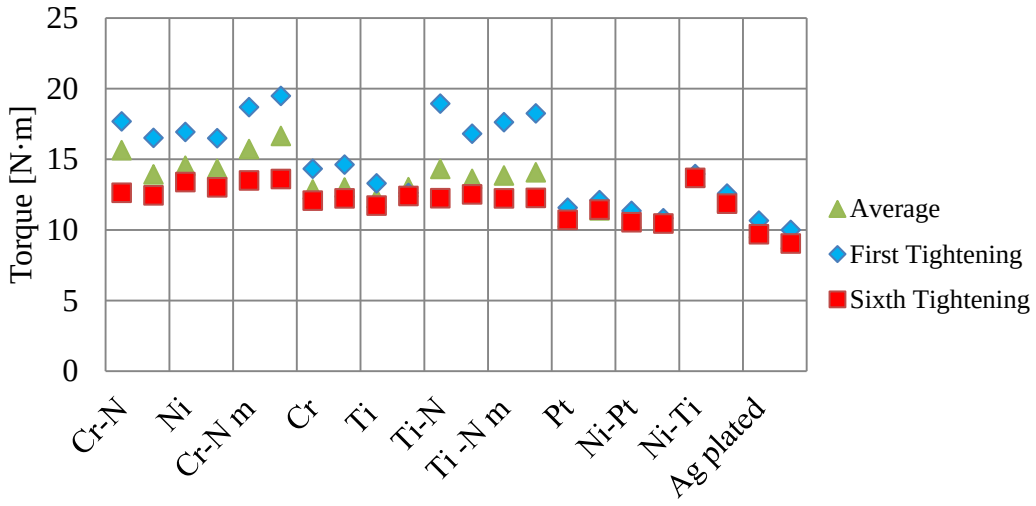

Figure 5.3: Torque at the End Load: Coatings

Figure 5.3 shows the torque at 11.6 kN for the first and sixth re-use, in addition to the average torque in order to highlight the consistency during re-uses, for the thin metal coatings, along with the silver coating results obtained in Section 3.3.3. The figure highlights a great deal of consistency for the Cr, Ti, Pt, Ni-Pt and Ni-Ti coatings over the six re-uses in each test. Furthermore, when comparing to the silver plated joint the consistent coatings showed slightly higher torque, from 15 N·m for Chromium to 11 N·m for Nickel-Platinum. Additionally, no differences were noticed between the dual-layer and the multi-layer configurations in the Ti-N and Cr-N coatings, with the torque at end load found inconsistent in all cases during the 6 cycles. Furthermore, the pure Nickel mono-layer was found inconsistent over the cycles, in contrast with the

same material in combination with Platinum and Titanium, which showed better results. In the figure, the torque required to reach the end load also takes into account the self-locking torque, which generally decreased over the cycles, as shown in Figure 5.4.

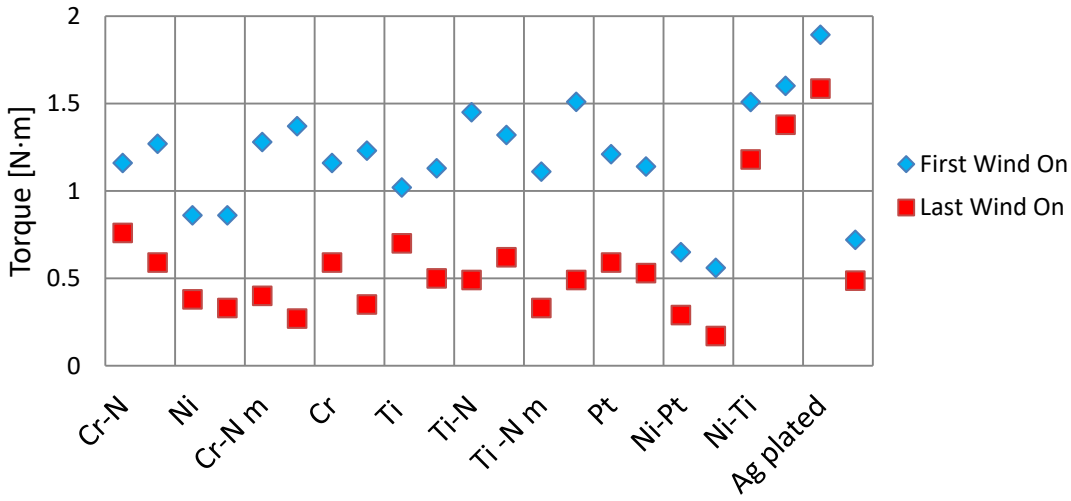

Figure 5.4: Self-Locking Torque: Coatings

As shown in Figure 5.4, the self-locking torque varied during the cycles, thus increasing the variance of the total torque required. However, as shown in most cases the variation in total torque is greater than the variation seen in locking torque, meaning it is attributable to changes in the coating. Thus, the CoF in the threads (measured by subtracting the self-locking torque) is also analysed. The CoF in the threads has been plotted, once again for the first and last re-uses, as well as the average during the six re-uses, and with the silver results also included for comparison (Figure 5.5).

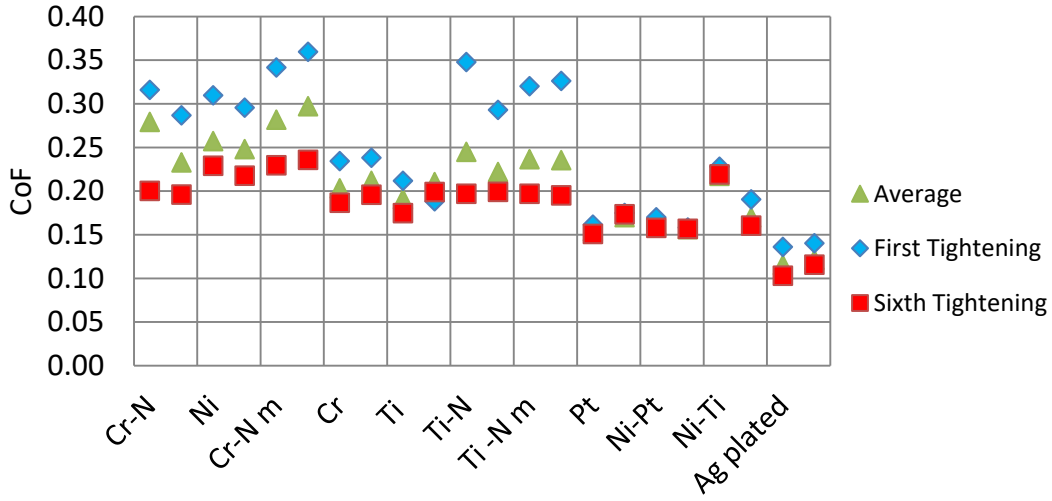

Figure 5.5: CoF: Coatings

As shown in Figure 5.5, the CoF in the threads for Cr, Ti, Pt, Ni-Pt and Ni-Ti were found to be consistent, and similarly stable throughout all six re-uses. However, these coatings experienced higher friction compared to electroplated silver (0.125), such as 0.22 for Chromium, 0.20 for Titanium, 0.15 for Platinum, 0.16 for Nickel-Platinum, and 0.20 for Nickel-Titanium.

Coatings containing Nitride (Cr-N, Cr-N multi, Ti-N and Ti-N multi) were found ineffective, with high scatter in values, ranging, for instance, from 0.2-0.32 for Chromium-Nitride or 0.2-0.35 for Titanium-Nitride. Pure Nickel was identified as inconsistent in contrast with Platinum and Titanium, where better performance was observed. The CoF in the threads experienced with the Platinum and Titanium, mono layer or linked with Nickel, were found to be the most consistent with re-uses, similarly to the silver plated samples.

Furthermore, as further explained in Section 5.4.1, the hardness of the metal coatings and the CoF were found to be strongly related, similarly to the silver coating analysed in Section 3.4.4, and in accordance with previous studies (Holmberg & Matthews 2009). In fact, soft coatings tend to be easier to slide, while hard coatings are more wear resistant.

A similar analysis was undertaken for the paints, with the torque at end load plotted for all the alternatives, and compared to the silver results (Figure 5.6).

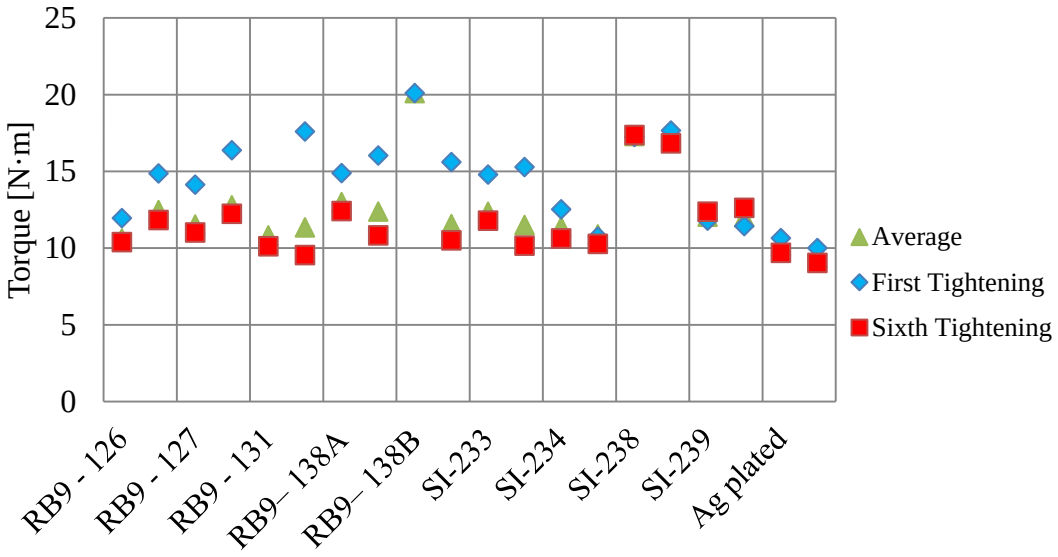

Figure 5.6: Torque at the End Load: Paints

Figure 5.6 shows the torque at end load for the paints, along with the silver coating, and highlights a marked consistency in the SI-234, SI-238 and SI-239 paints over the six re-uses. Compared to the plated silver, these paints experienced higher torque,

particularly SI-238, which has a torque 80% bigger than silver (10 N·m vs 18 N·m), while SI-234 experienced a torque of about 10-12 N·m and SI-239 of about 14 N·m, which are closer to the silver results. All the RB9 paints and SI-233 experienced a significantly higher torque during the first cycle, attributable to the reduction in self-locking torque during the initial cycles as shown in Figure 5.7, and to the high friction generated by the excessive thickness of the paints, as further explained later.

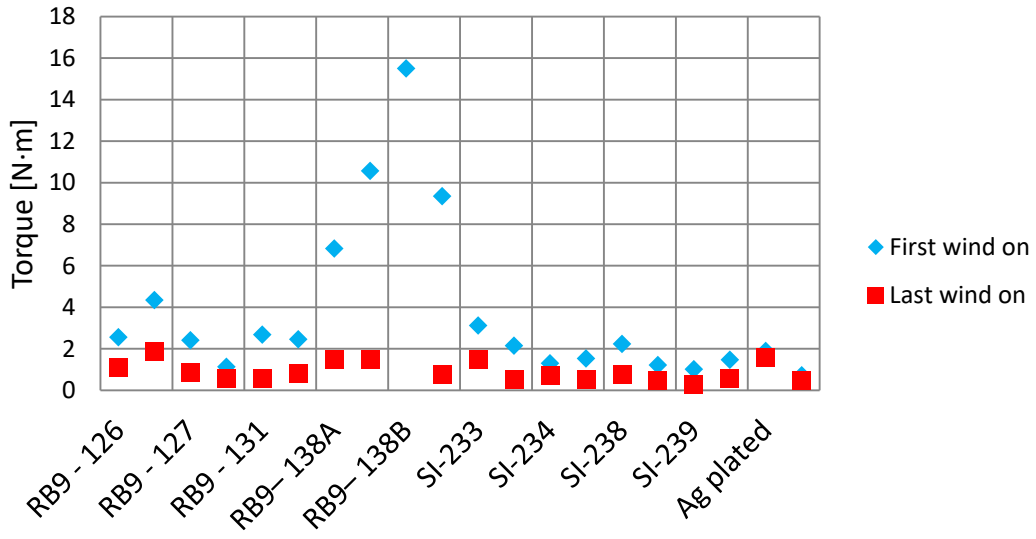

Figure 5.7: Self-Locking Torque: Paints

As shown in Figure 5.7 a higher self-locking torque in the first cycle was experienced in almost all the paints, with the RB9-138B being the highest at 15 N·m, which significantly damaged the threads.

Furthermore, similarly to the alternative metal coatings, the CoF in the threads was plotted, and compared to the silver results (Figure 5.8).

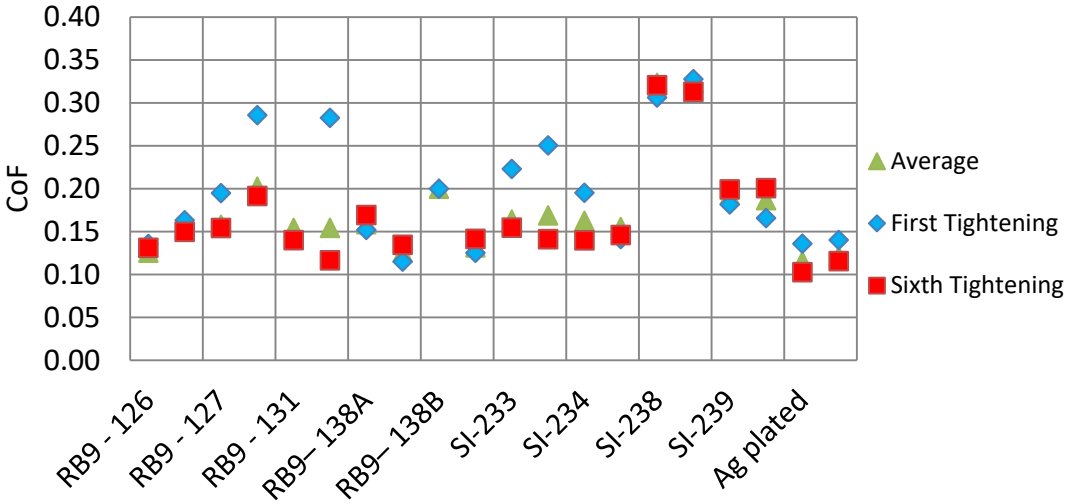

Figure 5.8: CoF: Paints

As shown in Figure 5.8, analysing the CoF in the threads for the paints, RB9-126, RB9-138A, SI-234, SI-238 and SI-239 were found to be fairly consistent over the six re-uses with a limited scatter. Similarly to the thin PVD films, the CoF was generally higher than silver, such as 0.13-0.16 for RB9-126, 0.11-0.18 for RB9-138A, 0.14-0.20 for SI-234, and 0.16-0.20 for SI-239. In particular SI-238 experienced the highest CoF in the threads with 0.32-0.33. Additionally, the CoF was found to be higher during the first cycle for almost all the alternatives, attributable to the excessive thickness of the paints which reduces the clearance of the fastener and increases the frictional forces in the contact.

As previously stated, the limited scatter in the CoF is important when predicting the specific torque required to achieved a given end load, preventing overestimation and underestimation of the clamping load which may lead respectively to the failure or the loosening of the joint.

In order to analyse the coating condition after the test, the nuts were sectioned and optically examined, as shown in Figure 5.9.

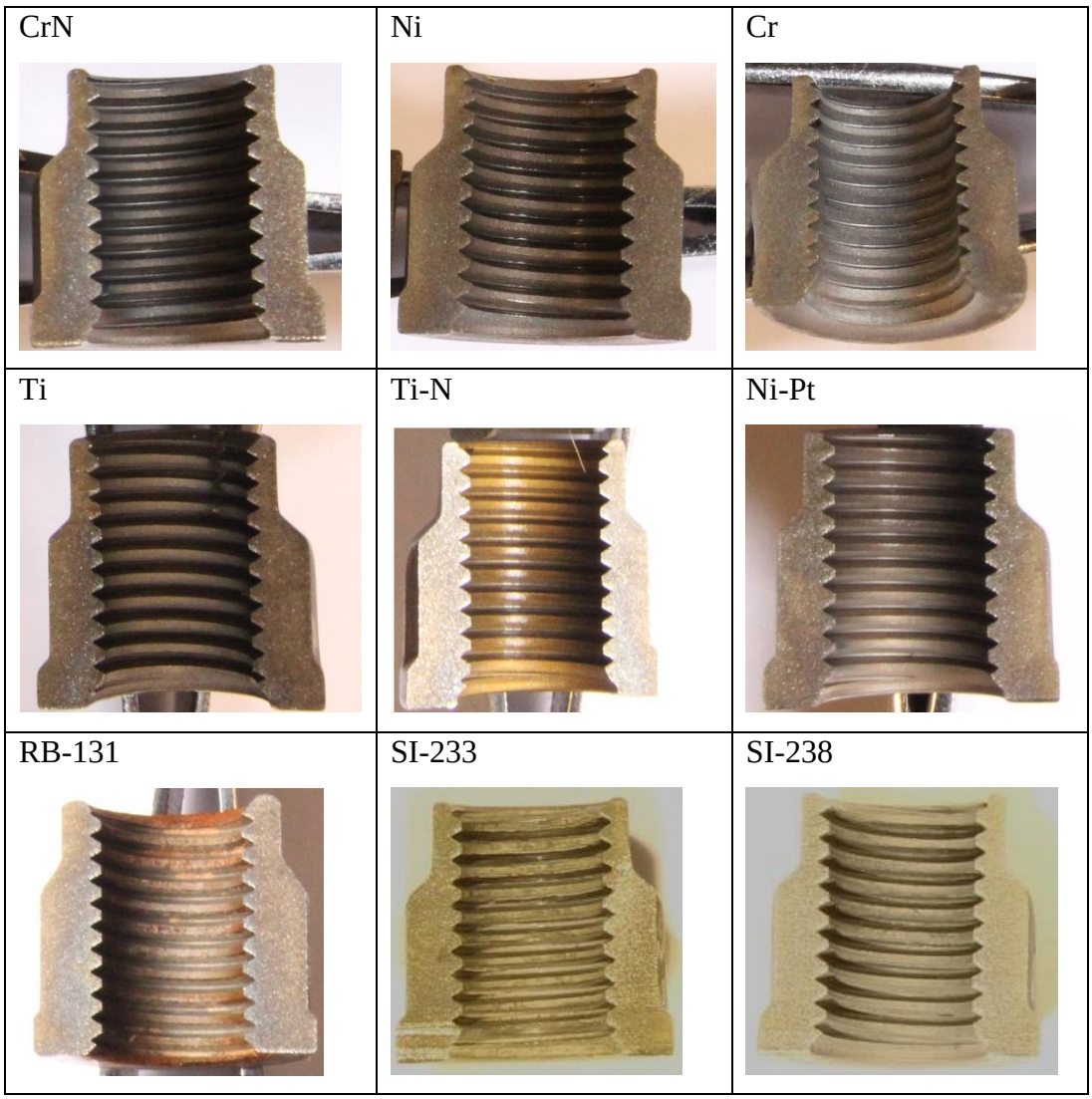

Figure 5.9: Coating and Paint Conditions After Test.

In Figure 5.9 clear examples of the coating conditions during the test are presented, highlighting that in most cases the alternatives had a similar colour to the substrate, with the exception of RB-131 and Ti-N. The metal coatings and the SI paints experienced slight removal, while the RB paints were found to be significantly deformed and removed from the substrate (Figure 5.10), likely due to their excessive thickness.

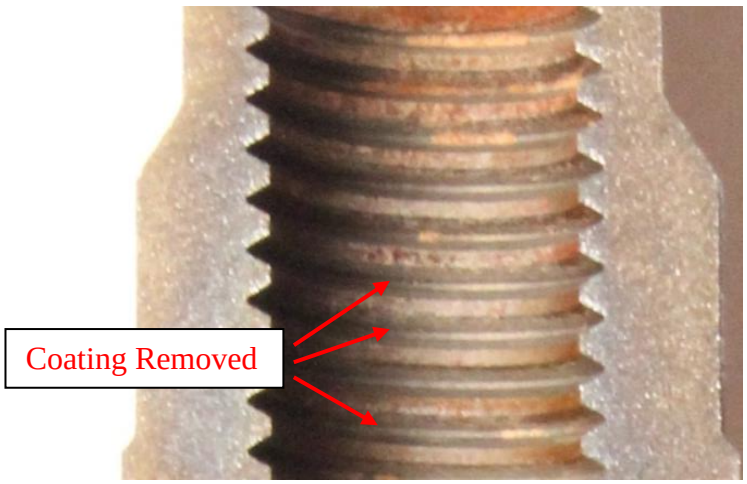

Figure 5.10: Close Up of the Thread Damage

As previously stated, the aims of this test were to analyse the consistency in the frictional properties of the alternative coatings, and assess the damage occurring to the coatings during the test. The consistency in the CoF is one of the key parameters which prevents failure or loosening of the bolted joint, by reducing risk of over-tightening or under-tightening respectively. For this reason, Cr-N (dual and multi-layers), Ni, and Ti-N (dual and multi-layers) were found inappropriate during the six cycles test and were therefore not taken into account in the next examinations. Additionally, the coating conditions were assessed to detect any removal of the coating, as it acts as a barrier between the thread surfaces. In fact, the RB paints, which were significantly damaged during the tests, were identified as unsuitable to replace silver and similarly not taken into account in the next experiments.

Successful		**Removed**	
THIN FILMS	**PAINTS**	**THIN FILMS** ***(Inconsistent results)***	**PAINTS** ***(excessive thickness)***
Pure Chromium	SI-233	Pure Nickel	RB9-126
Pure Titanium	SI-234	Chromium-Nitride (dual)	RB9-127
Pure Platinum	SI-238	Titanium-Nitride	RB9-131
Nickel-Platinum	SI-239	Chromium-Nitride (multi)	RB9-138A
Nickel-Titanium		Titanium-Nitride (multi)	RB9-138B

Table 5.2: Room Temperature Test Summary: Coatings and Paints

As shown in Table 5.2, the successful and unsuccessful alternatives are summarised, and the successful coatings will be analysed in the next experiment.

5.3.2 *Ageing Tests*

5.3.2.1 Test Procedure

The coatings and paints which satisfied the requirements in the previous test at room temperature were analysed after a thermal cycle, as previously performed for the silver coating in Section 3.2.3.3. As previously described in the selection procedure (Section 5.2), the requirements for the selection were the consistency in the CoF and the damage assessed after the test. So that, the severe damaged RB paints were removed, along with the inconsistent thin coatings, such as Cr-N, Ni and Ti-N. The remaining alternatives are shown in Table 5.2.

Assembled joints were thermally aged at 760º C for 50 hours, as this represents the service temperature, and their ability to prevent seizure investigated at room temperature post-cooling. In the preliminary step, the nuts were crimped in the chimney section and the torque required to reach the end load was first evaluated using the load cell. Afterwards, the joints were re-assembled to the same torque with a Waspaloy spacer replacing the load cell. The spacer had similar dimensions to the load cell, and was used because the load cell could not be subjected to the ageing process. Mobil Jet Oil II was once again used as a lubricant. After cooling down to room temperature, the joints were unscrewed on the test rig, and the torque profile measured for each.

Afterwards, in order to compare the CoF in the pre- and post-ageing conditions, the joints were re-tightened using the thrust bearing and the load cell, and applying the lubricant beforehand, as previously performed with the silver coating (Section 3.2.3.3 and Section 3.3.4), as shown in Figure 5.11.

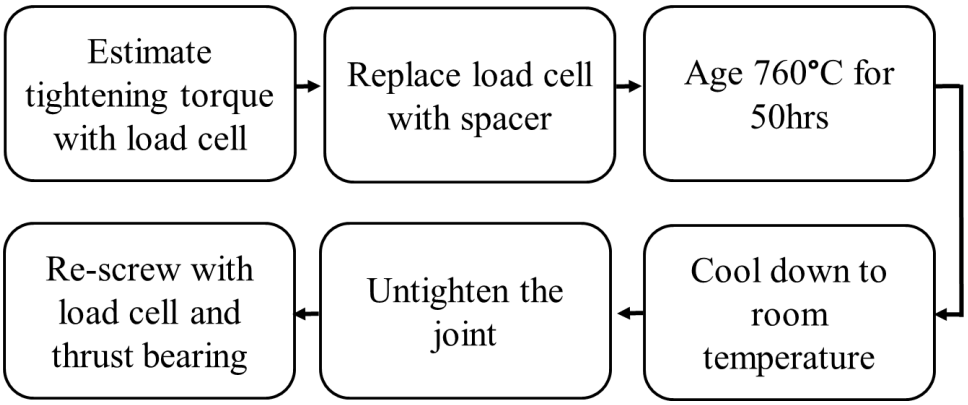

Figure 5.11: Heat Treatment Test

The aim of this test is to assess the ability of the alternatives to withstand the thermal cycle without failure, and to analyse the CoF after ageing and compare them to the silver plated joints.

5.3.2.2 Results

Three samples for each alternative has been tested, and results are shown in Table 5.3, and compared to the silver coating result obtained in Section 3.3.4.

COATING	Pre-ageing			Post-ageing		Successful Test?
	Tightening Torque [N·m]	Untightening torque [N·m]	CoF (avg)	Break Torque [N·m]	CoF (avg)	
Silver	16	12.7	0.120	33.8 ± 5	0.231	YES
Pure Chromium	20	18.5	0.207	30 ± 3.5	0.504	YES
Pure Titanium	21.2	17.7	0.201	30 ± 5	0.538	YES
Pure Platinum	19	15.2	0.162	42 ± 11	0.388	YES
Nickel- Platinum	16.8	14.3	0.159	36 ± 8.5	0.424	YES
Nickel- Titanium	26.1	22	0.194	56 ± 1	0.317	YES
PAINT						
SI-233	21.6	17.5	0.166	27.5 ±1.5	0.244	YES
SI-234	20	16.6	0.159	32.7 ±0.5	0.386	YES
SI-238	25	20.6	0.211	31.5 ±3.8	0.211	YES
SI-239	20.8	17.1	0.19	38 ± 2	0.228	YES

Table 5.3: Heat Treatment Test: Results

Table 5.3 shows the results of the Heat Treatment test for the alternative coatings and paints. The ‘Tightening Torque’ and ‘Untightening Torque’ columns are obtained at room temperature before the thermal cycle, when the load cell is used to accurately reach the end load required. The ‘CoF’ columns (pre-ageing) shows the average CoF in the threads calculated at room temperature, which was obtained in the previous section (Section 5.3.1). The ‘Break Torque’ column shows the torque required to unscrew the joint after cooling down to room temperature.

The break torque highlighted a significant increase from the untightening torque pre-ageing and a significant scatter in values. The increase, such as from 17.7 N·m to 30 N·m for Titanium, from 15 N·m to 42 N·m for Platinum, from 22 N·m to 56 N·m for Nickel-Titanium, or from 17 N·m to 38 N·m for SI-239 was caused by an increase of CoF in the threads (examined below) along with the seizure experience in the bearing surfaces, which can also depend on the chemical affinity between the mating parts, as widely discussed in the literature (Kuznetsov & Freitag 1966). Additionally, the significant standard deviation in the break torque values, such as 8.5 N·m in the Nickel-Platinum and 11 N·m in the Platinum was also attributed to the unpredictable seizure between the mating bearing surfaces. In fact, after unscrewing, clear signs of seizure were apparent on the seating faces of the joint, in the spacer and in the washers, as shown in Figure 5.12.

Figure 5.12: Seizure in the bearing Surfaces

The last column in Table 5.3 shows the CoF in the threads measured after the thermal cycle, using the load cell and the thrust bearing. As highlighted in the table, the CoF for all the coatings and the majority of the paints tested experienced a significant increase, with the paint SI-238 being the exception. As shown in the table, most of them doubled in value, such as Chromium from 0.207 to 0.504, Titanium from 0.201 to 0.538, Platinum from 0.162 to 0.388, Nickel-Platinum from 0.159 to 0.424, and SI-234 from 0.159 to 0.386, similarly to the silver coating (from 0.120 to 0.231) previously tested in Section 3.3.4. On the other hand, three other alternatives experienced a lesser increase, such as Nickel-Titanium from 0.194 to 0.317, SI-233 from 0.166 to 0.244, and SI-239 from 0.190 to 0.228. Finally, as previously stated the paint SI-238 is the only alternative which experienced a reduction in the CoF, from 0.323 to 0.211.

Analysing the break torque and the CoF values, it was noted that seizure played the most important role. In fact, a clear example was seen for SI-238, where a reduction of the CoF did not cause a reduction of the break torque. Thus, this large increase of

torque, from 20.6 N·m pre-ageing to a 31.5 ± 3.8 N·m post ageing, was attributed to the seizure in the bearing surfaces. Generally however, the increase of the CoF in the threads experienced after ageing plays an important role in the increase of the break torque. In fact, as presented multiple times in this work, the tightening and untightening torque is a function of the CoF, as the torque increase with the increase of thread friction.

As previously stated in Chapter 2, a high CoF in the threads can lead to the failure of the joint. Thus a further analysis will be presented in Section 5.5.1, introducing a friction limit at which the joint may fail, and compare this value to the thread friction seen in this test.

The samples were once again visually examined using filtered lights, with the nuts again split in two after the test in order to analyse the thread condition. Unfortunately, in contrast with the bright silver previously analysed (Section 3.3.4), all the alternatives were found to be similar in colour to the substrate (Figure 5.13), and accurate examination was therefore difficult. However, a slight damage of the coating in the threads was observed.

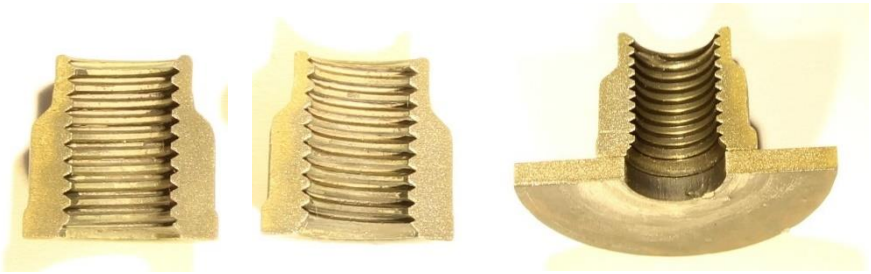

Figure 5.13: Coating Condition after the Heat Treatment Test (Nickel- Titanium)

5.4 CHARACTERASATION

5.4.1 *Nano-Hardness Test*

5.4.1.1 Test Procedure

In the previous test, all the coatings and the paints successfully passed the thermal cycle test, with none of them experiencing any seizure, despite a significant change in CoF. For this reason, they were further investigated using the nano-hardness test.

As previously described, the ageing process effected the frictional properties of the coatings and paints. In order to further analyse the ageing consequences to the coatings and paints, the hardness pre and post-ageing was measured through the nano-indentation machine described in Section 3.4.4. Similarly, the coating roughness was

analysed pre and post thermal cycle, to further investigate the ageing effects. The alternative coatings were once again compared to the currently used silver coating, in order to find the similarities and differences. As previously described, the hardness was measured on the flat bearing surface, as measurement of the threads was impracticable. The metal coated nuts were polished with 0.25 microns diamond suspension for two minutes and cleaned with acetone, while the paints were tested at original condition as either polishing or acetone cleaning would entirely remove the thin layer. In order to test the post-ageing condition, the coatings and paints were thermally treated at 760ºC for 50 hours and re-tested after cooling, as explained multiple times in this work (such as in Section 3.2.3.3 and in Section 5.3.2).

5.4.1.2 Results

The roughness and the hardness of the coatings and paints were measured pre- and post-thermal cycle, and compared to the silver coating results obtained in Section 3.4.4, as summarised in Table 5.4.

THINFILM	Roughness Ra[µm]		Hardness [GPa]	
	Pre-Ageing	Post-Ageing	Pre-Ageing	Post-Ageing
Silver	0.5-0.8	3.0-4.0	1.5-2.3	0.4-1.2
Pure Chromium	1.5-2.0	2.5	2.7-9.1	0.9-6.3
Pure Titanium	1.0-2.0	2.0-3.0	3.1-6.3	0.3-4.5
Pure Platinum	1.0	2.5	0.9-5.9	0.2-4.3
Nickel-Platinum (dual-layer)	1.5-2.0	2.0-3.0	1.4-6.0	1.4-6.6
Nickel-Titanium (multi-layer)	1.5-2.0	2.5-3.0	0.1-9.0	0.6-9.0
PAINT				
SI-233	2.5-3.0	3.0-3.5	0.13-0.9	0.05-1.3
SI-234	2.5	---	0.015-0.6	---
SI-238	2.5	3.0	0.18-0.5	0.013-0.3
SI-239	2.5-3.0	3.0-3.5	0.013-0.53	0.023-0.50

Table 5.4: Roughness and Hardness Pre and Post- Ageing

In the table, the previously tested silver coating was added, in order to easily compare to the alternatives. As shown in Table 5.4, the roughness significantly increased in all coatings and paints, as much as 1 µm to 2.5 µm for Platinum and 2.5 µm to 3.5 µm for SI-233, showing that the ageing process had effects on the alternatives, as was the case for the silver coating. For the case of mono-layer coatings, Chromium, Titanium and Platinum experienced a softening during the thermal cycle (Figure 5.14a), similarly to the silver coating (Section 3.4.4), leading to an increase in the CoF, as further discussed in Section 5.5.2. Alternatively, the dual-layer Nickel-Platinum and the multi-layer Nickel-Titanium, due to the mix of materials with different hardnesses, did not show a clear pattern, as shown in Figure 5.14b.

Additionally, the thin paints exhibited a very low hardness pre and post ageing, as low as 0.015 GPa. Interestingly, SI-234 was easily removed from the substrate, even with a delicate finger touch. The other three paints showed a slight decrease in hardness, as shown in Figure 5.14c.

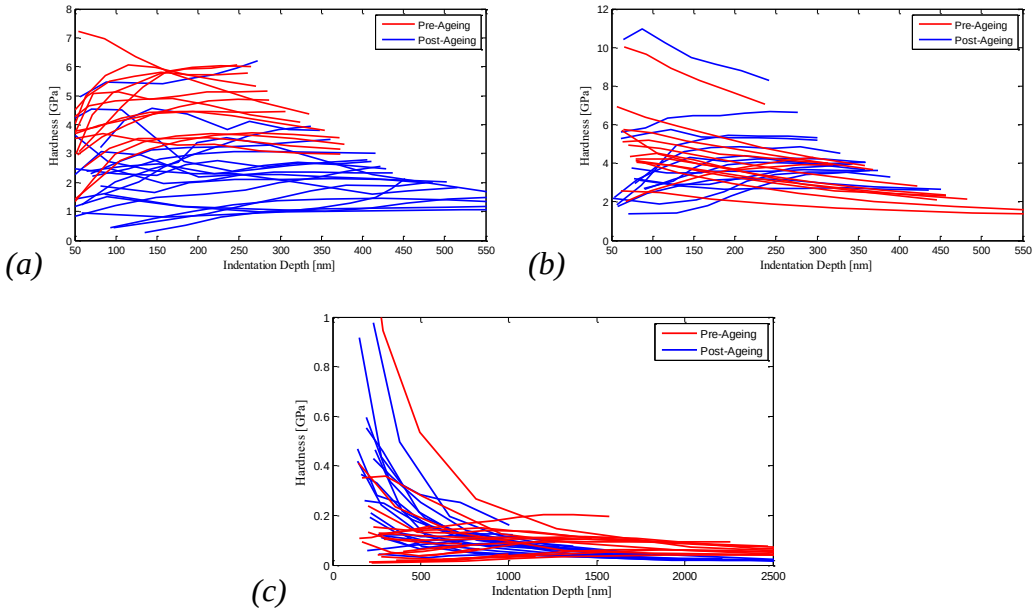

Figure 5.14: a) Pure Ti (Mono-layer) b) Nickel-Platinum (Multi-layer) c) SI-239 (Paint)

Figure 5.14 shows the three different trends experienced during the hardness test, with the coating hardness pre and post thermal ageing plotted against indentation depth, for Pure Titanium (a), Nickel-Platinum (b) and SI-239 (c). A further discussion of the underlying mechanisms observed here as well as a summary of these results will be presented in Section 5.5.2, where the successful alternatives are compared to the silver coating. Additionally, in APPENDIX B, the hardness test performed on the other coatings will be presented.

At this stage, a cost analysis was performed in order to determine the suitability of these materials in a future large scale production. Firstly, raw Platinum was found to be ten times more expensive than silver and thus, pure Platinum and Nickel-Platinum thin films were considered unsuitable for engine applications and not investigated further. Additionally, all the SI paints were found to be cost prohibitive for this application at this stage, and removed from the list. Furthermore, the paint SI-234 was also excluded as the nano-hardness test showed a poor behaviour of the paint as a consequence of the thermal cycle, being easily removed post cooling. Thus, the successful coatings after this analysis were established, as summarised in Table 5.5.

COATINGS
Pure Chromium
Pure Titanium
Nickel-Titanium

Table 5.5: Remaining Alternatives

The remaining pure Chromium, pure Titanium and Nickel-Titanium were found to successfully pass the tests of this study, and in order to assess which of them is the most suitable coating for aero-engine applications, further analysis will be undertaken, such as vibration testing, as further explained in Section 9.1.

5.5 DISCUSSION

In this section the limit of the CoF in the threads will be investigated in order to find how close the alternatives are from causing failure. Even the unsuccessful coatings are considered in this analysis in order to present an overview of all the alternatives. Additionally, the successful coatings are compared to the silver coating and their capabilities summarised. Finally, the limitations of this analysis are discussed along with future improvements.

5.5.1 *Thread Friction Limits*

The CoF in the threads in the alternatives after the thermal cycle in Section 5.3.2.2 was found to be higher than at room temperature, and significantly higher than the silver coating. As previously stated, a high CoF can lead to an increase of thread torque, and a subsequent failure of the joint. In this discussion all the coatings tested

in the heat treatment test are analysed in order to provide an overview of the variability in the coatings, although most of them were eliminated in the subsequent tests. The aim of this discussion is to draw a CoF in the threads limit at which the joint may undergo failure, and establish how each of the coatings stand compared to this.

5.5.1.1 Bolt Torsional Test

In order to define a limit of CoF in the threads to avoid the thread deformation, the Waspaloy bolt normally used in this work was tested with a pure torsional test until failure. Using the test rig previously described in Section 3.2, the ¼" (6.35 mm) bolt was rotated while two nut halves were clamped together in order to avoid any thread rotation (as shown in Figure 5.15), and the torque measured.

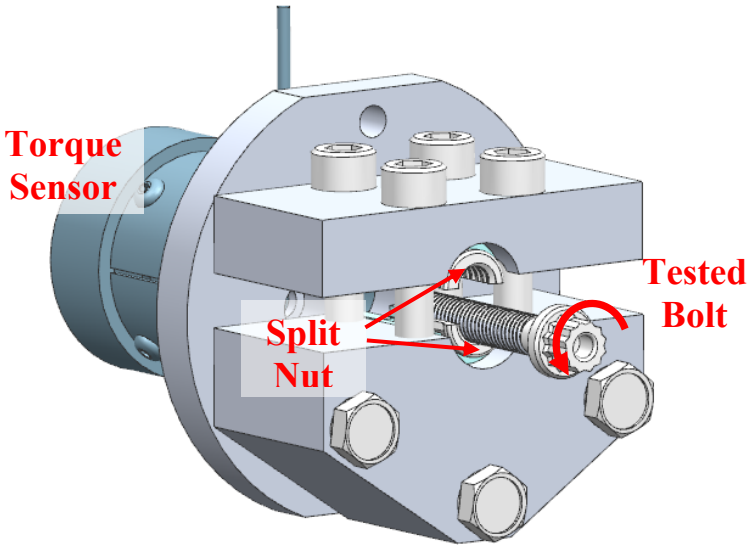

Figure 5.15: Torsional Test Rig

The test was done at room temperature, with bolts tested pre and post thermal cycle, once again at 760ºC for 50 hours. During post-processing, the resistance torque was plotted along with the angle of rotation, as shown in Figure 5.16.

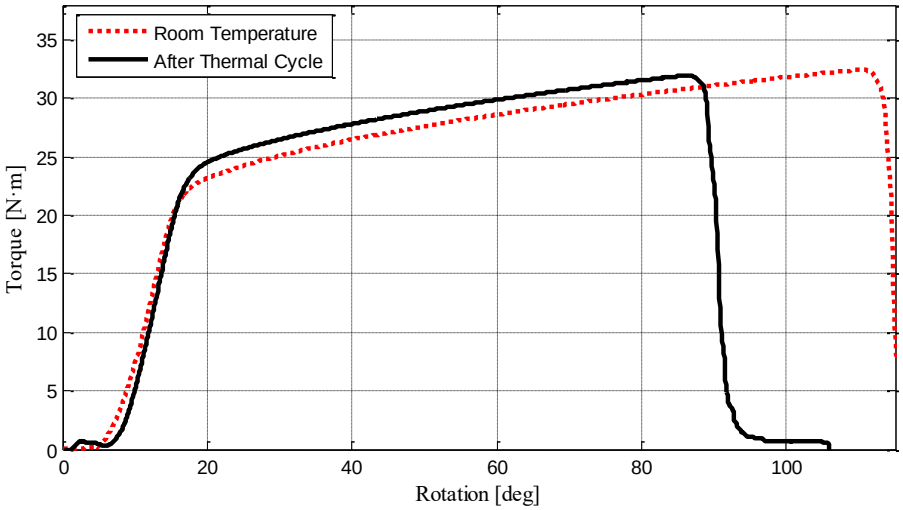

Figure 5.16: Torsional Test Result

As shown in Figure 5.16, the bolts start to plastically deform at 23 N·m, and fail at 32 N·m. It was found that the elongation reduced with the ageing cycle, as also seen in the literature (ASM International 2002). Additionally, the torsional test was validated using the Von Mises theory for a tension and torsion stress scenario (Equation (*5.1*) (Juvinall & Marshek 2006; Budynas & Nisbett 2010).

$$\sigma_x{}^2 + 3\tau^2 = S_y{}^2 \qquad (5.1)$$

As shown in the equation, for a purely torsional stress field (σ_x =0), the maximum shear stress is 0.577 σ_y, where Yield Strength (S_y) is 910 MPa for Waspaloy bolt (ASM International 2002). In case of failure, the Ultimate Strength is 1330 MPa, which gives a maximum shear stress of 780 MPa. Assuming the bolt as a bar, the shear stress due to the torsion was calculated using Equation (5.2, where T is the torque, J_p is the polar moment of inertia and d is the diameter (Juvinall & Marshek 2006; Budynas & Nisbett 2010).

$$\tau_{tors} = \frac{T\,r}{J_p} = \frac{16\,T}{\pi\,d^3} \qquad (5.2)$$

Using Equation (5.2, the maximum shear stress which the bolt can sustain breaking, calculated using the torque to break (32 N·m) and the mean radius (5.8 mm), is 783 MPa, in line with the maximum shear of the material previously calculated (780 MPa).

5.5.1.2 Joint Stress Analysis

The total torque required to tighten a bolt into a nut is the sum of four values as previously described in Section 2.1, which act differently on the bolt (Figure 5.17).

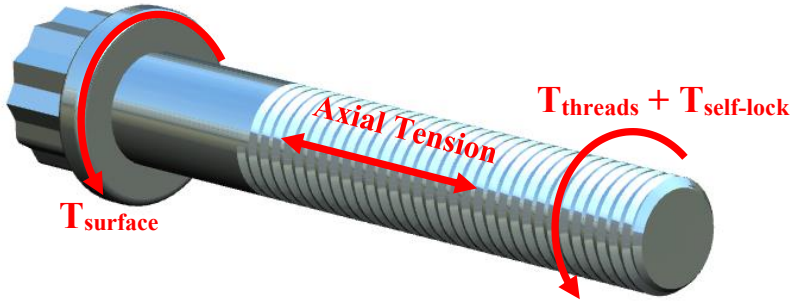

Figure 5.17: Force Diagram in the Bolt

The pitch torque, responsible for the axial tension on the bolt, is acting across the entire bolt shank, and the axial stress is calculated as:

$$\sigma_x = \frac{F}{Area_{sect}} \tag{5.3}$$

As shown in Equation (5.3, the axial stress is dependent on the clamping load and the cross sectional area, with the maximum value in the threads section, where the area is smaller.

The surface torque, the torque to overcome the friction in the bearing surface, is acting on the bolt head or on the nut depending on which part rotates. The torsional stress due to the surface torque is calculated using Equation (5.2, with the radius *r* being the bolt head diameter. As noted, the surface torque necessary to break the joint is higher than the thread torque, as the two act in different sections of the joint.

Two failure modes were identified in the broken joints; high CoF in the threads (Figure 5.18a), and high surface torque or severe seizure in the bearing surfaces (Figure 5.18b).

a) b)

Figure 5.18: Failure of Bolt: a) Torsion in the Threads b) Surface Torque

In Figure 5.18a, a deformed thread caused high CoF in the threads causing the joint to fail in the threaded section. On the other hand, Figure 5.18b shows a failure due to the surface torque, in particular a severe seizure between the spacer and the bolt head was seen in the preliminary test, when washers were not used in the assembly. A further schematic of the joints is presented in Figure 5.19 to summarise the failure modes.

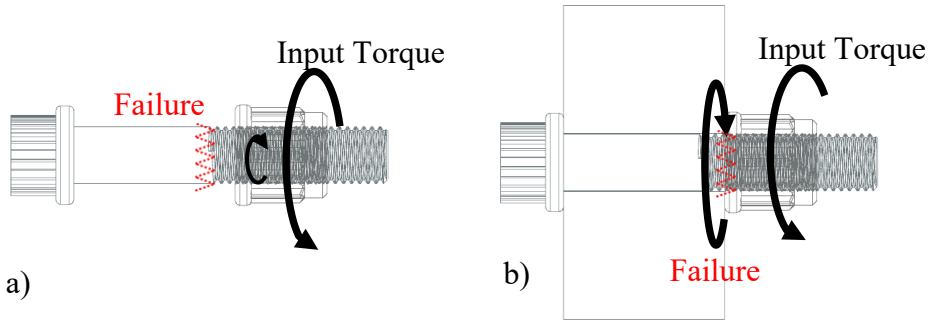

Figure 5.19: Schematic of the Failure Modes: a) Threads Friction and b) Bearing Seizure

As shown in Figure 5.19a, the high friction in the threads generates a resistance torque in the bolt, which leads to a failure of the bolt in the weakest section, at the start of the threaded part. On the other hand, in Figure 5.19b, the high friction in the bearing face generated high stresses which led to the failure of the joint in the torque application point, in the weakest component of the assembly, the bolt.

5.5.1.3 Alternative Coatings Analysis

During the bolt torsion test, the axial tension was not applied, thus in the thread friction limit analysis, the pitch torque was not taken into account. The resulting friction limit equation is a function of the clamping load, the resistance torque of the bolt, the self-locking torque and a geometrical factor as summarised in Equation (5.4.

$$\mu_{limit} = \frac{T_{limit} - T_{self-lock}}{F \cdot (r_1 \, cos\beta)} \qquad (5.4)$$

In Equation (5.4, F is the clamping load (varying from zero to11.6 kN), β and r_1 are geometrical factors from Rolls- Royce Design Standard JDS 829_03 (Rolls Royce 2011), 30º and 2.823 mm respectively. T_{limit} is the Yield or the Failure torque experienced in the torsion test, which is in the range of 22 to 25 N·m for the Yield and

28 to 32 N·m for the failure of the bolt. Finally, $T_{self\text{-}lock}$ was assumed in the range of 0.5 to 3 N·m, as typical values experienced in the experiments.

The Yield and the Failure areas were plotted along with the clamping load, with the values of coefficient of thread friction of the coatings and the paints experienced after the thermal cycle (Figure 5.20). The upper and the lower bounds of the failure and yield area were obtained using the minimum and maximum values of the self-locking torque and the failure or yield torque obtained in the torsional test.

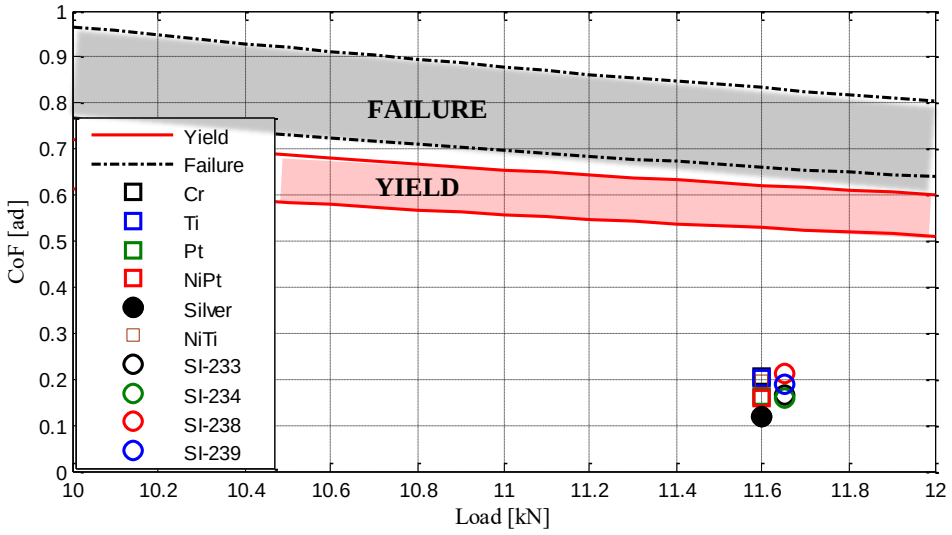

Figure 5.20: CoF Limits

As shown in Figure 5.20, none of the alternatives were in the failure zone, while the pure Chromium and pure Titanium were considerably close to the Yield zone. However, as noted in the graph, the Yield curve is dependent on the clamping load and the above mentioned films intersect the curve only at the end load. At approximately 10.5 kN, all the coatings are below the Yield curve. In reality, during the untightening, this clamping load is achieved in a fraction of a second.

Additionally, comparing the results with the silver plating, all the alternatives, apart from the paints SI-233, SI-238 and SI-239, increase the risk of yielding and failure in the joint.

Finally, as seen in Section 5.3.2.2, the CoF in the threads for the majority of the alternatives was found to be higher after the thermal cycle compared to the room temperature test. Thus, this analysis mainly aimed to analyse the friction post-ageing conditions, as the friction at room temperature was significantly below the Yield curves, as shown in Figure 5.21, and therefore did not pose a significant risk of failure in any case.

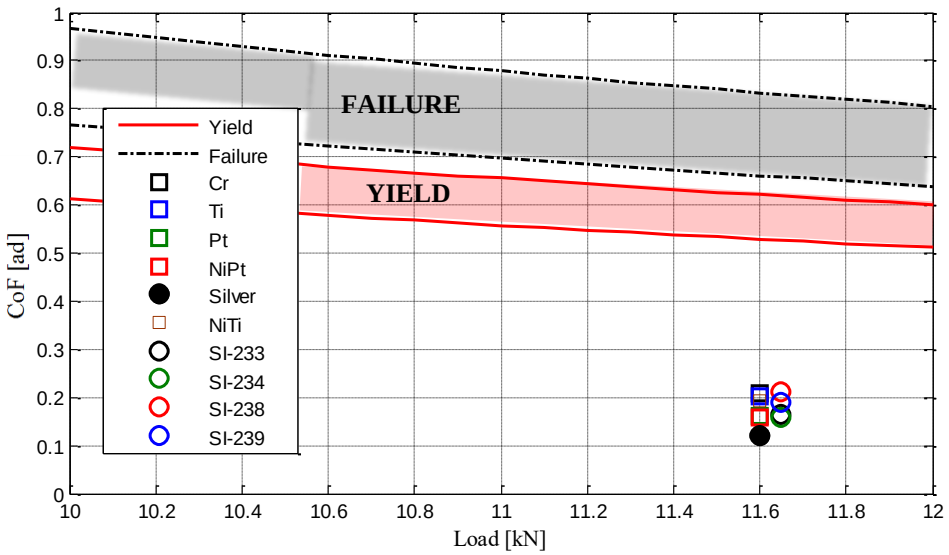

Figure 5.21: Friction Limits: Pre-Ageing

5.5.2 *Comparison with the Silver Coating*

The three successful coatings, pure chromium, pure titanium and Nickel-Titanium, were further analysed and compared to the currently used silver coating. Thus, the CoF, the hardness and the roughness pre and post thermal treatment were summarised in Table 5.6.

COATING	CoF Pre-ageing	CoF Post-ageing	Hardness Pre-ageing [GPa]	Hardness Post-ageing [GPa]	Roughness Behaviour with Ageing
Silver	0.12	0.23	1.9	0.8	Increase
Pure Chromium	0.21	0.50	5.9	3.6	Increase
Pure Titanium	0.20	0.54	4.7	2.4	Increase
Nickel - Titanium	0.19	0.32	4.6	4.8	Increase

Table 5.6: Alternatives Summary

As shown in Table 5.6, similarly to the silver coating, the pure metal coatings (Pure Chromium and the Pure Titanium) experienced a softening behaviour during the heat treatment, increasing the roughness and doubling the CoF. As previously stated in Chapter 3 for the silver, the softening of the coating causes the coating to be removed

from the threads during the screwing, and the CoF to increase, due to a like on like couple being formed.

Furthermore, the Nickel-Titanium multi-layer coating, as investigated by Liu & Duh (Liu & Duh 2008) in their work comparing different percentages of the two materials in thin films at high temperatures, showed an increase in hardness with the temperature up until 823ºK (550ºC), where the softening started, due to grain growth. Thus, the softening of the coatings after the heat treatment at 760 ºC was found to be the cause of the increase of CoF in the threads.

5.6 SUMMARY

Different coating alternatives were examined in order to replace the silver coating in aerospace fasteners, and summarised as follows:

- The 19 alternatives identified at the beginning of the work were reduced through a selection procedure to three which were pure chromium, pure Titanium and Nickel-Titanium, which successfully passed the test and the aerospace requirement. The unsuccessful alternatives have shown an inconsistency in the test result or were found unfeasible in terms of cost.
- The three successful alternatives, similarly to the silver coating analysed in Chapter 3, were found to be affected by the heat treatment. In fact, the increase of friction was found to be driven by the softening of the coatings, as highlighted by the nano-hardness test performed before and after the heat treatment.
- Analysing the importance of the joint failure due to the CoF in the threads, it was found that a low level of yield might be reached in the case of the thin films of Chromium and Titanium. However, the joints in aerospace applications are re-used exclusively during engine assembly. In fact, after a thermal cycle, the joints are replaced, such as during engine maintenance.
- In this work a selection procedure has been drawn, in order to understand the alternatives. However, more test samples are needed to validate the results obtained as in this study only few test repeats were performed due to shortage of samples. Furthermore, new materials and in particular alloys using the successful coatings can be investigated.
- From the coating selection, the cost of the coating materials was found to be the most important factor. In fact multiple alternatives, such as Platinum films

and SI paints, were removed from the list even if they successfully passed the tests. However, as cost and coating technologies are in continuous evolution, a future recovery is not unreasonable.

CHAPTER 6

ALTERNATIVE LOCKING DESIGN

6.1 INTRODUCTION

In Chapter 4 a FEA approach was developed to analyse the tightening process of silver coated joints, in order to examine the stresses and the contact pressure along the elliptical self-locking nut. The gradual decay in the locking torque of the coated joints over multiple reuses was attributed to plastic deformation in the threads and a severe removal of the silver coating caused by high contact pressure in the crimped section. Thus, in this chapter a new self-locking design will be investigated in order to solve these problems.

As seen in the literature, and previously described in Section 2.3, numerous self-locking features are available on the market, with most of them designed to deform elastically to prevent loosening. For example, the widely used elastic Nylock nuts use a nylon collar inside the standard nuts, which can deform elastically. It was found that the collar increases the CoF between the nut and the bolt threads, inducing an anti-loosening effect, as confirmed by the work of Kumar et al (Kumar 2014). However, the material of the collar can sustain a maximum temperature of 121 ºC, rendering them infeasible for high temperature applications. Furthermore, in the work of Zhang et al (Zhang et al. 2000) a FEA approach was used to develop a new locking design, which utilized shape memory alloys. These alloys deform elastically and prevent vibrational loosening. Despite the fact that the maximum operating temperature for aerospace applications is not mentioned in the study, the FEA approach was found to be promising. Additionally, a successful example of elastic locking design is shown in the work of Miyata et al (Miyata et al. 1991) which developed a new self-locking feature using a ‘skirt-like’ hollow flange for hexagonal nuts in order to effectively reduce loosening under vibrations. The FEA approach discussed in this work shares similarities with the work of Izumi et al (Izumi et al. 2005) which aimed to verify and expand conventional fastener theories. In their work they affirm that FEA can be successfully used to identify and analyse new self-locking features, and also suggest

that anti loosening systems can be obtained by modifying the fastener's design, supporting the findings of Junker (Junker 1969).

In the elliptical self-locking feature currently used in the aerospace industry and analysed in Chapter 4, the crimped area includes high contact stresses, localised in the small segment of the diameter. The scope of the work presented in this chapter is to develop a new locking design in order to distribute the contact stresses along the entire diameter. However, it should be simple, reliable and similar to the current design, suitable for harsh environments and light in weight. The aim is to explore whether a similar locking torque can be achieved by alternative manipulation of the threads, whilst still providing the self-locking torque required. Thus, the new design should operate within a lower stress field, with the silver coating less likely to be stripped off. Furthermore, the lower stress might allow alternative coatings to be used, which are currently not applicable at the current contact stresses. Finally, elastic deformation will also be an advantage with regard to multiple reuses for high temperature applications.

6.2 DESIGN & SIMULATION

6.2.1 *Design Concept*

In Chapter 4 the FEA approach was used to analyse the contact stresses in the elliptical self-locking nut, showing similar load and torque curves with respect to the experimental results. As previously described, the bolt, nut and load cell were modelled using the actual dimensions, with the nut screwing into the bolt for eight revolutions before clamping the load cell. In this chapter, instead of using a radially deformed nut, such as the elliptical shape typically utilised, an axial deformation in the nut is modelled, in order to distribute the contact pressure in the entire diameter of the threads.

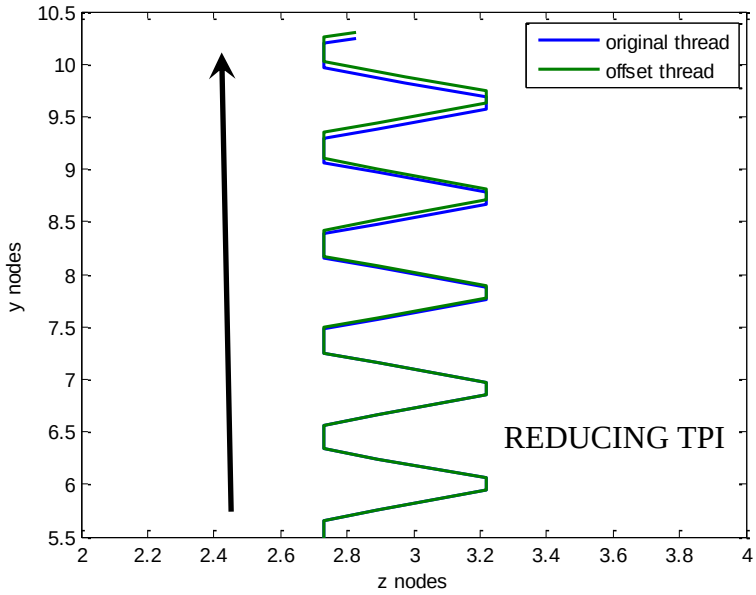

Figure 6.1: Nut Threads Axial Displacement: Stretching

As shown in Figure 6.1, a positive axial displacement stretches the nut, reducing the TPI, defined as 'threads per inch'. The deformation causes a tight contact between the bolt and nut threads, resulting in a locking system. Once the joint is tightened, it elastically deforms to accommodate the load, as shown in Figure 6.2.

The axial displacement has been applied over one, two, three and four threads at the chimney of the nut. In fact, in this section the nut wall is thinner, which allows the deformation to occur in the nut and not in the bolt.

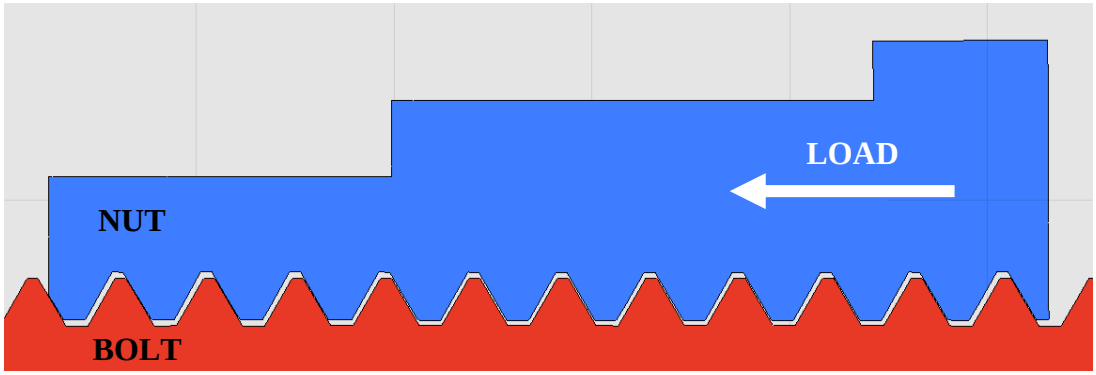

Figure 6.2: Bolt and Nut in Contact

One of the key requirements of the analysis is the self-locking torque, measured as the resistance torque prior to the clamping step. The ideal self-locking torque as specified in the Aerospace Standard nº128 (The Society of British Aerospace Companies Ltd 2006) should be approximately 2 N·m, so that an upper limit of 2.5 N·m and a lower limit of 1.5 N·m is applied. Additionally, as previously stated, it is preferable

to remain in the elastic range throughout the entire screwing process, in order to avoid any plastic deformation, allowing the joint to be re-used multiple times.

6.2.2 *Modelling Approach*

As previously described in Section 4.4, Solidworks 2012 was used to design the joint while Hypermesh v.11 (Altair 2013a) was used as a pre-processor, where the ¼" (6.35 mm) joint along with the load cell were meshed with a total of 87,500 nodes and 235,000 elements. The geometry was then imported into Matlab, and the coordinates of the nodes in the inner helix were identified. An axial displacement was applied to these nodes and all the nodes above, in order to maintain the thread angle of 60º (Figure 6.3). As the nut chimney is approximately 4 mm and the pitch is approximately 0.91 mm, the maximum number of threads moved is four, while the minimum investigated is one, the last revolution.

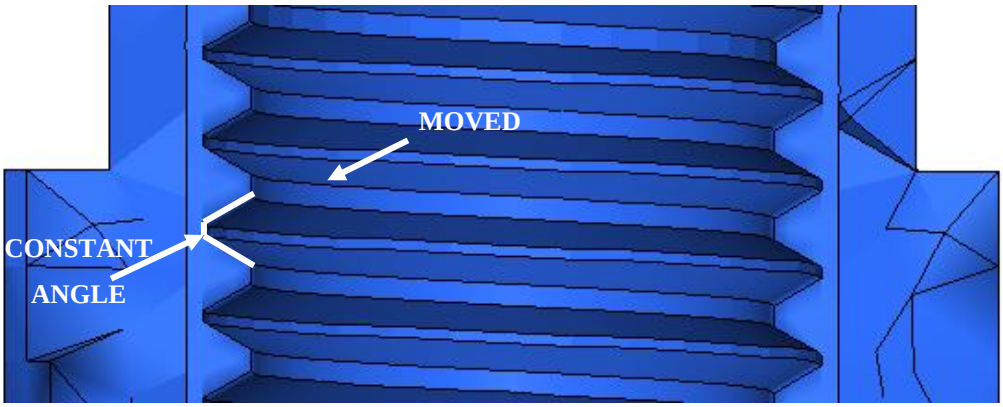

Figure 6.3: Axial Displacement

The steps defined in Chapter 4 are adopted again in this work, with the only exception being the crimping step. In fact, the elliptical deformation applied in the crimping step is not utilised in this work, as the axial deformation is previously applied during pre-processing as described above. The analysis is essentially a two steps process. Firstly the nut screws into the bolt for eight revolutions, and secondly the nut clamps the load cell until the required end load is reached. As in Chapter 4, the material used to define the bolt and the nut is Waspaloy, with an Yield strength of 897 MPa, obtained from the true strain true stress curve (ASM International 2002).

One of the input parameters in the model is the friction behaviour of the surfaces in contact. As clearly defined in Section 4.3, the relationship between the contact pressure and the CoF in the threads was analysed through the pin on disc tests and is again utilised in this simulation. As previously described, the pin on disc testing was

done using a silver coated disc and an Inconel pin in a range from 50 to 1,500 MPa, in the presence of lubricant. Finally, the thermal and tightening speed effects are not taken into account, with the aim of reducing the solving time, as the simulations already took 3-4 days each to solve in the University cluster.

Afterwards, the results were analysed using Hyperview (Hyperworks) (Altair 2013b), and in particular the Von Mises stresses and the contact pressure in the threads were examined, along with the torque and load profile.

6.2.3 *Results & Selection for Manufacture*

The approach explained in Section 6.2.1 was initially explored by Guy (Guy 2015), as a final year project. This project was linked to this PhD, and the student used the previously created model under supervision. The study ran over forty simulations, using the previously defined model and a macro to simply apply the displacement to the threads. From this several promising results were obtained, as shown in Figure 6.4, which were further examined to higher accuracy in this work. The self-locking torque is plotted against axial displacement for a number of tests under a range of 'threads moved' (Figure 6.4).

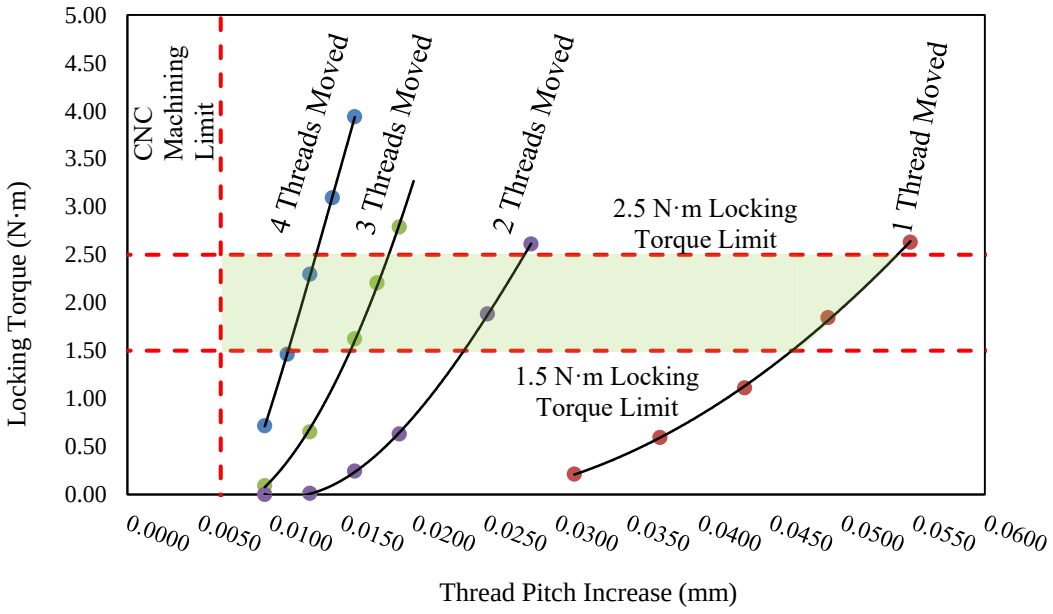

Figure 6.4:Self-locking Torque for Different Candidates (Guy 2015)

As shown in Figure 6.4, self-locking torque increases with the axial reduction (decreasing TPI), and with the number of threads moved. Thus, to achieve the same result moving less threads, a bigger displacement was required. In the Figure, a CNC machining limit was imposed, as a standard CNC milling machine allows an error of

10 µm over a linear displacement of 170 mm (Guy 2015). Thus, in a linear displacement of 3.9 mm (the length of the chimney), the smallest reduction that can be physically manufactured was 0.00654 mm, which had no effect in the final selection. A further limit was the stress value at which the silver starts to strip (750 MPa (Section 4.7.3)).

Based on the work of Guy, four cases were identified and further explored with respect to the nature of the threads contact.

In order to convert the linear displacement to the actual TPI value, Equation (*6.1* was used.

$$TPI_{new} = \frac{mm/inch}{\left(\frac{mm/inch}{TPI_{old}} + displ\right)} \tag{6.1}$$

where *mm/inch* is the conversion between millimeters and inches (25.4 mm/inch), the TPI_{old} is the standard 28TPI (UNF ¼" (6.35 mm)) and *displ* is the axial displacement in mm.

The selected candidates are summarised in Table 6.1.

Candidate	**TPI_{new}**	**Threads Moved**	**Self-locking Torque**
1	27.65 TPI	4	1.5 N·m
2	27.60 TPI	4	2.3 N·m
3	27.5 TPI	3	1.9 N·m
4	27.25 TPI	2	1.9 N·m

Table 6.1: Variable Pitch Candidates

In Table 6.1 the four candidates selected are summarised, including the self-locking torque experienced in the simulations. Additionally, candidate 3 shown in Table 6.1 is the combination of two models, which gave a thread deformation of 27.47 and 27.52 TPI, which are rounded to 27.50 TPI. As previously anticipated, in order to achieve the required self-locking torque with fewer threads moved, a larger axial

displacement is necessary, as highlighted in Table 6.1. The stresses and the contact pressure at zero load and at the end load of 11.6 kN for the Candidate 1 are extrapolated and presented in Figure 6.5 and Figure 6.6.

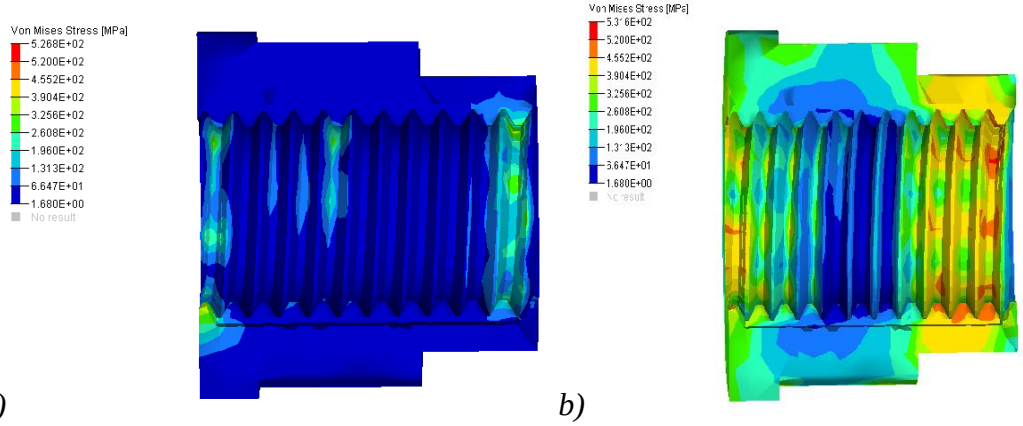

a) *b)*

Figure 6.5: Stress along the Nut. a) At Zero Load b) At End Load (Candidate 1: 27.65 TPI)

In Figure 6.5 the Von Mises stresses are shown at zero load (Figure 6.5a) and at the end load (Figure 6.5b), highlighting that the maximum stresses do not exceed the Yield strength (of 897 MPa). Furthermore, it is evident that the nut is subjected to a level of stress even at zero load, thought to be due to the interaction between the 28 TPI bolt and the deformed nut threads, generating the resistance torque. Additionally, the stresses experienced were lower compared to the elliptical nut observed in Section 4.6, where a stress value of 990 MPa was identified. This comparison will be further analysed in Section 6.5.3.

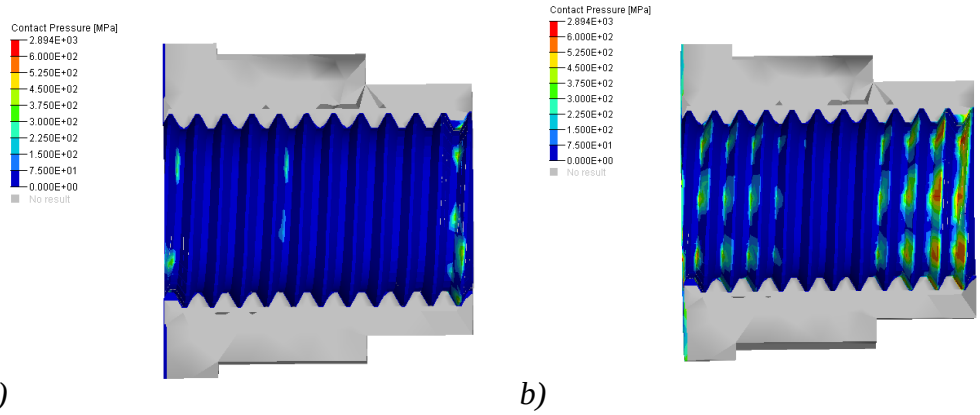

a) *b)*

Figure 6.6: Contact Pressure along the Nut. a) At Zero Load b) At End Load (Candidate 1: 27.65 TPI)

In Figure 6.6 the contact pressure field is shown at zero load (Figure 6.6a) and at end load (Figure 6.6b), highlighting that the contact pressure increases throughout the

tightening process. Additionally, a non-uniform pressure distribution was identified, due to the geometrical modelling and the contact algorithm utilised by the software (Kloosterman 2002). This effect was also seen and examined in Chapter 4, as both the bolt and the nut were modelled as polygons, interacting with each other with a limited impact to the results.

Furthermore, in Chapter 4 a contact pressure of 750 MPa was identified as the cause of the stripping of the silver from the substrate. As shown in Figure 6.6b, the contact pressure never exceeds 600 MPa here, which will be further investigated in Section 6.5.3, where the elliptical crimp results will be compared to the axial deformation result. The alternative candidates defined in Table 6.1 showed similar results as summarised in Figure 6.7 and are presented in APPENDIX C.

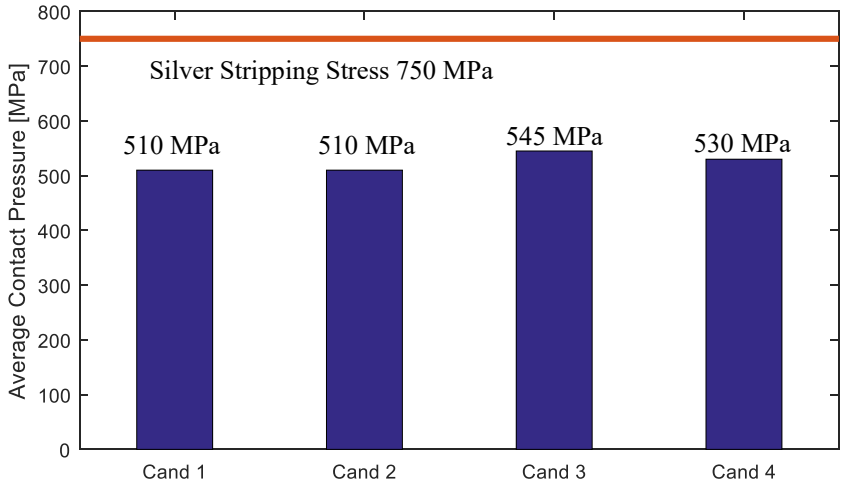

Figure 6.7: Average Contact Pressure at the End Load

As shown in Figure 6.7, the four candidates experienced an average contact pressure lower than 750 MPa, the stress value at which the silver coating removal begins. The four candidates were found similar, due to the contact pressure being evenly distributed over a large area, with the small pitch difference playing a minor role.

In order to further examine the elastic behaviour of the joint, the strain in the nut at the end load is analysed and plotted in Figure 6.8.

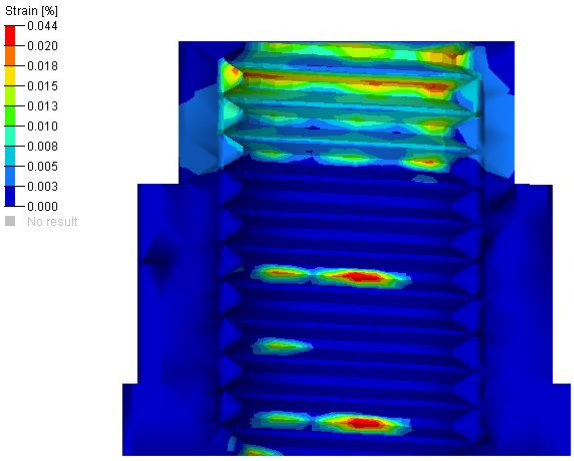

Figure 6.8: Residual Strain at End Load

As shown in Figure 6.8, the residual strain was found to be lower than the elastic limit of 0.2%, which means that an elastic behaviour is theoretically achieved. Thus, the joint can be re-assembled multiple times without inducing plastic deformation, and with the stresses distributed across the entire diameter instead of having peaks in a small portion of the crimped section, as shown in Section 4.6.

6.2.4 ***Further Analysis***

Two additional analyses were performed with the purpose of further investigating the manipulation of threads, such as the thread offset and the TPI increase (Figure 6.9).

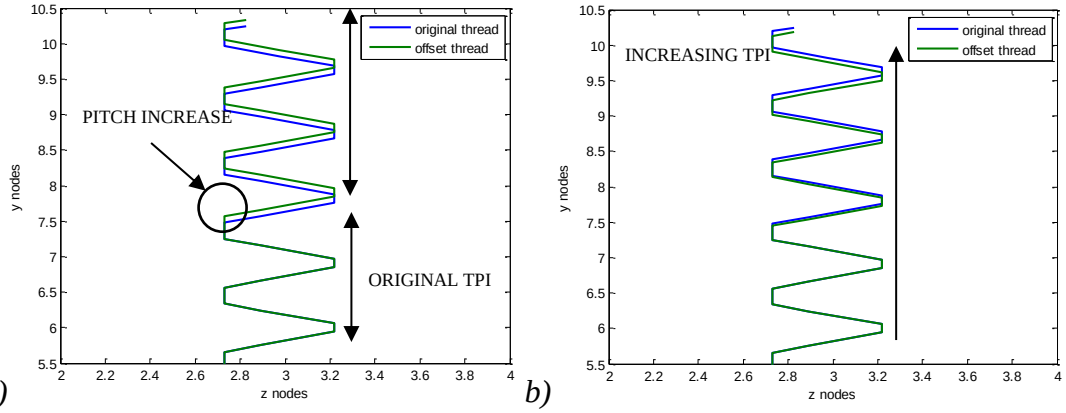

a) *b)*

Figure 6.9: (a) Pitch Offset and (b) TPI Increase

A pitch offset (Figure 6.9a) is a single axial displacement in one of the threads at the nut chimney. In practise, the TPI changes for a revolution and then goes back to normal. However, two problems were found to affirm that this option is not feasible. Firstly, compared to the 'stretching' method, a larger deformation is necessary in order to achieve the 2 N·m self-locking torque required (0.045 mm compared to

0.025 mm in the stretching), and since this displacement is applied to a single thread, it generates stresses which exceed the material yield limit. Secondly, considering future large scale production, the thread geometry may be difficult to machine, end in fact, at this moment a tool capable to precisely and quickly machine this design has not been identified.

In the second scenario (Figure 6.9b) the principle is the same as the decrease of TPI previously discussed, applying an axial deformation in the last threads in order to achieve the self-locking torque required. Instead of 'stretching' the nut, a negative displacement is applied, thus 'squashing' it. However, high stresses are generated in the joint during screwing on, as high as 850 MPa compared to the 530 MPa in stretching (Figure 6.10). Thus, for this reason the TPI decrease has been preferred in this work. However, as explained in Section 7.3 a future evaluation is needed in order to fully evaluate the design.

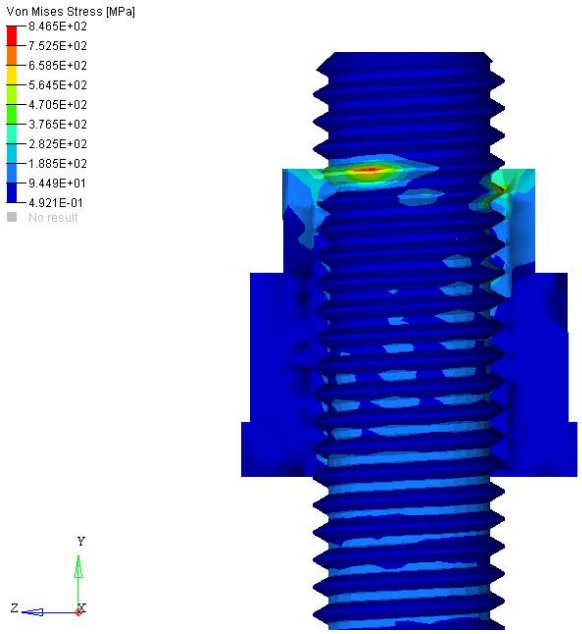

Figure 6.10: TPI Increase

6.3 MANUFACTURE

Following the candidates identified by Guy (Guy 2015) and subsequently explored in Section 6.2.3, the test samples were manufactured. In this section the machining process is described, including development of the g-code program, followed by the CNC machining and finally the application of the silver coating.

6.3.1 *Manufacturing Process Development*

The four candidates (Table 6.1) that meet the requirements have been machined with a CNC vertical milling machine. The g-code files required by the machine, controlled by Siemens software (Siemens 840D ShopMill Control), have been written using the software Vero Edgecam 2015. Five different programs were developed in order to machine the external nut shape and the four different candidates.

In the first program, the hexagonal shape was obtained from a ½" (12.7 mm) bar. The hex shape was designed using Solidworks 2012, and then imported into Edgecam. The nut dimensions were similar to the silver nuts previously tested (Section 3.2.2) with the only difference being the simplified hexagonal shape (9/16" (14.29 mm)) instead of the double hexagonal (12 points), due to the machining equipment.

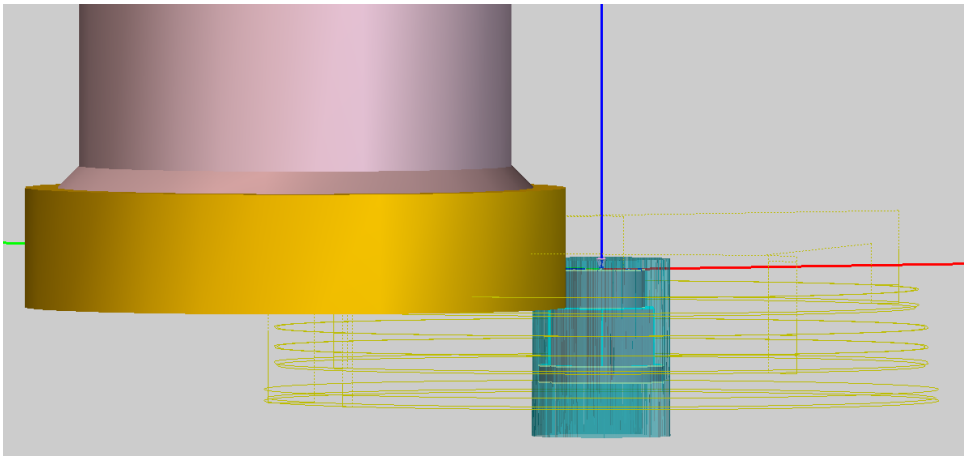

Figure 6.11: Hexagonal Shape Program

In this program a 50 mm shoulder milling cutter with 90º inserts was used. Firstly, the top of the bar was machined flat. The second operation was roughing, in order to machine the external shape, consisting of a 3.5 mm high top circle, followed by the 5 mm high hexagonal shape, and the 1.5 mm bottom circle. These were executed through seven passes, with a maximum cutting depth of 2 mm. The bottom circle was extended for 5 mm, in order to allow the nut to be latterly cut. The finishing operation was deemed necessary as the inserts at this point were found to be damaged. As such, the cutter was lifted from the work piece and the program paused, allowing the technician to change the inserts. Thereafter, a 0.2 mm finishing operation was performed, in order to achieve the right size and a suitable surface finish.

Additional programs were developed to define the machining processes for the internal threads. The only differences between the four programs are the pitch size

and the number of the threads deformed. For this operation the nut, previously cut from the bar was positioned upside down, with the standard 28 TPI side facing up in order to check the thread size in situ.

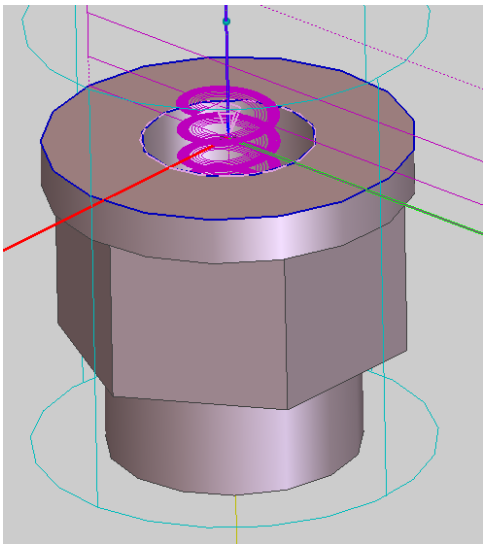

Figure 6.12: Threading Program

Prior to commencing this second sequence of machining operations, the bottom of the nut was cleaned using the 50mm cutter previously used, in order to clean the surface and achieve the required thickness. A 5.5 mm drill was used to make the internal hole, using speeds and feeds from the tool manufacturer, as further detailed in Section 6.3.2. After drilling, the tool was lifted 200 mm in order to check the drill and the hole conditions. After this a single point threading tool was used, to perform the internal threads. The tool geometry was defined within the program and the machining of the two different helixes designed, one for the standard thread size and the other depending on the thread candidate (Table 6.1). From a starting diameter of 5.5 mm to the maximum internal diameter of 6.35 mm, both helixes were machined in 6 passes. The cutting pass along with the feed rate and the spindle speed were once again specified in the program, based on suggestions from the tool manufacturer.

6.3.2 ***Machining***

A 1060 HS VMC, 3-axis CNC vertical machine was used to machine the nuts, as presented in Figure 6.13.

Figure 6.13: CNC Machine 1060HS VMC

The nuts were made from Inconel 718, as were the standard nuts tested in the previous chapters. Inconel 718 has similar properties to Waspaloy, the other nickel super-alloy adopted in this work, but is easier to machine. The external shape was manufactured using a 50 mm Walker shoulder mill, F4041, and WSM35S inserts (4 teeth and 4 cutting edges per insert) (Figure 6.15a). As previously described, the inserts were as expected found to be deteriorated at the end of the roughing operation, and thus replaced for the finishing operation. Thereafter, the nuts were parted off and cleaned using a lathe, with the result shown in Figure 6.14.

Figure 6.14: Finished Hexagonal Shape

The second g-code program was used to drill and tap the nut, using a different program for each candidate (Table 6.1). A 5.5 mm CoroDrill Delta-C solid carbide drill (Sandvik Coromant R840-0550-30-A0A 1220, Figure 6.15b), was used to drill the nut. As this type of drill is self centering, a centre spot drill was not utilized. After cleaning the hole, the internal threads were manufactured using a grooving tool,

Supermini Type 105 from Horn Cutting Tools Ltd (Figure 6.15c). As previously stated, the cutting parameters were defined in the g-code program, following the tool manufacturers suggestions as summarised in Table 6.2.

Tool	**Cutting Speeds**
Shoulder Mill Walker F4041	Cutting speed= 35 m/min, 0.1 mm/rev/tooth. Spindle speed= 223 rpm Feed rate= 90 mm/min.
Drill Sandvik Coromant CoroDrill Delta-C	Spindle speed= 1,160 rpm Plunge feed= 92.6 mm/min
Single point threading tool Horn Cutting Tools Supermini Type 105	Spindle speed= 2,000 rpm Feed rate= 32 mm/min.

Table 6.2: Cutting Parameters

The internal threads were initially machined in six passes, using two different spirals as previously explained. The standard threads were positioned facing up, in order check the internal fit. As the tool was found to be deflected by the workpiece, resulting in incorrect machining, further passes were performed upon checking the depth of the threads with a standard ¼" (6.35 mm) bolt. Up to five additional spring passes (0.025mm each) were required in order to reach the necessary fit. This fit variability was due to the poor machinability of the Inconel and the low stiffness of the threading tool, as further examined in Section 6.5.4.

Figure 6.15: Cutting Tools: a) Walker shoulder mill F4041, b) Solid Carbide Drill 5.5 mm, c) Supermini Type 105

During all the operations described above, the coolant (Castrol Hysol MB 50, concentration 7%) was used, in order to reduce the temperature of the workpiece and the cutting tools. A machining time of 90 minutes was required to manufacture each candidate. Finally, the nuts were cleaned to remove residual swarf and prepare for the coating to be applied.

6.3.3 *Coating*

12 nuts were machined in total, three for each different candidate (Table 6.1). The nuts were shipped to a coating company and were electroplated with silver. The silver coating had a thickness of 5 microns, in order to be comparable to the generally used nuts described in Chapter 3.

Figure 6.16: Machined Coated Nut

Figure 6.16 shows a machined nut after the silver coating was applied. Thus, the candidates were tested and compared to the elliptical nuts.

6.4 TESTING RUSULTS

Three samples of each of the four candidate nuts (Table 6.1) were tested using the procedure explained in Section 3.2.3.2 and used extensively in this work. The nuts were tested at room temperature for six tightening cycles using Inconel bolts (AS48824, Section 3.2.2) as counterparts. Mobil Jet Oil II and the thrust bearing were once again applied, along with a rotating speed of 3 rpm during wind on/ off and 0.5 rpm during the loading/ unloading. The end load reached during the test was 11.6 kN (as per Rolls- Royce Design Standard JDS 829_03 (Rolls Royce 2011)) and torque, load and position were acquired at 200 Hz. Afterwards, the condition of the silver coating was analysed and the experimental results were compared with the FEA prediction.

In the experimental test, three types of result were identified in the twelve nuts tested, as summarised in Table 6.3, with no immediate correlation between geometry and failure observed, as further detailed later in this section.

Candidate	Condition		
	SAMPLE 1	**SAMPLE 2**	**SAMPLE 3**
1 (27.65 TPI)	Successful (1A)	Successful (1B)	Failed (1C)
2 (27.60 TPI)	Successful (2A)	Deformed (2B)	Failed (2C)
3 (27.50 TPI)	Successful (3A)	Successful (3B)	Deformed (3C)
4 (27.25 TPI)	Successful (4A)	Deformed (4B)	Failed (4C)

Table 6.3: Testing Results

Firstly, three joints failed (1C, 2C, 4C), as the failure torque of 28-30 N·m (previously seen in Section 5.5.1) was reached during the first wind on (Figure 6.17).

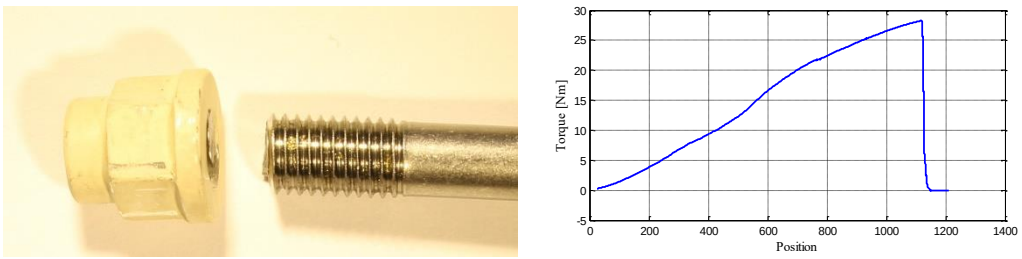

Figure 6.17: Failed Test: a) Broken Joint and b) the Torque Profile (Sample 2C)

As shown by the example result from sample 2C, in Figure 6.17b, the torque linearly increased until 28 N·m, when a sudden drop indicated the failure of the joint (Figure 6.17a). As further examined in the following sections, the high torque was generated by the tight fit of the machined threads.

Three other joints (2B, 3C, 4B) experienced a high self-locking torque during the first wind on (up to 22 N·m), damaging the internal and external threads (Figure 6.18a). However, the joint did not fail as above and the self-locking torque eventually reduced in the subsequent cycles (Figure 6.18b).

a) 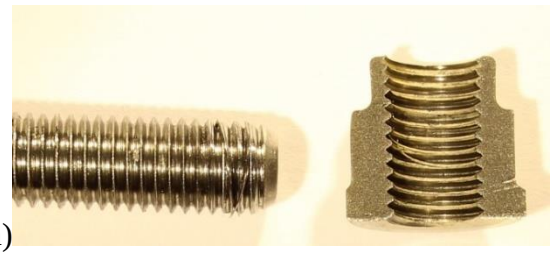 b) 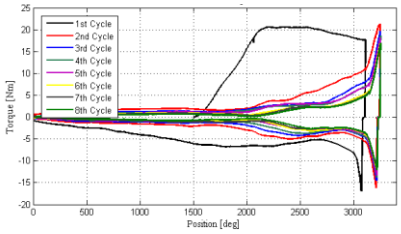

Figure 6.18: Damaged Joint: a) Deformed Threads (Sample 4B) and b) the Torque Profile (Sample 4B)

As shown by the example result from sample 4B in Figure 6.18b, in the first cycle a wind on torque of 20 N·m was reached, and the final clamping was not performed, in order to avoid any further damage. In the second cycle, the self-locking torque dropped to 10 N·m and the final clamping was then completed. During the following cycles, the self-locking torque continued to reduce, eventually stabilising at 5 N·m in the sixth cycle. A further two cycles were performed in order to prove the elastic behaviour following the initial plastic deformation in the first cycles.

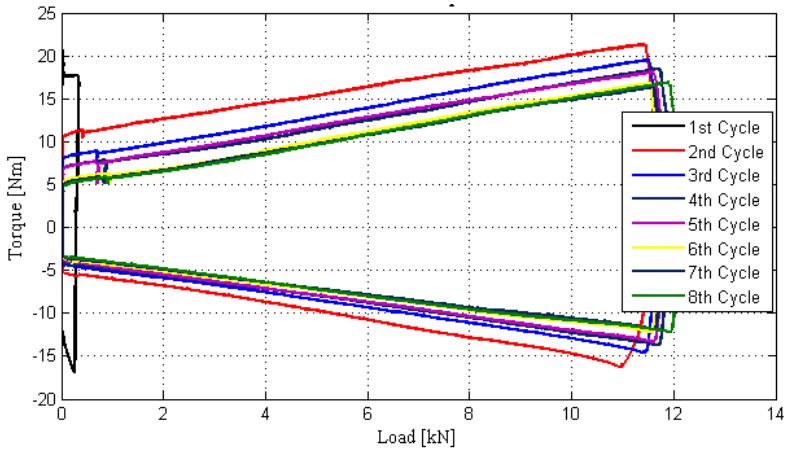

Figure 6.19: Load versus Torque: Elastic Behaviour (Sample 4B)

The remaining six joints (1A, 1B, 2A, 3A, 3B, 4A) successfully completed the six cycle test, and the torque profile and load-torque curve have been plotted in Figure 6.20 and Figure 6.21.

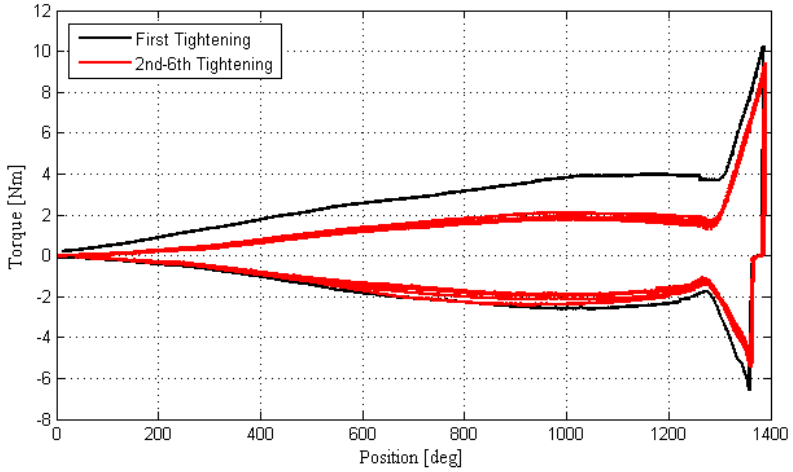

Figure 6.20: Self-Locking Torque (Sample 3A)

As shown by sample 3A given in Figure 6.20 as an example, the torque in the first cycle was found to be higher compared to the remaining cycles, where a highly repeatable torque was achieved. Additionally, the 2 N·m locking torque predicted by

the FEA was verified in the test, as further examined in Section 6.5.1. Furthermore, the self-locking torque gradually increased until a stabilization, in contrast with the sinusoidal pattern experienced with the elliptical nuts (Section 3.3). This aspect will be further detailed in Section 6.5.3, where the new design will be compared to the typical elliptical shaped nuts.

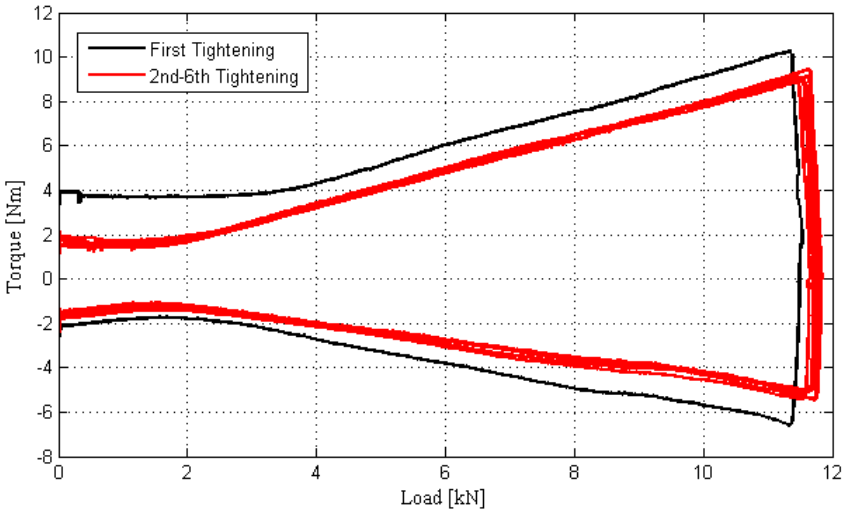

Figure 6.21: Load versus Torque (Sample 3A)

As further shown for the successful joints in Figure 6.21 and Table 6.4, the first cycle experienced a higher torque compared to the successive cycles, followed by high repeatability in the subsequent cycles, proving that elastic deformation was achieved, as shown in Table 6.4.

Sample	**Tightening Torque at End Load[N·m] (Self-locking Torque [N·m])**					
	1st	2nd	3rd	4th	5th	6th
1A(27.65TPI)	10.75 (5.2)	9.83 (3.2)	9.90 (3.0)	9.62 (2.9)	9.69 (2.8)	9.63 (2.6)
1B(27.65TPI)	9.80 (3.1)	9.27 (1.1)	9.26 (0.9)	9.18 (0.9)	9.25 (0.8)	9.10 (0.8)
2A(27.60TPI)	10.66 (2.5)	10.18 (1.2)	10.00 (1.0)	9.50 (1.0)	10.18 (0.9)	10.0 (0.9)
3A(27.50TPI)	10.25 (3.8)	9.13 (1.9)	9.42 (1.7)	9.13 (1.5)	8.95 (1.5)	8.99 (1.5)
3B(27.50TPI)	10.61 (5.1)	9.44 (2.7)	9.29 (2.1)	9.02 (1.9)	9.12 (1.8)	9.98 (1.8)
4A(27.25TPI)	11.63 (3.7)	9.82 (1.2)	9.80 (1.1)	9.80 (1.0)	9.81 (0.9)	9.80 (0.9)

Table 6.4: Torque at End Load for the Successful Nuts

As previously highlighted, the three behaviours described could not be linked to a specific thread geometry, as the three failed joints are from different candidates. Similarly to the higher torque experienced in the first cycle, this variance was likely a product of the manufacturing process and will be further discussed in Section 6.5.4. After testing the nuts were cut with the EDM technique in two halves, and the silver coating conditions analysed, as performed previously in this work.

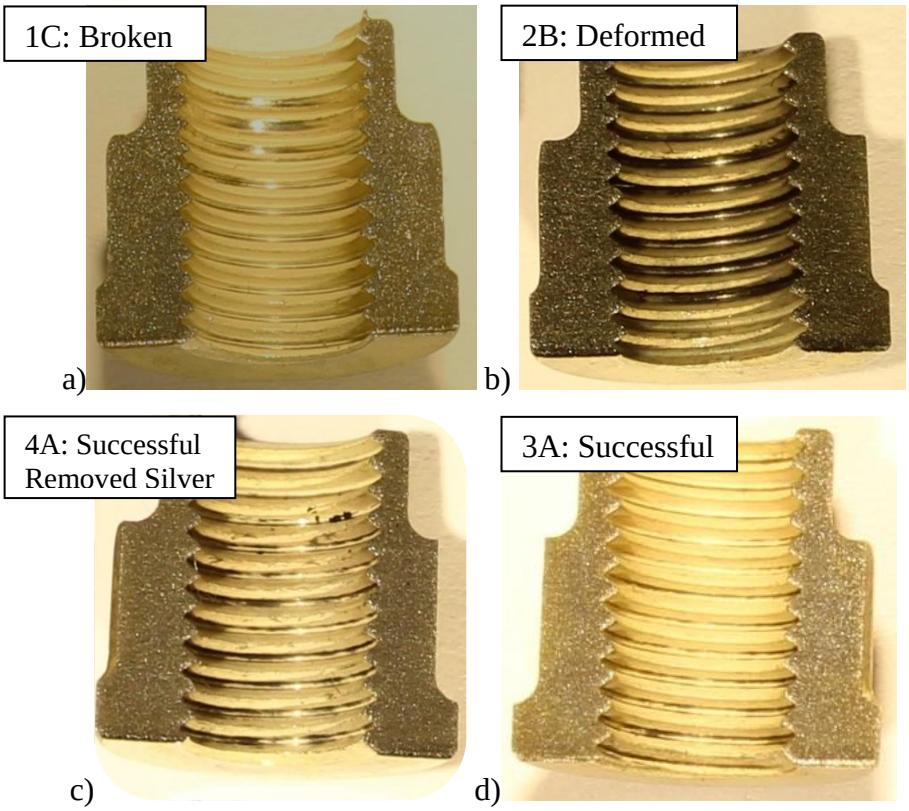

Figure 6.22: Coating Conditions: a) Broken Joint (Sample 1C), b) Deformed Joint (Sample 2B), c) Removed Silver (Sample 4A), d) Intact Coating (Sample 3A)

As shown by the examples 1C, 2B, 4A and 3A in Figure 6.22, four different conditions were identified in the nut analysis. An example of the failed joint is presented in Figure 6.22a (sample 1C), showing a silver coating bright in colour. This was due to the high contact pressure in the deformed area, responsible for the failure. In Figure 6.22b (sample 2B) and Figure 6.22c (sample 4A) two examples of different levels of removal were seen, with the variance depending on the self-locking torque during the first cycle. In fact, the nuts presented in Figure 6.22b and Figure 6.22c reached 20 N·m and 5 N·m self-locking torque respectively during the first cycle. Finally, in Figure 6.22d (sample 3A), an example of a successfully tested nut is presented, showing the silver coating almost intact despite withstanding all six cycles. The silver removal

process will be further analysed in Section 6.5.4, where the possible causes of these differences will be presented.

6.5 DISCUSSION

In this Section the experimental results are compared to the FEA prediction in terms of the cycle profiles and pressure distribution. Additionally, the new design is compared to the elliptical shaped nut examined in the previous chapter. Finally, the last point of discussion considers the variability seen in the test results.

6.5.1 *FEA & Experiment*

The results obtained from the experimental test (Section 6.4) were compared to the profile curves obtained from the FEA (Section 6.2).

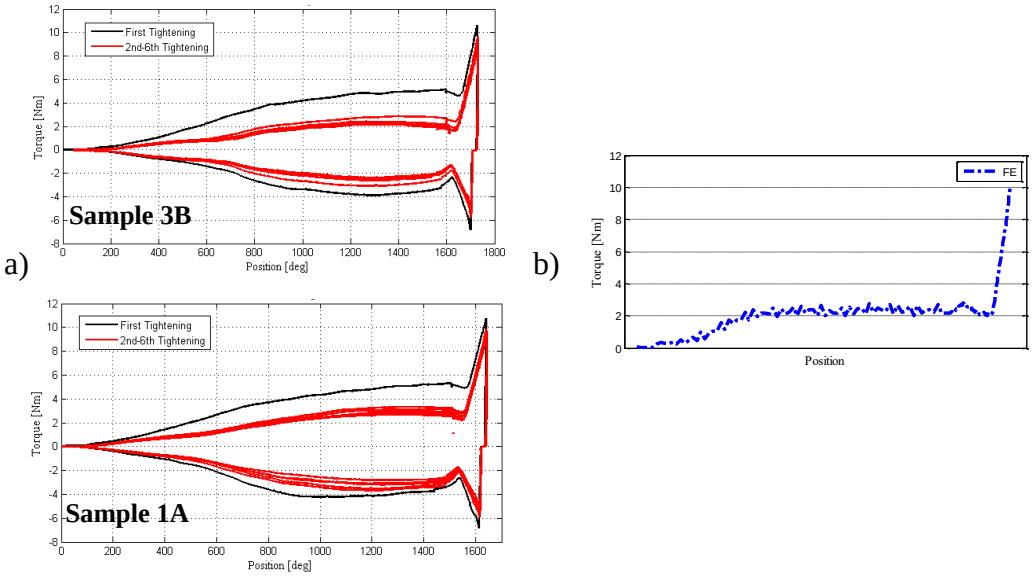

Figure 6.23: FEA and Test Comparison: Torque Profile, a) Testing, b) FEA.

As shown in Figure 6.23 the 2 N·m self-locking torque prediction in the FEA (also presented in Table 6.1) is close to all the successful test results, as seen for the samples 3B and 1A in Figure 6.23, where the silver coating was found undamaged. Additionally, the load-torque curve extrapolated from the FEA and experimental results were compared (Figure 6.24), indicating the expected behaviour.

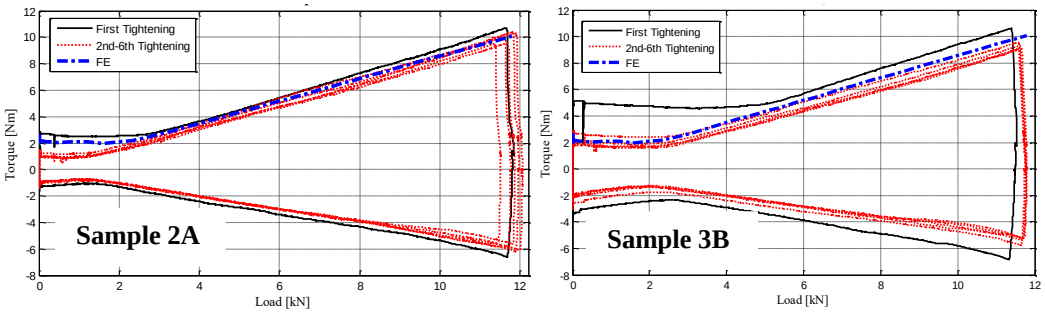

Figure 6.24: FEA and Test Comparison: Load/ Torque Profile

As seen in all the successfully tested nuts and using samples 2A and 3B in Figure 6.24 as examples, the predicted results obtained from the FEA are fully verified by the experimental outcomes, with minor divergence due to the frictional properties used in FEA model. In fact, as previously explained in Section 4.7, the pin on disc test used to characterise the silver coating was found to be particularly inaccurate at low pressure (below 50 MPa).

6.5.2 ***Pressure Distribution***

The pressure distribution in the new design has been examined through the FEA model, and further validated by analysing the silver coating status after the test. Thus, the contact area and the contact pressure extrapolated from the FEA at the end load were plotted in Figure 6.25.

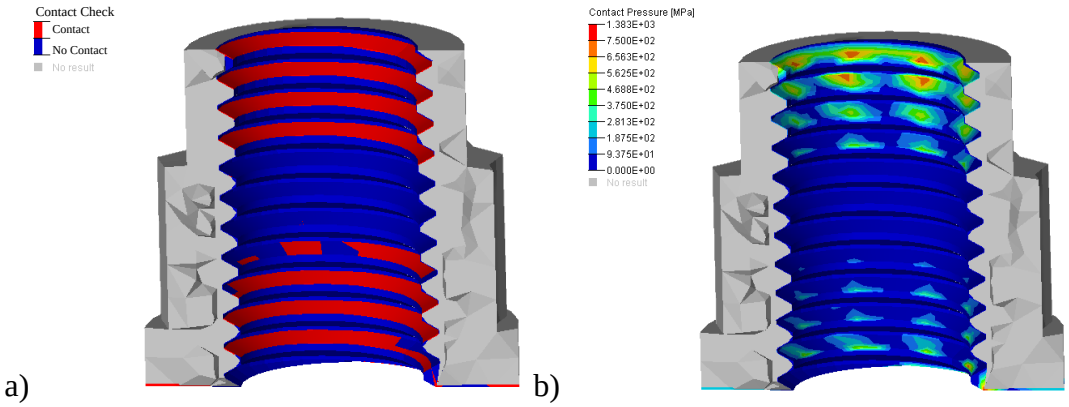

a) b)

Figure 6.25: a) Contact Area, b) Contact Pressure at End Load (Candidate 3)

In Figure 6.25a, the contact area at end load is presented. As shown, the threads in contact are the first and last four of the nut. In Figure 6.25b, the contact pressure in the nut is displayed. In Section 4.7.3 the contact pressure causing the silver coating to strip was identified as 750 MPa. In Figure 6.25b, the contact pressure exceeding 750 MPa is red in colour. Thus, the contact pressure experienced in the nut during the

tightening is below the stripping limit, except in a few small areas. This behaviour of the new design was further confirmed by analysing the silver coating condition after the test (Figure 6.26).

Figure 6.26: Silver Coating Condition (Sample 3A)

As shown in Figure 6.26, in sample 3A for example, the silver was found to be generally intact, further validating that the contact pressure experienced during the cycles does not reach the stripping limit. Furthermore, the FEA was simulated exclusively for the first tightening, while the silver coating in the figure was analysed after six cycles, still showing intact conditions.

6.5.3 *Elliptical vs Axial Locking Features*

The axially deformed nuts were compared to the generally used elliptical nut, in order to further analyse the new locking design. Firstly, the results from the six cycle test for the elliptical shape and an example of the new design were plotted (Figure 6.27, sample 3A).

a)

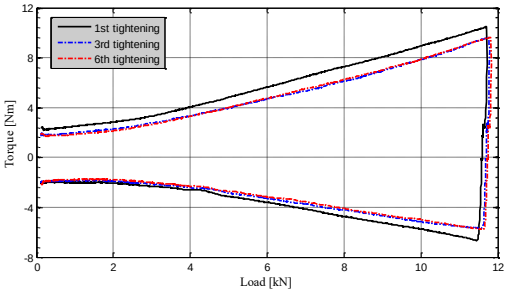

b)

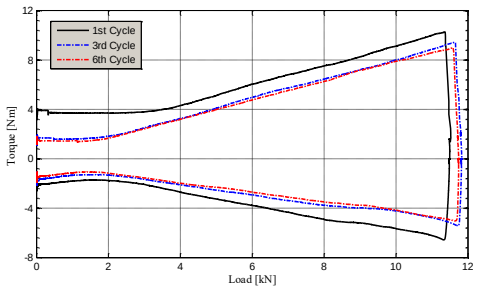

Figure 6.27: Six Cycles Test: a) Elliptical Nut b) Axial Deformed Nut (Sample 3A)

As shown in Figure 6.27, similar curve profiles were obtained with the two designs, showing a higher torque in the first cycle compared to the following cycles, and a

similar torque value at end load. Furthermore, both designs were found to be highly repeatable, as highlighted by the third and sixth cycle curves being almost identical. Additionally, the areas of the threads in contact were also examined for the two designs using the FEA approach and plotted in Figure 6.28.

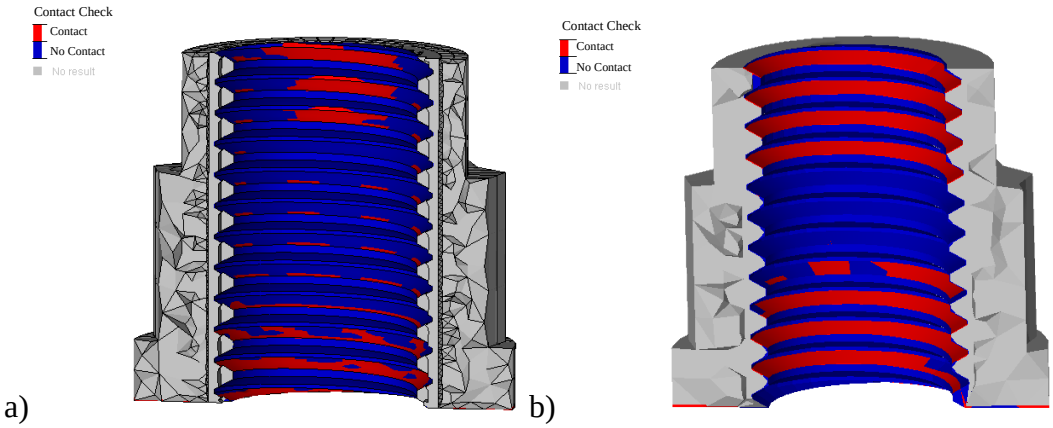

a) b)

Figure 6.28: Contact Area: a) Elliptical Nut, b) Axial Design (Candidate 3)

As shown in Figure 6.28, in the new design (Figure 6.28b) the area in contact is larger compared to the elliptical design (Figure 6.28a), with obviously lower resulting pressure for the same clamping load, as previously described in Section 6.5.2. The pressure distribution was also investigated by analysing the condition of the silver coating after the six cycle test for the two designs, as shown in Figure 6.29.

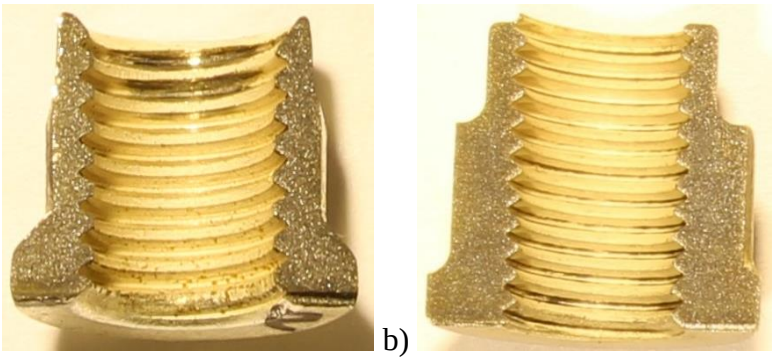

a) b)

Figure 6.29: Silver Conditions: a) Elliptical Nut b) Axial Design (Sample 3A)

As shown in Figure 6.29, the new design presented a silver coating almost intact (Figure 6.29b), compared to the elliptical design (Figure 6.29a). In fact, the current design was found to have been significantly damaged, particularly in the chimney, where high contact pressures were known to have been induced (Section 4.7.2). With this analysis the more distributed contact pressure in the new design was further validated.

6.5.4 *Variability*

As previously anticipated, during the machining process (Section 6.3) the tendency of the threading tool to be deflected was observed. This issue was attributed to the nut material (Inconel 718) and, in fact, in a preliminary study using steel or aluminium as the nut material, this issue was not seen. In the experimental work, this problem was found to cause high contact pressure and the consequent removal of the silver coating (Figure 6.30), sometimes even resulting in complete failure of the joint.

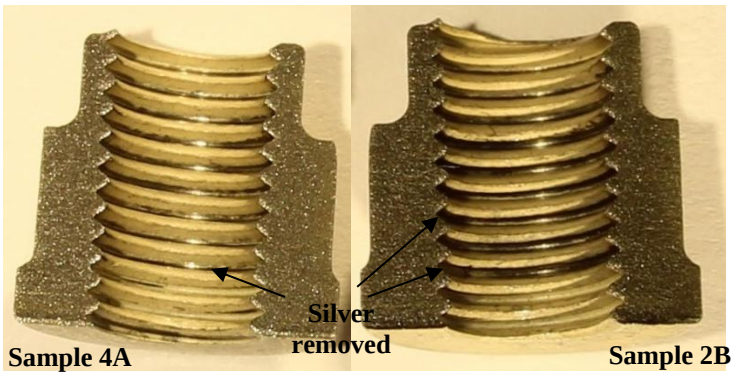

Figure 6.30: Thread Root in the Nut

As shown in Figure 6.30 using samples 4A and 2B as examples, the silver coating was found to have been removed from the root of the threads in particular, highlighting an area of high contact pressure, attributable to the inaccuracy of the single point threading tool during the manufacturing process. The tool issue was further highlighted by the removal of silver from the undeformed threads (first eight threads), which should experience a lower pressure.

However, this problem could be solved in two ways. Firstly, a more rigid tool is necessary in order to reduce the machining time and achieve the required geometry with a smaller number of passes. Additionally, in this work the thread fit was checked using a male counterpart, which was found to be inaccurate and non-repeatable. Thus, a quick and reliable measuring technique could be developed in order to check the thread dimensions, in particular the depth of the root and axial displacement.

6.6 SUMMARY

In this chapter a new self-locking design was developed and the analysis is summarised as follows:

- The axial deformation in the threads are promising for a future development of the new self-locking device. In fact, it was found that as little as two threads

can actually produce the required locking torque. However, further tests and investigation are needed in order to fully describe the capabilities of this design.

- The FEA analyses and the successive examination of the coating condition after the test have shown that fully elastic deformation occurs in the threads, increasing the chance to have a repeatable tightening cycle. This consistency is one of the key parameters for characterising the bolted parts, allowing the necessary torque for a datum load to be calculated.
- During the test of the axial deformed nuts several joints failed to complete the six cycles, which was attributed to a machining issue. In fact, the single-point tool used to manufacture the threads was found to be unsuitable for cutting Inconel. However, a different tool, along with a measurement technique could improve the design.
- The FEA was used as the initial approach to investigate the different design options. The results obtained from the experimental test showed good agreement with the FEA results, further validating the reliability of this approach in order to develop a new design of self-locking devices. As also seen in Chapter 4, the FEA is confirmed as an economical investigation tool for joint application.
- In this work the new axial deformed design was compared to the elliptical nuts used in the rest of this thesis. Improvements were identified in the stripping mechanism and in the contact pressure distribution, confirming that the new design is promising. However, further analysis and test are needed in order to fully understand the new design behaviour.

CHAPTER 7

DISCUSSION

7.1 INTRODUCTION

In the first half of this thesis, the tightening mechanism of the crimped nuts has been investigated, showing that common equations used to calculate the CoF have inaccuracies, and that the coefficient depends on the pressure. In this chapter the challenge of the calculation of the CoF in self-locking coated nuts is further discussed, along with the two approaches used to investigate the tightening mechanism, such as the FEA and the experimental study.

Additionally, as seen in chapter 5 and 6, two different approaches were used to reduce the silver removal issue, such as a new locking feature and a silver coating replacement. In this chapter the two approaches are compared, and their limitations summarised. Finally, future directions and recommendations in the short and long term are discussed, considering the tests required in order to make a final decision with respect to the silver removal issue.

7.2 MEASURING FRICTION IN BOLTED JOINTS: EXPERIMENTAL & FINITE ELEMENT APPROACHES

As introduced in Section 2.2.2, in the analytical calculations normally used in the aero-engine industry, an average CoF is used, calculated at an average contact pressure. However, in Chapter 3 and 4 the tightening mechanism was investigated through an experimental study and a FEA, finding an irregular pressure distribution along the threads, and identifying a localised high pressure in the crimped area. Additionally, the CoF of the silver coating was found to be speed and pressure dependent. Thus, this thesis highlighted the inaccuracy of the equations normally used in the aero-engine industry (Motosh 1976) to calculate the clamping load for a datum tightening torque. On the other hand, the FEA has matched the experimental tightening curve, using the pressure dependant friction curve from a simple pin on disc test, highlighting its applicability in the estimation of friction in joints made from or containing materials with pressure dependant properties.

However, in many respects this issue is likely to be a consequence of the nature of the coated crimped joints in this study. As highlighted, the behaviour of the silver coating is pressure and speed dependant, with the crimp further concentrating contact pressures. In a more typical joint, whilst the contact pressure will still vary between threads, the impact of this change in the absence of the coating/ crimp will be less pronounced. For example, for a steel on steel interface with light lubrication (Bickford 1998), the CoF is between 0.1 and 0.2 (depending on the surface conditions) and shows minimal variation with pressure and speed, meaning in this case the more general thread friction equation would be more accurate.

Additionally, the differences between the analytical and the FEA methods to calculate the CoF in this study are not significant, converging at the end load to a value of 0.125, as discussed in Section 4.7.4. In many respects it is this value under high load that is the most important, because as shown, it is this value that is linked to failure (snapping) of the bolt. Furthermore, whilst the FEA does appear a good tool for estimating behaviour, some inaccuracies were found as a result of the pin on disc test not being accurate enough, due to the equipment used and the coating layer in the sample.

As discussed, both experimental and FEA approaches were used in this study, highlighting the ability of the FEA to investigate the failure sites. In particular high spots of the contact pressure distribution was found, and can be particularly hard to identify in small joints, such as those investigated in this study. With the continuing development of the FEA codes with improved solving methods, in the future the analysis can include the thin layer of coating and the temperature effect can be investigated.

Indeed, the FEA study undertaken has contributed to the literature of the fasteners analysis through this approach. In fact, the fully dynamic investigation of the tightening mechanism, which include a self-locking feature, and a pressure dependent CoF is considered the novelty of this thesis in the FEA literature.

Whilst the benefits of the FEA study are clear, the experimental study remains fundamental to analyse the global behaviour of the joints, as it takes into account geometrical anomalies that in the FEA are not modelled. Also the repeatability of the joints should be assessed experimentally, in order to investigate the reliability of the fastener to be used in the aero-engine industry.

In conclusion, the FEA approach should be use as first step in the analysis and development of self-locking fasteners, and the experimental study to validate the results.

7.3 LIMITATIONS OF THE NEW LOCKING DESIGN & COATING REPLACEMENT

In this study two different approaches have been investigated to minimise the removal of the silver from the crimped nuts, such as a coating replacement and a new self-locking design. However, both approaches were found to have limitations and more analysis is needed in order to complete the studies.

In the coating replacement study, the CoF in the threads was the key parameter to be examined. However, the surface torque was found to have an important effect in the test. In fact, in a preliminary test where washers were not used in the heat treatment test, the failure of the joints was experienced due to seizure in the seating face. Thus, more tests are needed in order to fully understand the influence of friction and seizure in the bearing surface. However, in the current platform the bearing friction is not measurable, thus a number of changes and new sensors can be implemented in order to measure and isolate this parameter.

Additionally, a pin on disc experiment should be performed using the different coating alternatives at room temperature and after heat treatment, in order to better understand the tribological behaviour of the coatings. Thus, the relationship between the friction and contact pressure can also be used to simulate the tightening process using the FEA technique, similarly to the silver coating analysis performed in Section 4.

Four different tests were performed on the alternative coatings in order to identify if there were any appropriate replacements for the silver. However, due to the shortage of testing samples, only a limited number of tests could be performed, and more repeats would be necessary in order to further validate the conclusions drawn.

In the new locking design study, significant margins of improvement were seen with respect to the reduction of contact pressure in the threads and consequent silver removal. However, several limitations were found in this study and further investigation are needed.

For example, in Section 6.2.4 the TPI increase analysis was explained and was excluded due to the higher stresses compared to the TPI decrease, generated during screwing. However, the contact distribution examination has latterly shown a more

uniform contact distribution when the joint is loaded, as shown by the comparison in Figure 7.1.

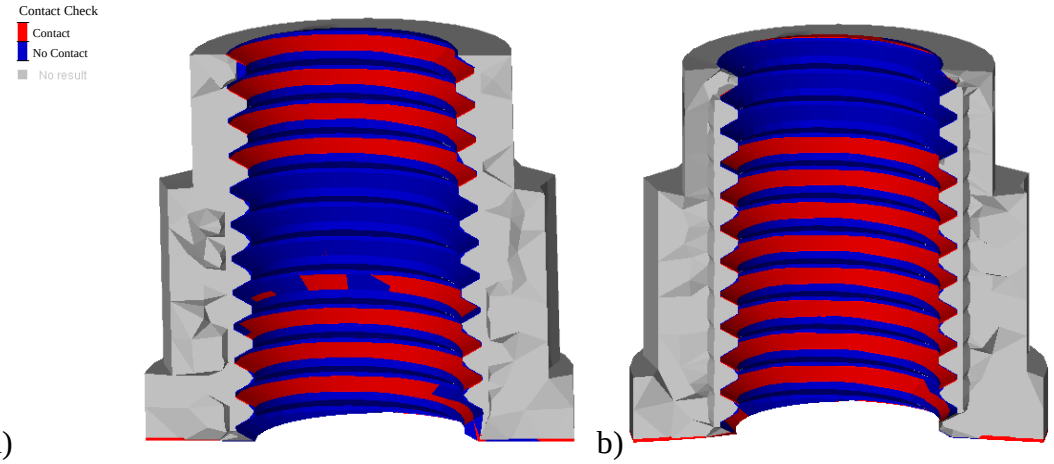

Figure 7.1: Contact Area: a) TPI Decrease and b) TPI Increase

As shown in Figure 7.1, the area of the threads in contact when the end load is reached is significantly different for the two designs. In the TPI decrease analysis (Figure 7.1a), the threads in contact are the first and the last four, with the three threads in the middle not in contact. However, the scenario seen for the TPI increase, with the first eight threads in contact (Figure 7.1b), is preferable as it is similar to the typical contact in the standard fasteners without the self-locking feature. Thus, further investigations should be undertaken in order to analyse this design, including FEA and experimental testing.

As an initial trial of this thread cutting process, a single point cutting tool has been used. However, in a future mass production this method would not be feasible, and a quicker and easier method must be developed. A new tapping method could be achieved using two male thread taps, one with the standard 28 TPI thread, tapping from the bottom of the nut and the other one with the deformed TPI, tapping from the chimney. In fact, during the design process, the deformed threads were preferred in the end of the chimney rather than in the middle of the nut, in order to simplify future production. Furthermore, a small mating thread could be machined on top of the taps to avoid any mismatch, as shown in Figure 7.2.

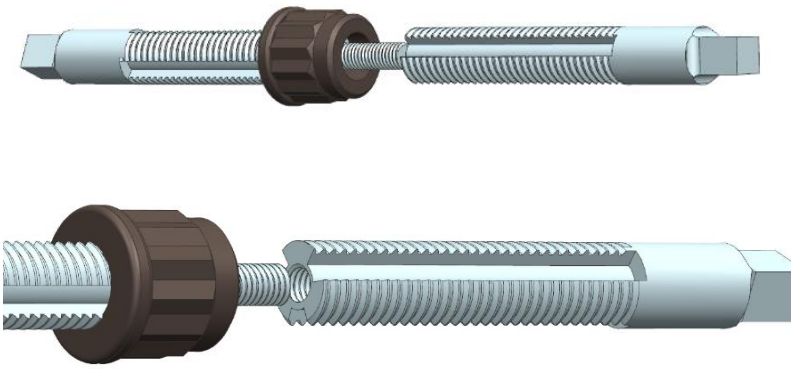

Figure 7.2: Possible Quick Machining Device

This option requires a bigger initial investment to develop the tools, but will ultimately reduce the machining time, which will be essential for a future industrial production. Additionally, in this thesis the ageing capabilities of the silver nuts and the alternative coatings were analysed in order to understand the ability to withstand the high temperature without any seizure occurring. The same test should therefore be performed for the new design. However, as previously explained, the contact stresses experienced with the new design are smaller, and the seizure is less likely to occur in any case.

7.4 FUTURE DIRECTIONS

The two possible solutions investigated in this thesis can be classified as long term, as both approaches need further tests and validations, in order to be implemented in the aero-engine industry. However, due to the promising results of the small change in the locking design seen in Chapter 6, an improvement in the contact distribution can be investigated and achieved in order to minimise the silver removal in the short term.

In Section 6.2.3 the FEA results of the new locking design showed a lower stress field compared to the currently used crimped nuts. From this, seizure and galling are less likely to occur and a new investigation eliminating the low friction coating should be performed. As the FEA analysis was found to be a reliable resource, new simple pin on flat tests should be used to define the pressure-friction dependency, using uncoated solution (lubricated only) or either different alternatives, such as another thin coating. However, in case of an uncoated solution, the CoF in the joint, would be as high as 0.8 (Fox & Liang 2010), being a like on like couple as previously discussed in

Section 2.2.5. This effect would lead to the seizure of the joint (Robinson 2009), and would be likely experienced even with a new crimp design reducing the contact pressure. Additionally, the operating temperature will further promote seizure, as seen by the uncoated seating face. Hence, even if uncoated nuts are fine with cold re-uses, they are likely to fail after service. Thus, the most encouraging solution would be a change in the crimp design, which would prevent the in service coating removal, solving the issues related, as detailed in Section 2.4. Additionally, a protective thin coating would prevent the seizure and reduce the friction.

Additionally, in this work 19 different coatings were tested based upon previous selection of the available technologies and materials. However, these coating methods are subject to continuing development, in terms of new technologies, new materials and related cost. In the coming years, new alternatives should therefore be available for this application, and in particular different alloys could be investigated, also using the combination of the three successful thin films, Chromium, Titanium and Nickel-Titanium.

In this work the anti-vibration capabilities of the new design were not tested. In order to prove the design or either the new coating, further investigations are needed, For example, the Junker test machine (Deutsches Institut für Normung 2004) as previously defined throughout this thesis is widely accepted to assess the locking properties of the fasteners, and will be further explained in Section 9.1. With these tests, the ability of the new design to prevent the self-loosening of the joint can be explored.

Finally, in order to validate the alternative coatings, as previously discussed, the tribological behaviour should be fully understood, through pin on disc test at room temperature and after heat treatment, and the chemical performance with the aero-engine materials investigated and documented in order to draw a final decision. Through this combination of tests a final long term decision point can be reached, and the approach of a modification of the crimp combined with a new coating rigorously explored and validated.

CHAPTER 8

CONCLUSIONS

8.1 INTRODUCTION

In this thesis the tightening process of silver coated locking nuts was investigated in a novel way, using different approaches. An innovative test platform was developed to experimentally examine the nuts currently used in aero-engine applications, where the CoF in the threads was continuously monitored during the tightening process. Furthermore, the FEA approach was for the first time employed to analyse the contact between the threads, along with the pressure and the stresses due to the crimped section. Additionally, different alternatives were explored to investigate how the silver coating might be replaced or avoided entirely, through use of a variety of testing technique. Finally, an original design of self-locking nut was considered, utilising an axial deformation in the chimney of the nut, rather than the current radial crimp. In this section the conclusion of the areas investigated are discussed and summarised.

8.2 SILVER MECHANISM

In Chapter 3 the silver coating was experimentally analysed, using a newly developed test platform. Coated joints were tested at room temperature and after a thermal cycle, and the frictional capabilities assessed. During the tightening, the CoF in the threads was found to be dependent on the clamping load, with a low value of approximately 0.125 at end load of 11.6 kN. In the six cycle test, the friction was found to be consistent over the cycles, which is essential in the bolted joint design.

Silver coated nuts were thermally aged at 760ºC, and the frictional properties assessed post cooling. Significant silver removal and transfer to nearby parts was observed during the test, with the CoF in the threads considerably increasing to 0.24. However, none of the tested joints experienced any failure. An additional test was also performed, to investigate the nano-hardness of the silver coating pre and post thermal cycle. A softening of the material was noticed, with the pre-aged hardness of 1.9 ± 0.4 GPa dropping to 0.8 ±0.4 GPa after ageing. It is thought that annealing and the consequent removal of the silver, generate a like on like contact, causing an increase in the CoF. The relationship between the tightening speed and the CoF was

also investigated across a speed range of 0.5 rpm to 32 rpm. As seen in previous studies, the increase in tightening speed leads to an increase in the CoF. Thus, an assembly standard specifying the tightening speed is strongly recommended in order to estimate the torque required to reach the required load.

The mechanism of the silver coating was fully understood using this approach, through the room temperature cycle, the thermal ageing and the nano-hardness test. For this reason, the same approach was used to investigate new silver alternatives, as performed in Chapter 5.

Finally, a sinusoidal pattern in the self-locking torque during the wind-on and off was found. The cause was identified as arising due to the shape of the bolt being slightly oval, due to the process by which the threads are machined. Despite being within the tolerance of the bolt, the elliptical crimp interacts with the oval bolt, generating this unusual torque pattern.

8.3 FINITE ELEMENT INVESTIGATION

In Chapter 4, a 3D dynamic FEA approach was adopted to analyse the contact mechanism in the elliptical crimped nut during the tightening, as it was found to be too complex to characterise using only the experimental data. The silver coating frictional properties were investigated using a pin on disc test, and implemented as an input to the model. A good agreement between the simulation and the experimental results was achieved, for example comparing the torque profiles. Thus, this approach can be employed to develop new self-locking methods, and analyse the performance of alternative coatings.

The stress distribution was analysed during the whole simulation, and a concentrated stress was identified in the crimp section. As the stresses were higher than the yield strength of the Inconel, the threads plastically deformed. Additionally, by comparing the silver stripping in the nut and the contact pressure in the simulation, a contact pressure of approximately 750 MPa was identified as the cause of the removal of the silver, particularly in the crimped section of the nut.

Furthermore, the reduction in torque experienced in the second tightening cycle was found to be caused by the increase of clearance in the joint, due to the removal and compression under load of the silver coating. The different equations used to calculate the CoF during the tightening were compared using FEA methods. With this method in fact, the friction can be calculated on a nodal basis, instead of using the total torque

and load. It was further highlighted that the CoF obtained in the experimental work did not show a true average, compared to the FEA results. However, the different methods converge to a single value at the end load, which is the most significant, despite the differences at low load due to the weaknesses of the calculation methods.
The pin on disc test was used to provide an input to the FEA model for the CoF at various contact pressures. The relationship seen in the experimental test was also confirmed and the tribological mechanism of the silver investigated. Analysing the friction and the coating condition, three different contact behaviour phases were identified, such as the adhesion at low pressure, followed by a shearing of the silver and finally a progressive damage with an increase in friction.

8.4 ALTERNATIVE COATINGS

In Chapter 5 a coating selection procedure was developed in order to investigate a replacement for the silver as a low coefficient coating in the threads for the elliptical self-locking nuts. Similar to the test performed with silver in Chapter 3, the alternative coatings were tested at room temperature and after heat treatment, assessing the CoF and the ageing behaviour.
An initial selection of 19 metal coatings and paints were analysed, with pure Chromium, pure Titanium and multi-layer Nickel-Titanium found to fulfil the requirements. These three showed a consistent low CoF during re-uses at room temperature, such as 0.21 for the Chromium and 0.20 for the Titanium and 0.19 for the Nickel-Titanium.
However, similarly to the silver analysed in Chapter 3, friction properties of the alternative coatings were found to be affected by the thermal ageing, at 760ºC for 50 hours, increasing the thread friction post treatment, such as 0.50 for the Chromium, 0.54 for the Titanium and 0.32 for the Nickel-Titanium. However, no seizure was experienced during the test, which is fundamental in the aero-engine industry.
As the aim of this research was only to find a selection procedure of coatings, more repeats are needed to validate the results, along with different tests in order to assess the friction properties and the self-locking capabilities of the coatings, such as through the pin on disc test, previously done for the silver coating and the vibration test as further explained in Section 9.1. Additionally, further alloys can be employed in the analysis, such as manufacturing new coatings using the successful materials tested in this research.

Furthermore, investigating the limit torque to break the joints, a low level of thread yield was found to be likely to occur during the untightening, due to the high CoF after ageing, in the case of pure Chromium and pure Titanium. However, during the engine maintenance, after a thermal cycle, the joints are fully replaced.

The cost of the raw materials and the technology used were found to have a significant effect in the coating selection. On the other hand, as the cost is continuing to reduce as coating processes improve, a future resume of the removed materials is not implausible.

8.5 ALTERNATIVE LOCKING DESIGN

In Chapter 6 a new self-locking design, which is applied through an axial deformation at the chimney of the nut, was considered in order to replace the radially deformed nuts for aerospace applications, found to cause the high contact pressure in the crimped section. The new approach was firstly analysed with the FEA technique, and the best candidates machined through a CNC milling machine. Afterwards, the new designed nuts were tested and the results compared with the FEA results and the current radial design.

The FEA was used to investigate the different solutions. As also seen in Chapter 4, the model shown similar results to the experiments, further confirming the capabilities of the FEA as an economical tool to investigate contact and stress problems. The elastic deformation was achieved in the new axial design, further validated by the experiments as multiple re-uses were performed. The CoF was found consistent during the test, a key parameter for the bolted joints designer, as the torque required to reach the end load is directly proportional.

This study confirmed that the self-locking torque required for this application can be achieved with a tiny axial deformation in a small portion of the nut, which produces a resistant torque while screwing. However, more tests are needed to fully characterise the new design capabilities, such as the vibration test. For example, the transverse loading Junker test can be adopted to assess the anti-loosening capabilities. A further examination would be the heat treatment test, in order to analyse the capabilities in an engine environment. Additionally, during the experimental test, several joints failed the six cycle test, which can be solved in future. In fact, it is thought that a stiffer machining tool for cutting Inconel is required, along with a measuring technique to analyse the deformation and the depth in the threads.

Finally, the new axial design was compared to the typically used radially crimped nut, showing a reduction in the stripping process of the silver, further highlighting the lower pressure distribution in the threads.

CHAPTER 9

RECOMMENDATIONS FOR FURTHER WORK

9.1 VIBRATION TESTING

In this work the self-locking torque was the only parameter used to establish the anti-loosening capabilities of the bolted joints, and the anti-vibration capabilities were not taken into account. However, as a new locking method was identified as a possible replacement, a comparison with the current design with respect to the loosening capabilities was found to be necessary. As previously defined, among the currently available vibration test platforms, the Junker test machine (Junker 1969) is the most common used for a wide range of applications. Additional standard tests are also available for aerospace applications, such as the SAE standard (SAE International 2014), which similarly aims to evaluate the ability to prevent loosening by monitoring the reduction of the clamping load along with the vibration cycles.

Comparing the two standards, a different type of loosening is considered. In fact in the Junker test, the loosening is caused by a pure transversal load, while in the SAE standard the loosening is caused by impact, as compared in Figure 9.1.

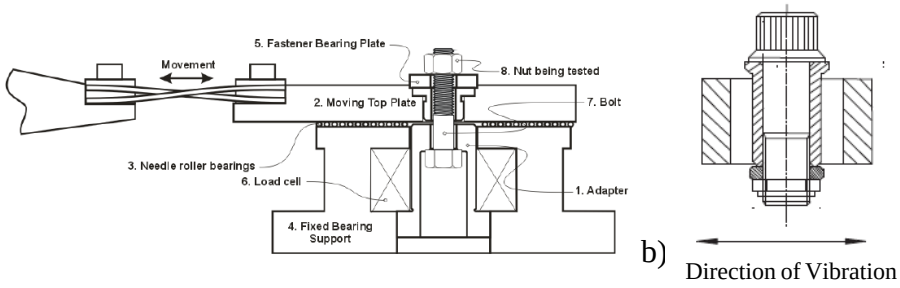

Figure 9.1: Junker Test (Eccles 2010) and SAE Vibration Test (SAE International 2014)

As shown in Figure 9.1a, in the Junker test the bolt clamps two plates, the bottom one is fully constrained to the base, while the top one is driven by a motor and an eccentric shaft, with the load cell clamped on between. On the other hand, in the SAE standard (Figure 9.1b) the bolt is tightened in a hollow cylinder, which is free to move in a slot. Interestingly, in the SAE test the relative displacement between the bolt head and the

nut is measured to indicate the untightening, while in the Junker test the clamping load is also monitored throughout the entire test. In fact, due to the shock loads in the SAE test, the load cell cannot withstand the impacts. A further difference between the two tests is the stiffness required in the Junker platform, due to the motor and the motor directly applying the transversal loads, while in the SAE test the speed is the most influential factor.

Following these standards, a new platform is currently being developed following this thesis in the University of Sheffield, aiming to test the self-locking fasteners using both techniques.

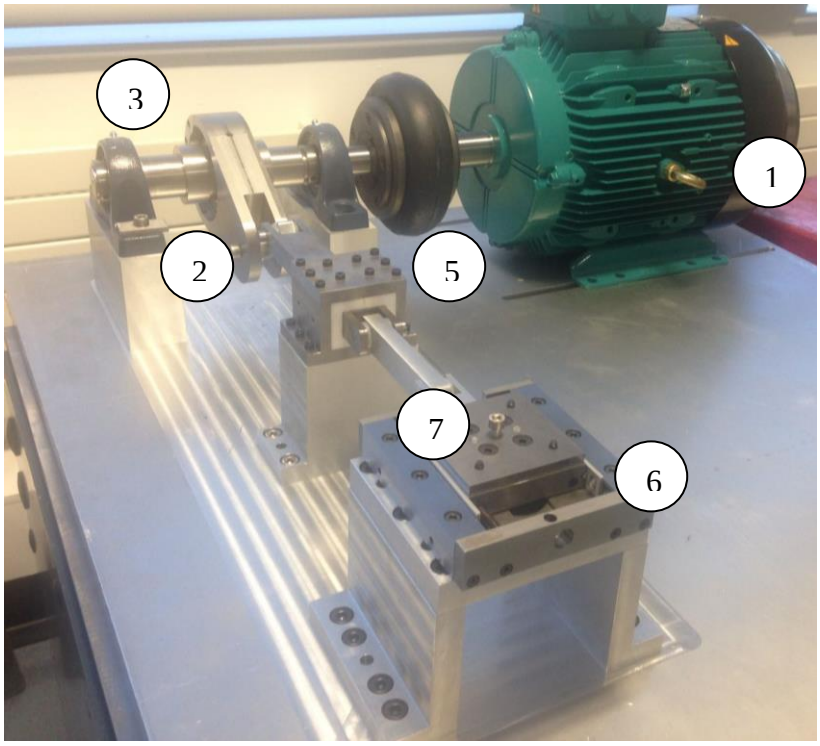

Figure 9.2: New Test Platform Being Developed in the University of Sheffield

As shown in Figure 9.2, an electric motor (1) drives a lever arm (4) through an eccentric shaft (3). The lever arm is connected with a pin to a bar, which is connected to a linear slider (5), in order to only transmit horizontal load to the test specimen. Through another bar, the top plate (6) clamping the fastener (7) vibrates. The load cell is placed between the bolt and the bottom plate, which is fixed to the test rig table.

A 7.5kW electric motor can rotate to a maximum speed of 1800 rpm, thus the test can be performed up to 30Hz. Additionally, the eccentric shaft can be easily changed in order to apply a different displacement. Simply changing the top plate and the joint sleeve, both the Junker and the SAE tests can be performed in the test rig.

The aim of the test is to monitor the clamping load or the joint displacement with respect to the test cycles, in order to assess the locking torque of the silver coated nuts, and compare the results with the other locking designs. Additionally, a new locking design can be tested and improved and the influence of the initial preload in the self-loosening process can be evaluated.

9.2 BEARING FACE FRICTION

In Section 5 different coatings were analysed as potential replacements of the silver used in nuts for aero-engine applications. The seizure seen in the bearing surfaces during the experimental tests, particularly during the thermal cycle, showed the importance of investigating the contact and the coefficient of bearing friction in the joints. With the current platform configuration, a thrust bearing is used and the bearing torque subtracted during post-processing. However, the test rig can be updated to accommodate a further torque sensor, in order to measure the bearing torque continuously alongside the thread torque and clamping load. Thus, CoF in the threads and bearing friction can be plotted independently with respect to load, and the different coating alternatives compared. An ultimate objective of this analysis would be develop of a new coating method, using different coatings in the threads and in the bearing surface, depending on the contact behaviour.

9.3 PUBLICATIONS ARISING FROM THIS WORK

1. Tronci, G., Marshall, M.B., 2016, “Understanding the behaviour of silver as a low friction coating in aerospace fasteners”, *Tribology International*.

2. Tronci, G., Marshall, M.B., 2015, “Understanding the behaviour of silver as a low friction coating in aerospace fasteners”, *Proceedings of the 42nd Leeds-Lyon Symposium on Tribology*, September 7-9, 2015, Lyon, France.

3. Tronci, G., Marshall, M.B., 2015, “Mechanical behaviour of silver as a low friction coating in aerospace fasteners”, *Proceedings of the 9th International Charles Parsons Turbine and Generator Conference*, 15-17 September 2015, Loughborough, UK.

REFERENCES

ABAQUS, 2013. *Abaqus 6.13 Documentation*, Dassault Systèmes.

Altair, 2013a. HyperMesh 11.0 User Guide.

Altair, 2013b. HyperWorks 11.0 Desktop User's Guide.

Arnell, R.D. & Soliman, F. a., 1978. The effects of speed, film thickness and substrate surface roughness on the friction and wear of soft metal films in ultrahigh vacuum. *Thin Solid Films*, 53(3), pp.333–341.

ASM International, 2002. *Atlas of Stress-strain Curves*,

Barrett, R.T., 1990. Fastener design manual. *Nasa Rp-1228*.

Bi, Q., Zhu, S. & Liu, W., 2013. High Temperature Self-Lubricating Materials. *Tribology in Engineering*, pp.109–134.

Bickford, J., 1998. Handbook of Bolts and Bolted Joints. , p.911.

Budynas, R. & Nisbett, K., 2010. *Shigley's Mechanical Engineering Design*, McGraw-Hill Education.

Cheatham, C.A., Acosta, C.F. & Hess, D.P., 2009. Tests and analysis of secondary locking features in threaded inserts. *Engineering Failure Analysis*, 16(1), pp.39–57.

Chen, S. et al., 2010. Research on deformation and stress distribution on thread teeth at conic thread connections. *Zhongguo Jixie Gongcheng/China Mechanical Engineering*, 21(17), pp.2044–2049.

Chesson, E. & Munse, W.H., 1965. Studies of the behavior of high-strength bolts and bolted joints.

Deutsches Institut für Normung, 2004. *Design guide for railway vehicles and their components – Bolted joints – Part 4: Securing of bolted joints. DIN 25201-4*,

Dragoni, E., 1994. Effect of Thread Pitch and Frictional Coefficient on the Stress Concentration in Metric Nut-Bolt Connections. *Journal of Offshore Mechanics and Arctic Engineering*, 116(21).

Eccles, W., 2010. *Tribological Aspects of the Self-Loosening of Threaded Fasteners*.

Eccles, W., Sherrington, I. & Arnell, R.D., 2010. Towards an understanding of the loosening characteristics of prevailing torque nuts. *Proceedings of the Institution of Mechanical Engineers, Part C: Journal of Mechanical Engineering Science*, 224(2), pp.483–495.

El-Sherbiny, M. & Salem, F., 1986. Tribological Properties of PVD Silver Films. *A S L E Transactions*, 29(2), pp.223–228.

Englund, R. & Johnson, D., 1997. Finite element analysis of a threaded connection compared to experimental and theoretical research. *Journal of Engineering Technology*.

ExxonMobil, 2015. Mobil Jet Oil II.

Fastenal: Industrial & Construction Supplies, 2005. *Technical Reference Guide*,

Finkelston, R.J., 1972. How much shake can bolted joints take. *Machine Design*, 44, pp.122–125.

Fischer-Cripps, A.C., 2011. Nanoindentation Instrumentation. *Nanoindentation*, pp.199–211.

Fox, G.R. & Liang, H., 2010. Wear Mode Comparison of High-Performance Inconel Alloys. *Journal of Tribology*, 132(2).

Fukuoka, T. et al., 1985. A stress analysis of threaded portions in fastening. *Bulletin of JSME*, 28(244).

Fukuoka, T., 2005. Finite element analysis of the thermal and mechanical behaviors of a bolted joint. *Journal of Pressure Vessel Technology-Transactions of the Asme*, 127(4), pp.402–407.

Fukuoka, T., Nomura, M. & Morimoto, Y., 2006. Proposition of Helical Thread

Modeling with Accurate Geometry and Finite Element Analysis. *Transactions of the Japan Society of Mechanical Engineers Series A*, 72(723), pp.1639–1645.

Goodier, J.N. & Sweeney, R.J., 1945. Loosening by vibration of threaded fastenings.

Groper, M. & Hemmye, J., 1983. Partial slip damping in high strength friction grip bolted joints. *Proceedings of the Fourth International Conference of Mathematical Modeling*.

Guy, J., 2015. Friction Modification for Aerospace-Engine Fasteners. *Master Degree Dissertation*.

Haviland, G., 1983. *Designing with threaded fasteners*, Newington Conn.: Loctite Corp.

Hess, D., 1998. Vibration- and Shock- Induced Loosening. In *Handbook of Bolts and Bolted Joints*.

Holmberg, K. & Matthews, A., 2009. *Coatings Tribology: Properties, Mechanisms, Techniques and Applications in Surface Engineering*, Elsevier.

Houghton, A., 2015. Use of Tribological Design and Surface Engineering to Improve Riser Valve Components.

Ibbotson, A.B. & Talbot, F.J., 1877. Improvement in forming threads on screw bolts and nuts. *US Patent 191,968*.

Indestructible Specialist Coatings Manifacture, 2016. *IP9136-R1 - Graphite Filled Skydrol Resistant Dry Film Lubricant*,

Izumi, S. et al., 2005. Three-dimensional finite element analysis of tightening and loosening mechanism of threaded fastener. *Engineering Failure Analysis*, 12(4), pp.604–615.

Jiang, Y. et al., 2004. An Experimental Study of Self-Loosening of Bolted Joints. *Journal of Mechanical Design*, 126, pp.925–931.

Jiang, Y., Zhang, M. & Lee, C.-H., 2003. A study of early stage self-loosening of bolted joints. *Journal of Mechanical Design, Transactions of the ASME*, 125(3),

pp.518–526.

Junker, G.H., 1969. New Criteria for Self-Loosening of Fasteners Under Vibration. *SAE Technical Paper*, No. 690055.

Juvinall, R.C. & Marshek, K.M., 2006. *Fundamentals of Machine Component Design*, Wiley.

Kasei, S., 2007. A Study of Self-Loosening of Bolted Joints Due to Repetition of Small Amount of Slippage at Bearing Surface. *Journal of Advanced Mechanical Design, Systems, and Manufacturing*, 1(3), pp.358–367.

Kasei, S., Ishimura, M. & Ohashi, N., 1988. On self-loosening of threaded joints in the case of absence of macroscopic bearing-surface sliding. Loosening mechanism under transversely repeated force. *Journal of the Japan Society for Precision Engineering*, 54(7), pp.1381–1386.

Kim, J., Yoon, J.-C. & Kang, B.-S., 2007. Finite element analysis and modeling of structure with bolted joints. *Applied Mathematical Modelling*, 31(5), pp.895–911.

Kloosterman, G., 2002. *Contact methods in finite element simulations*,

Kogut, L. & Etsion, I., 2002. Elastic-Plastic Contact Analysis of a Sphere and a Rigid Flat. *Journal of Applied Mechanics*, 69(5), p.657.

Kulak, G., Fisher, J. & Struik, J., 1987. Guide to design criteria for bolted and riveted joints.

Kumar, S.N., 2014. Investigation on the self loosening behavior of hexagonal nut and nylock nut in curvic coupling under transverse loading. *IOSR Journal of Mechanical and Civil Engineering (IOSR-JMCE)*, pp.63–66.

Kuznetsov, V.D. & Freitag, E.H., 1966. *Metal transfer and build-up in friction and cutting*,

Lawrence, H. & White, C.H., 1861. Lock for Nuts of Railroad-bolts.

Lehnhoff, T.F. & Bunyard, B.A., 2000. Bolt thread and head fillet stress concentration

factors. *Journal of Wessel Pressure Technology*, 122, pp.180–185.

Liao, R., Sun, Y. & Zhang, W., 2009. Nonlinear analysis of axial-load and stress distribution for threaded connection. *Chinese Journal of Mechanical Engineering*, 22(6).

Liu, K.T. & Duh, J.G., 2008. Hardness evolution of NiTi and NiTiAl thin films under various annealing temperatures. *Surface and Coatings Technology*, 202(12), pp.2737–2742.

Mackerle, J., 2003. Finite element analysis of fastening and joining: A bibliography (1990-2002). *International Journal of Pressure Vessels and Piping*, 80(4), pp.253–271.

Marechal, N., Pauleau, Y., et al., 1994. Sputter-deposited lubricant thin films operating at elevated temperatures in air. *Surface and Coatings Technology*, 68–69, pp.416–421.

Marechal, N., Quesnel, E., et al., 1994. Tribological properties of thin silver films sputter-deposited on superalloy substrates. *Thin Solid Films*, 249(1), pp.70–77.

Marshall, M.B., Zainal, I. & Lewis, R., 2011. Influence of the Interfacial Pressure Distribution on Loosening of Bolted Joints. *Strain*, 47, pp.65–78.

Martínez, M.. et al., 2011. Influence of thread geometry on the performance of retaining anaerobic adhesives. *International Journal of Adhesion and Adhesives*, 31(6), pp.429–433.

Maruyama, K., 1973. Stress Analysis of a Bolt-Nut Joint by the Finite Element Method and the Copper-Electroplating Method. *The Japan Society of Mechanical Engineers*, 16(94).

Military Specification, 1991. *MIL-S-8879C, Screw threads, controlled radius root with increased minor diameter.*,

Miyata, C., Tsumura, T. & Iwato, I., 1991. A Proposed Skirtlike, Hollow Flange Design for Self-Locking Hex Nuts. *JSME International Journal. Ser. 3, Vibration, Control Engineering, Engineering for Industry*, 34(2), pp.286–289.

Motosh, N., 1976. Development of design charts for bolts preloaded up to the plastic range. *Journal of Manufacturing Science and Engineering*, 98(3), pp.849–851.

Nassar, S. a. et al., 2007. Effect of Tightening Speed on the Torque-Tension and Wear Pattern in Bolted Connections. *Journal of Pressure Vessel Technology*, 129(3).

Nassar, S. a., Matin, P.H. & Barber, G.C., 2005. Thread Friction Torque in Bolted Joints. *Journal of Pressure Vessel Technology*, 127(4), p.387.

Nassar, S. a., Wu, Z. & Yang, X., 2010. Achieving Uniform Clamp Load in Gasketed Bolted Joints Using a Nonlinear Finite Element Model. *Journal of Pressure Vessel Technology*, 132(3).

Nassar, S. a. & Yang, X., 2007. Novel Formulation of the Tightening and Breakaway Torque Components in Threaded Fasteners. *Journal of Pressure Vessel Technology*, 129(4), p.653.

Nassar, S. a. & Zaki, A.M., 2009. Effect of Coating Thickness on the Friction Coefficients and Torque-Tension Relationship in Threaded Fasteners. *Journal of Tribology*, 131(2).

Oskouei, R.H., MKeikhosravy, M. & Soutis, C., 2009. Estimating clamping pressure distribution and stiffness in aircraft bolted joints by finite-element analysis. *Proc. IMechE,J. Aerospace Engineering*, 223.

Pai, N.G. & Hess, D.P., 2002a. Experimental Study of Loosening of Threaded Fasteners Due To Dynamic Shear Loads. *Journal of Sound and Vibration*, 253(3), pp.585–602.

Pai, N.G. & Hess, D.P., 2002b. Three-dimensional finite element analysis of threaded fastener loosening due to dynamic shear load. *Engineering Failure Analysis*, 9(4), pp.383–402.

Panja, B. & Das, S., 2013. A Study of Anti-Loosening Ability of 5/8 BSW Fasteners under Vibration with High Tension Steel and Stainless Steel Bolts. In *1st International and 16th National Conference on Machines and Mechanisms*.

Pattinson, G. & Pallett, L., 2015. Fastener Coating Selection. *Rolls-Royce Internal*

Report.

Pattinson, G. & Reade, G., 2012. Materials Capability Acquisition Overview: Silver Replacement on Threaded Fasteners. *Internal Report*.

Pauleau, Y., 1996. *Protective Coatings and Thin Films: Synthesis, Characterization, and Applications*, Springer Science & Business Media.

Pearce, M.B., 1973. A Study of Vibration-Resistant Fasteners (No. 730825). In *SAE Technical Paper*.

Petrova, a. P. & Lukina, N.F., 2008. Adhesive technologies in aircraft construction. *Polymer Science. Series D*, 1(2), pp.83–90.

Reedy, E.D., 2006. Thin-coating contact mechanics with adhesion. *Journal of Materials Research*, 21(10), pp.2660–2668.

Roberts, E., Anderson, M. & Gould, S., 1997. Solid lubricant coatings- Their performance and applicability at temperature extremes. *Protective coatings and thin films- Synthesis, characterization and applications*, pp.135–156.

Robinson, M., 2009. STC-3069 Literature Review: Anti-Seizure Coatings for Threaded Fasteners. *Rolls-Royce Internal Report*.

Rolls Royce, 2011. JDS 829.02 Torque Tightening of Unified Threaded Fasteners. *Internal Standard*, pp.1–14.

Rolls Royce, 2015. RRES90027 Torque Tightening of Unified Threaded Components. *Internal Standard*.

SAE International, 2014. Aerospace Standard AS7251-C.

Sase, N. et al., 1998. An anti-loosening screw-fastener innovation and its evaluation. *Journal of Materials Processing Technology*, 77(1), pp.209–215.

Sase, N. et al., 1996. Evaluation of anti-loosening nuts for screw fasteners. *Journal of Materials Processing Technology*, 56(1–4), pp.321–332.

Sauer, J., Lemmon, D. & Lynn, E., 1950. Bolts: how to prevent their loosening.

Mechanical Design.

Saunders, E.A. et al., 2016. Understanding the “blue spot.” *Engineering Failure Analysis*, 61, pp.2–20.

Shoberg, R., 2000. Engineering fundamentals of threaded fastener design and analysis. I. *Fastening*.

Sliney, H.E., 1982. Solid lubricant materials for high temperatures - a review. *Tribology International*, 15(5), pp.303–315.

Smith, C., 1990. *Carroll Smith’s Nuts, Bolts, Fasteners and Plumbing Handbook: Technical Guide for Racer, Restorer and Builder*, Motorbooks.

Tanaka, M. & Yamada, A., 1986. The Behaviour of Fasteners under External Loading. *Bulletin of JSME*, 248(41).

Temitope, S.J., 2015. Condition Monitoring of Bolted Joints. *PhD Thesis*, (June 2015).

The Society of British Aerospace Companies Ltd, 2004. *AS42910 Nut, Self-Locking, Bi-Hexagon, Waspaloy*,

The Society of British Aerospace Companies Ltd, 2006. *Technical Specification No. 128*,

Voevodin, A.A., Muratore, C. & Aouadi, S.M., 2014. Hard coatings with high temperature adaptive lubrication and contact thermal management: review. *Surface & Coatings Technology*, 257, pp.247–265.

Williams, J.A. & Dwyer-Joyce, R.S., 2000. Modern Tribology Handbook,. In *Modern Tribology Handbook*. CRC Press, p. 1760.

Yamamoto, A. & Kasei, S., 1984. A solution for self-loosening mechanism of threaded fasteners under transverse vibration. *Bull. Jpn. Soc. Precis. Eng.*

Yang, G. et al., 2011. Member stiffnesses and interface contact characteristics of bolted joints. *Proceedings - 2011 IEEE International Symposium on Assembly and Manufacturing, ISAM 2011*, pp.0–5.

Yang, G. et al., 2013. Three - Dimensional Finite Element Analysis of the Mechanical Properties. *Chinese Journal of Mechanical Engineering*, 26(3).

Yang, S.H. et al., 2003. A wear map of bearing steel lubricated by silver films. *Wear*, 255(7–12), pp.883–892.

Zadoks, R.I. & Kokatam, D.P., 1999. Three-dimensional finite element model of a threaded connection. *Computer Modeling and Simulation in Engineering*, 4(4), pp.274–281.

Zadoks, R.I. & Kokatam, D.P.R., 2001. Investigation of the Axial Stiffness of a Bolt Using a Three-Dimensional Finite Element Model. *Journal of Sound and Vibration*, 246(2), pp.349–373.

Zhang, M., Jiang, Y. & Lee, C.-H., 2006. An Experimental Investigation of the Effects of Clamped Length and Loading Direction on Self-Loosening of Bolted Joints. In *Journal of Pressure Vessel Technology-Transactions of the ASME*. ASME, pp. 388–393.

Zhang, M., Jiang, Y. & Lee, C.-H., 2007. Finite Element Modeling of Self-Loosening of Bolted Joints. In *Journal of Mechanical Design, Transactions of ASME*. ASME, pp. 218–226.

Zhang, X.R., Nie, J.X. & Hou, G., 2000. Development of Anti-Loosening Nuts Using Shape Memory Alloys. *Materials Science Forum*, 327–328, pp.35–38.

Zhu, J., 2012. Rolls-Royce – Anti-Seizure Coatings for Bolts. *Internal Report*.

Zou, Q. et al., 2007. Effect of Lubrication on Friction and Torque-Tension Relationship in Threaded Fasteners. *Tribology Transactions*, 50(1), pp.127–136.

APPENDICES

APPENDIX A LabVIEW Code

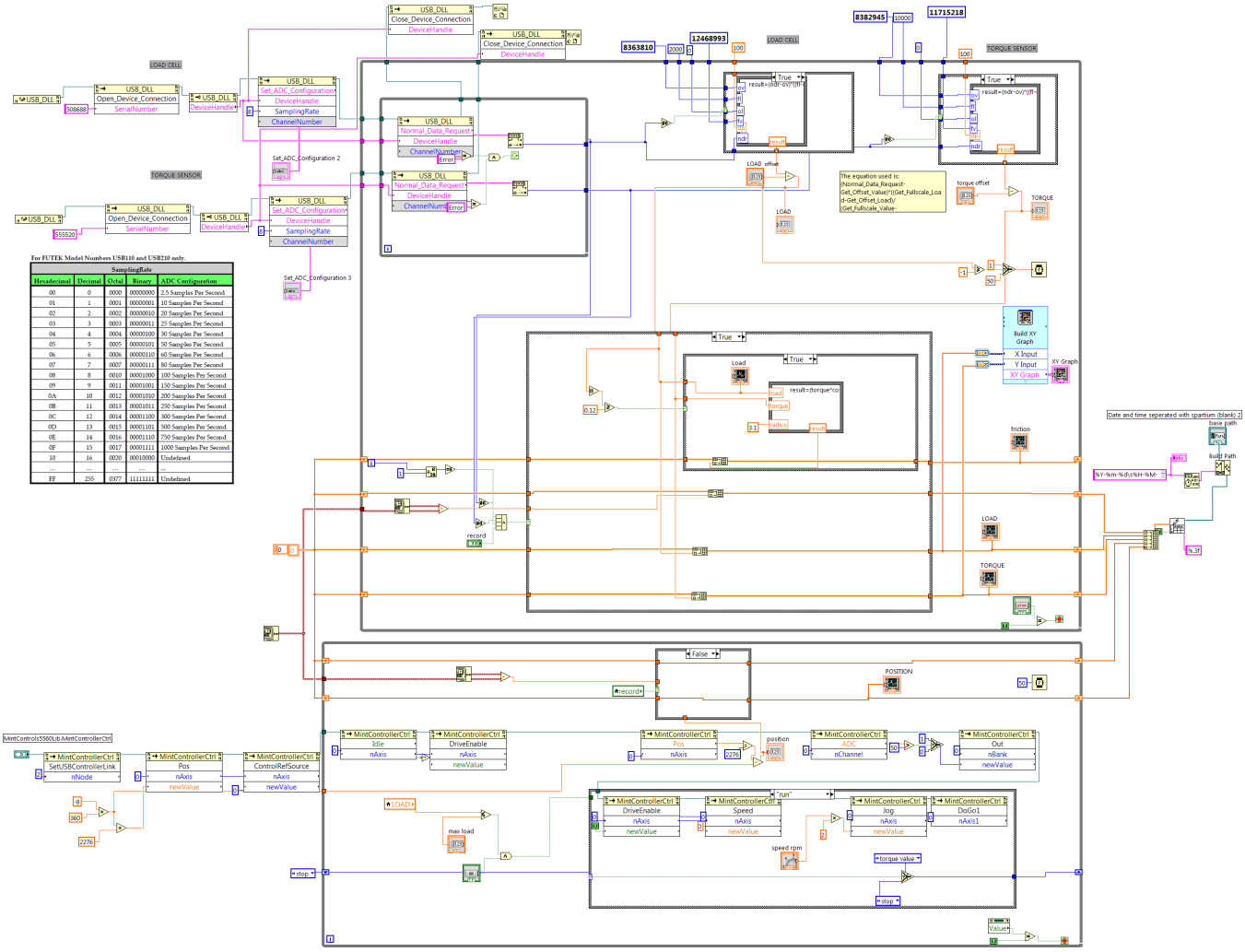

APPENDIX B Alternative Coating: Nano-Hardness

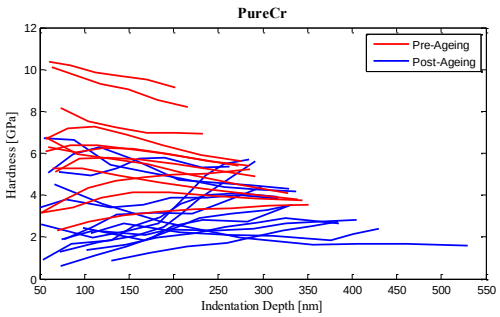

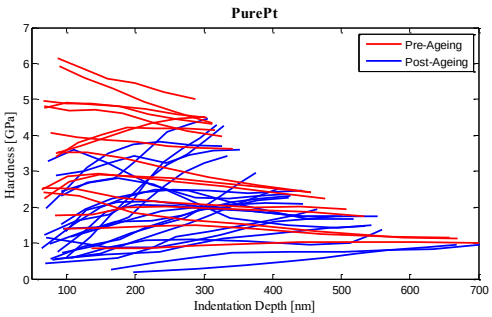

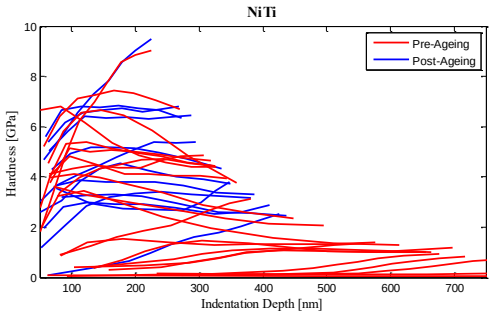

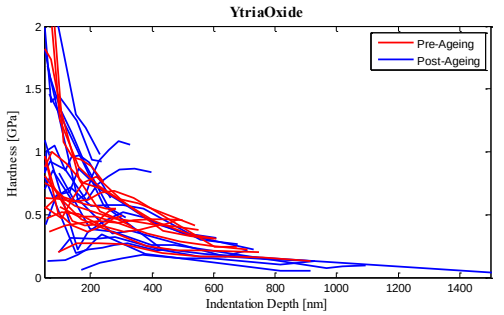

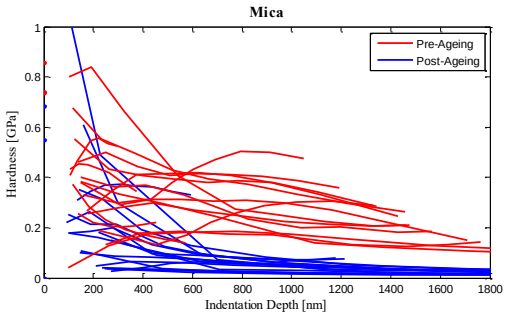

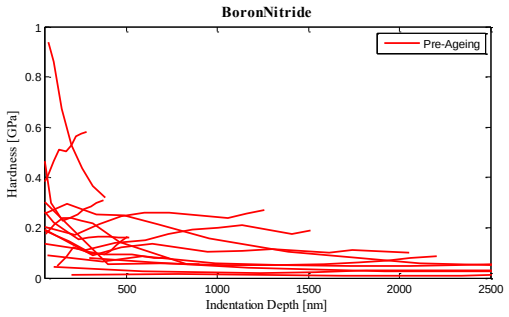

APPENDIX C Variable Pitch: FEA Results

Candidate 2 *(27.6 TPI for 4 threads)*

A) Von Mises Stresses at Zero Load

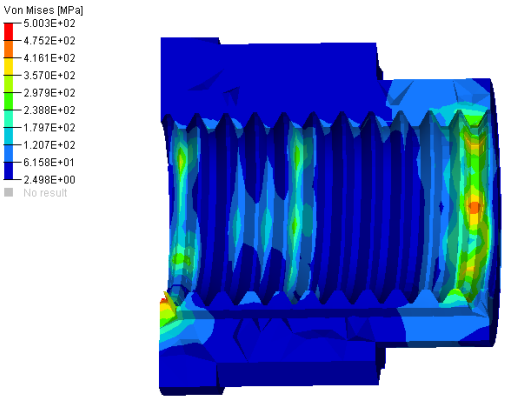

B) Von Mises Stresses at End Load

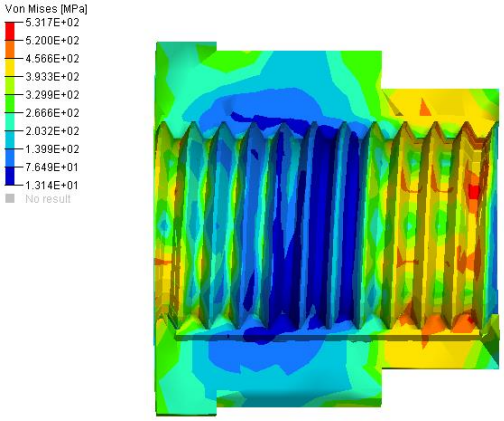

C) Contact Pressure at Zero Load

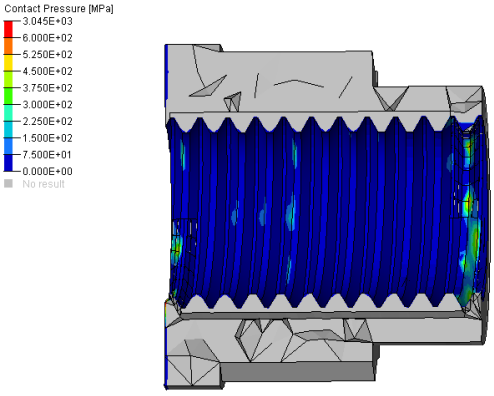

D) Contact Pressure at End Load

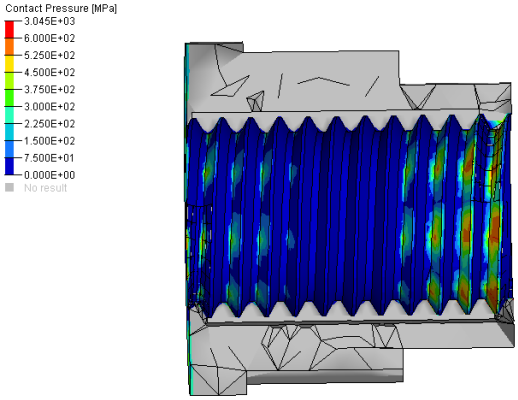

Candidate 3 *(27.5 TPI for 3 threads)*

A) Von Mises Stresses at Zero Load

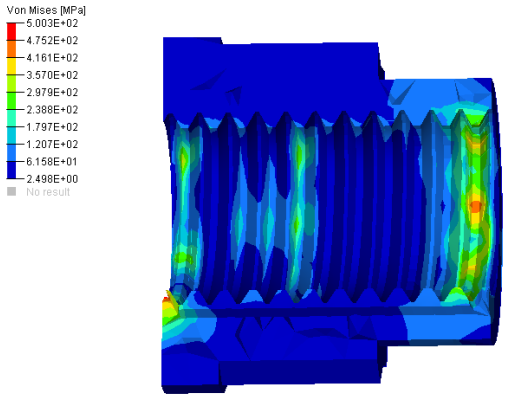

B) Von Mises Stresses at End Load

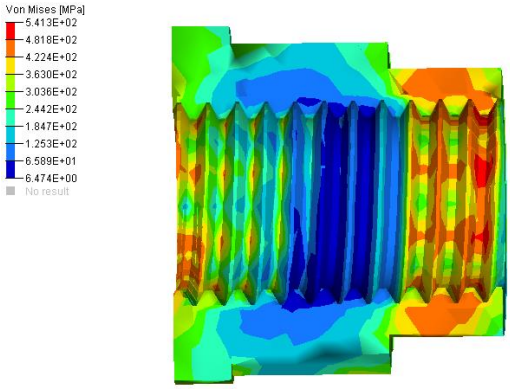

C) Contact Pressure at Zero Load

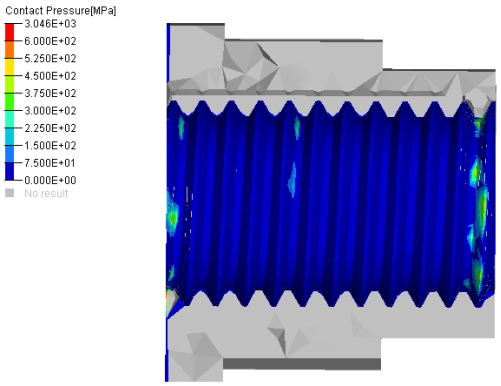

D) Contact Pressure at End Load

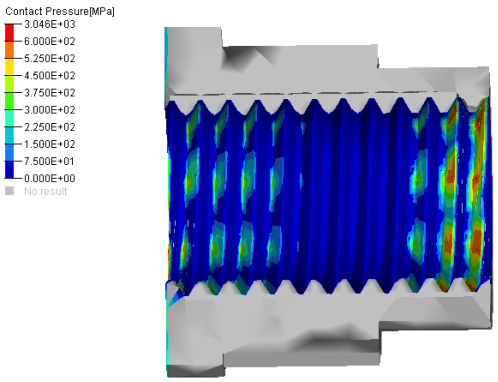

Candidate 4 *(27.25 TPI for 2 threads)*

A) Von Mises Stresses at Zero Load	B) Von Mises Stresses at End Load
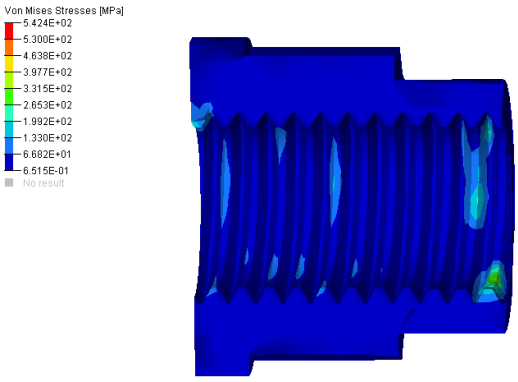	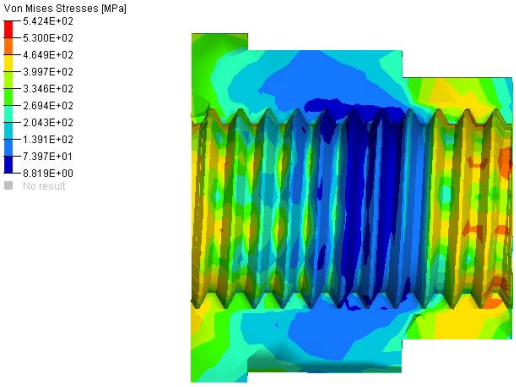
C) Contact Pressure at Zero Load	D) Contact Pressure at End Load